

For Reference

NOT TO BE TAKEN FROM THIS ROOM

For Reference

NOT TO BE TAKEN FROM THIS ROOM

Ex LIBRIS
UNIVERSITATIS
ALBERTAEensis



UNIVERSITY OF ALBERTA
LIBRARY

Regulations Regarding Theses and Dissertations

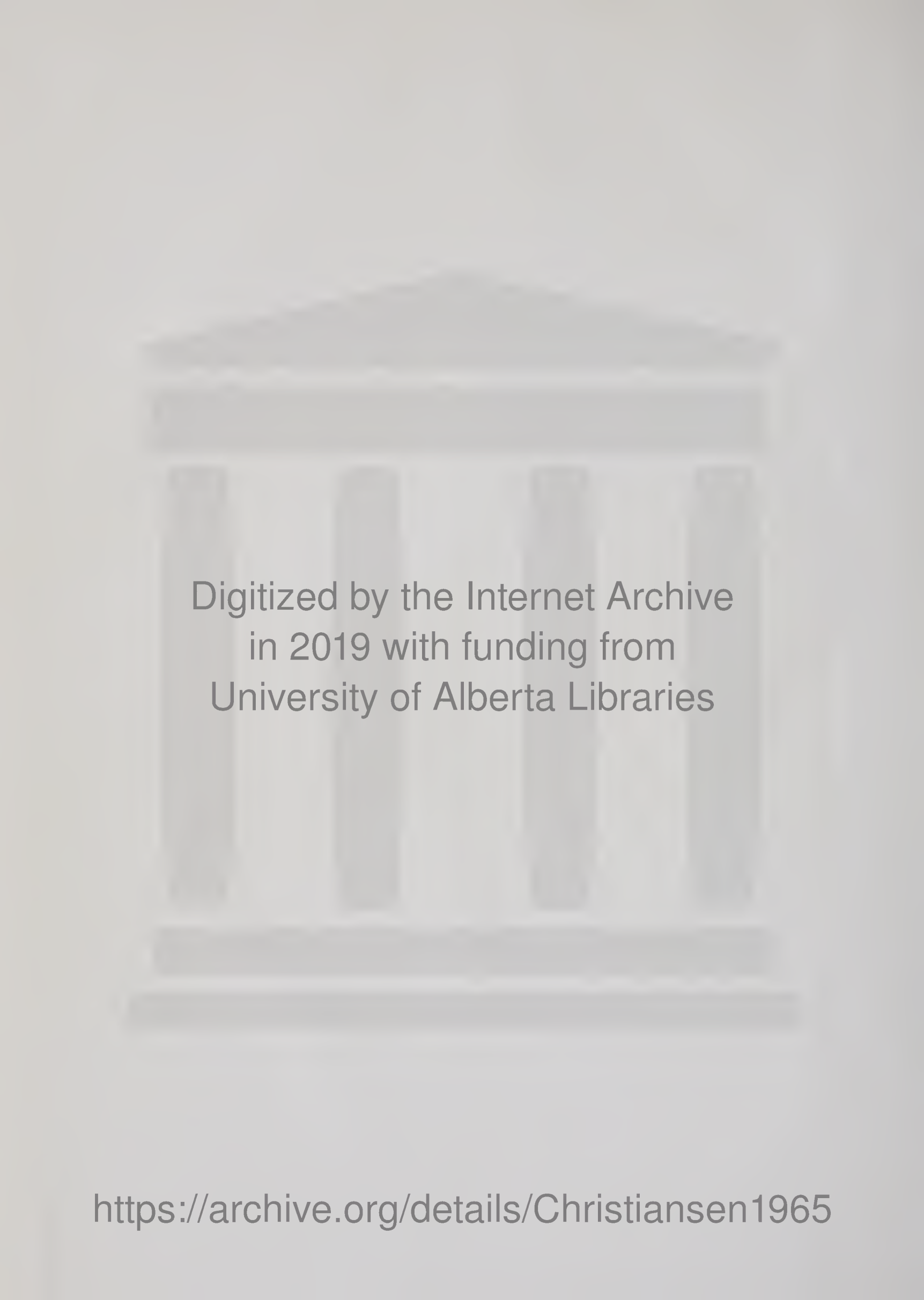
Typescript copies of theses and dissertations for Master's and Doctor's degrees deposited in the University of Alberta Library, as the official Copy of the Faculty of Graduate Studies, may be consulted in the Reference Reading Room only.

A second copy is on deposit in the Department under whose supervision the work was done. Some Departments are willing to loan their copy to libraries, through the inter-library loan service of the University of Alberta Library.

These theses and dissertations are to be used only with due regard to the rights of the author. Written permission of the author and of the Department must be obtained through the University of Alberta Library when extended passages are copied. When permission has been granted, acknowledgement must appear in the published work.

This thesis or dissertation has been used in accordance with the above regulations by the persons listed below. The borrowing library is obligated to secure the signature of each user.

Please sign below:

A faint, grayscale background image of a classical building, possibly a temple or a large library, featuring a series of columns supporting a classical entablature and a pediment. The building is set against a light, cloudy sky.

Digitized by the Internet Archive
in 2019 with funding from
University of Alberta Libraries

<https://archive.org/details/Christiansen1965>

THE UNIVERSITY OF ALBERTA

THE DEVELOPMENT OF AIR VELOCITY PROFILES
IN A VERTICAL TUBE WITH A
DIVERGING CONICAL INLET

by

S.E. Christiansen

A THESIS

SUBMITTED TO THE FACULTY OF GRADUATE STUDIES
IN PARTIAL FULFILMENT OF THE REQUIREMENTS FOR THE
DEGREE OF MASTER OF SCIENCE

IN

CHEMICAL ENGINEERING

FACULTY OF ENGINEERING

DEPARTMENT OF CHEMICAL AND PETROLEUM ENGINEERING

EDMONTON, ALBERTA

JUNE, 1965

UNIVERSITY OF ALBERTA
FACULTY OF GRADUATE STUDIES

The undersigned certify that they have read, and
recommend to the Faculty of Graduate Studies for acceptance
a thesis entitled THE DEVELOPMENT OF AIR VELOCITY PROFILES
IN A VERTICAL TUBE WITH A DIVERGING CONICAL INLET submitted
by Svein Erik Christiansen in partial fulfilment of the re-
quirements for the degree of Master of Science in Chemical
Engineering

Date . June 11, 1965 .

ABSTRACT

An experimental study of the development of air velocity profiles in a vertical 6.255 inside diameter aluminum tube with a diverging conical entrance was undertaken. Fully developed velocity profiles were obtained with a total head pitot tube for Reynolds numbers ranging from 9000 to 56000. The development of the center-line velocity along the tube axis was measured with a travelling carriage.

Various means for correlating velocity profiles were investigated, from the simple power law, universal velocity distribution, Gill and Scher's improved correlation (based on a modified mixing length theory) to the correlation derived by Pai. The different relations which have been derived for the region near the wall were analyzed and compared.

The experimental results correlated very well with an equation of the form suggested by Bogue, a modified universal velocity distribution which takes into account deviations from the universal velocity distribution with radial position. However, no significant effect of Reynolds number could be observed over the limited range investigated. The equation derived by Pai also correlated the data very well and since it has the advantage of being valid from the center-line to the wall, it would seem to be the most advantageous correlation over the range of Reynolds numbers investigated.

The center-line velocity was found to reach its maximum, and constant value, at 40 diameters downstream from the entrance. The hydrodynamic starting length was found to increase with increasing Reynolds number.

ACKNOWLEDGEMENT

The author wishes to express his sincere thanks to Dr. I.G. Dalla Lana for his guidance, encouragement and helpful criticism during the course of this project.

The financial assistance of the National Research Council of Canada is gratefully acknowledged.

TABLE OF CONTENTS

	<u>Page No.</u>
LIST OF TABLES	
LIST OF FIGURES	
I. INTRODUCTION	1
II. THEORY	
1. The Correlation of Experimental Velocity Profiles in Circular Ducts	4
2. The Development of Velocity Profiles in the Entrance Section of Circular Ducts	20
III. EXPERIMENTAL PROGRAM	
1. Equipment and its Operation	24
2. Experimental Procedures	39
IV. EXPERIMENTAL RESULTS AND DISCUSSION	
1. Fully Developed Flow	49
2. The Entrance Section	61
V. CONCLUSIONS	80
NOMENCLATURE	83
BIBLIOGRAPHY	85
APPENDIX A - EXPERIMENTAL AND CALCULATED DATA	87
APPENDIX B - AN ERROR ANALYSIS	145
APPENDIX C - OPERATION AND MAINTENANCE OF AIR SUPPLY UNIT	152

LIST OF TABLES

<u>Table</u>		<u>Page No.</u>
1	Entrance Velocity Profiles - Old Vanes	92
2	Entrance Velocity Profiles - New Vanes	93
3	Calibration of Orifice	94
4	Friction Factor	94
5 - 6	Traverse at Right Angle	95
7 - 14	Fully Developed Velocity Profile	97
15 - 18	Power Law Distribution	106
19	Power Law Exponent - Velocity Ratio	110
20 - 23	Semilogarithmic Velocity Distribution	112
24 - 27	Universal Velocity Distribution	118
28	Velocity Distribution Close to the Wall	124
29 - 32	Velocity Distribution of Gill and Scher	128
33 - 36	Velocity Distribution of Pai	134
37	Entrance Velocity Profiles	138
38 - 41	Center-Line Velocity	139
42 - 43	Center-Line Velocity, Using Wall Taps	143

LIST OF FIGURES

<u>Figure</u>		<u>Page No.</u>
1	Schematic Equipment Diagram	31
2	Entrance Velocity Profiles	32
3	Inlet Arrangement with Vanes Inside Tee	33
4	Connection from Entrance Cone to 6.255 inch Tube	34
5	Entrance Section	35
6	Pitot Tube	36
7	Wall Tap	36
8	Static Pressure Probe	36
9	Carriage	37
10	Schematic Carriage Arrangement	38
11	Calibration of Orifice	45
12	Traverses of 90° to One Another	46
13	Center-Line Velocity Using Carriage Static Pressure Probe and Wall Taps	47
14	Plot of Friction Factor Versus Reynolds Number for 6.255-inch Aluminum Tube	48
15	Fully Developed Velocity Profiles	66
16	Ratio of Average to Maximum Fluid Velocity	67
17	Power Law Exponent	68
18	Velocity Distribution, Power Law	69
19	Velocity Deficiency Law	70
20	Universal Velocity Distributions	71
21	Empirical Correction Function for $u^+ - y^+$ Correlation	72

<u>Figure</u>		<u>Page No.</u>
22	Corrected Universal Velocity Distribution	73
23	Velocity Distributions Based on a Modified Mixing Length	74
24	Velocity Distribution	75
25	Entrance Velocity Profiles	76
26	Dimensionless Velocity Profiles	77
27	Semilogarithmic Representation of Point Velocities Measured Near to the Entrance	78
28	Center-Line Velocity Versus Distance from the Entrance	79

I. INTRODUCTION

Experimental studies on the development of velocity profiles for air flowing upwards in a vertical tube with a diverging conical entrance were carried out by Bowers(1) and Sandall(2) in the Department of Chemical and Petroleum Engineering at the University of Alberta. Their studies encompassed air flows ranging in Reynolds numbers from roughly 1000 to 30,000. However, both of these earlier workers were, to some extent, limited in the scope and generality of their measurements.

The bulk of the difficulties which they encountered originated with an air supply subject to excessive ambient temperature and pressure changes, and from the lack of a suitable means of calibrating their hot wire anemometer at low velocities. To minimize these difficulties, the following changes have been made to the experimental equipment:

1. an air compressor of higher compression and volumetric capacity, Re up to 55,000 in the test section, has been installed;

2. with an after-cooler the air supply temperature could be controlled within $\pm 1^{\circ}\text{F}$;

3. further changes in the vertical tube entrance geometry were necessary to assure radial symmetry of the developing velocity profiles;

4. calibration of secondary velocity-measuring devices was eliminated by using a pitot total head tube of very small diameter for all air velocity measurements (Re from 9,000 to 55,000);

5. a travelling probe which measured center-line velocity was used to indicate the velocity profile development along the tube axis.

Using the improved experimental equipment, the following objectives were undertaken in this study:

1. to determine the velocity profiles for various values of Reynolds numbers corresponding to experimentally verified fully developed turbulent flows;

2. to define the distances along the tube axis in which fully developed flows would be encountered;

3. to review and test various published velocity correlations for their suitability in correlating the measured fully developed profiles;

4. to examine the axial development of the velocity profile in the entrance region using constancy of the center-line velocity as the criterion rather than constancy of the wall shear stress.

The problem of correlating experimentally measured velocity profiles in generalized mathematical terms has been and continues to remain the subject of considerable discussion. A truly universal function which relates local mean velocity

to radial position is not available hence the worker in this area, faced with the need for a velocity profile relationship, is restricted to using, in direct or modified form, the various relationships which have been proposed. The following section discusses ways of correlating velocity profiles in tubes with special reference to the flow of Newtonian fluids such as air.

II. THEORY

1. The Correlation of Experimental Velocity Profiles in Circular Ducts

In the case of laminar flow, theoretical relationships to predict velocity profiles have been derived. Turbulent flow cannot be analyzed satisfactorily from a theoretical standpoint and so, only empirical or semi-empirical relationships to predict velocity profiles in fully developed turbulent flow have been obtained. The condition of fully developed flow is referred to as the condition where the velocity profile, and in particular the center-line velocity, has reached its "constant" value. The various approaches to correlate mean point velocity in turbulent flow are discussed in four sections as follows:

- a. Power Law Distributions
- b. Logarithmic Distributions Including the Universal Velocity Distribution
- c. Improved Universal Velocity Distributions Near the Wall
- d. Other Distributions in the Turbulent Core

a. Power Law Distributions

The power law of velocity distribution for turbulent flow in circular ducts represents a simple way of analyzing data. Using a power function with a single term, the power

law is given by

$$\frac{u}{u_m} = \left(\frac{y}{R}\right)^{\frac{1}{n}} \quad (1)$$

This form was tested by Nikuradse(6) and was found to correlate his experimental data well, however, the exponent n varied from 6 at a Reynolds number of 4000 to 10 at a Reynolds number of 3,240,000.

It is interesting to note that equation (1) can be derived from the Blasius friction-factor equation which relates the friction factor to the Reynolds number in the following way

$$f = C (Re)^{-1/4} \quad (2)$$

Using this approach, Prandtl(3) obtained

$$\frac{u}{u_m} = C' \left(\frac{y}{R}\right)^{\frac{1}{7}} \quad (3)$$

which is only valid for Reynolds number up to 100,000 for which the Blasius friction-factor equation is applicable.

With a reliable functional relationship between the exponent n and the Reynolds number the power law would represent a useful and simple way of correlating velocity data.

b. Logarithmic Distributions Including the Universal Velocity Distribution

Several velocity distribution equations have been derived(3) in the form of semi-logarithmic functions. One

of the earliest approaches was that of Prandtl. Using his mixing length theory, he defined the total shear stress by the sum of the viscous and the turbulent shear stresses as follows:

$$\tau = \tau_L + \tau_T = \frac{\mu}{g_c} \frac{du}{dy} + \frac{\rho}{g_c} \left(l \frac{du}{dy} \right)^2 \quad (4)$$

Neglecting viscous shear, and assuming the shear stress to be constant and equal to the shear stress at the wall, Prandtl obtained

$$\tau = \tau_w = \frac{\rho}{g_c} \left(l \frac{du}{dy} \right)^2 \quad (5)$$

By introducing the friction velocity, $u^* = \left(\tau_w \frac{g_c}{\rho} \right)^{1/2}$, equation (5) can be simplified to

$$u^* = l \frac{du}{dy} \quad (6)$$

If the mixing length, l , is assumed to be a linear function of y , equation (6) may be integrated, yielding

$$u = \frac{u^*}{K} \ln y + C \quad (7)$$

Prandtl employed the boundary condition, $u = u_m$, for $y = R$ and obtained

$$u = u_m + k u^* \ln \frac{y}{R} \quad (8)$$

In spite of the number of drastic assumptions which were incorporated, its

predictions(3) compare well with the experimental data.

von Karman(3) showed that for flow at a distance from the wall, the shear stress is given by

$$\tau = \frac{\rho K^2 \left(\frac{du}{dy}\right)^4}{g_c \left(\frac{d^2u}{dy^2}\right)^2} \quad (9)$$

Introducing Prandtl's mixing length theory, and rearranging, gives

$$l = K \frac{\frac{du}{dy}}{\frac{d^2u}{dy^2}} \quad (10)$$

By using the linear shear stress distribution, $\tau = (1 - \frac{y}{R}) \tau_w$,

in equation (9) and rearranging, the following differential equation was obtained.

$$\frac{d^2u}{dy^2} = \sqrt{\frac{\rho}{g_c \tau_w}} \frac{1}{\sqrt{1 - \frac{y}{R}}} K \left(\frac{du}{dy}\right)^2 \quad (11)$$

After integrating equation (11) twice, and applying the boundary conditions,

$$\frac{du}{dy} = \infty, \quad \text{for } y = 0$$

and

$$u = u_m, \quad \text{for } y = R,$$

von Karman obtained,

$$u = u_m + \frac{1}{K} u^* \left[\ln \left(1 - \sqrt{1 - \frac{y}{R}} \right) + \sqrt{1 - \frac{y}{R}} \right] \quad (12)$$

The constant, K , appearing in the equations of both Prandtl and von Karman, is considered to be a universal constant and its value has been experimentally determined at small distances from the wall(6).

Wang(3), using a similar approach involving an expression for the mixing length based on an actual velocity distribution, obtained

$$u = u_m + \frac{u^*}{K} f(y, R) \quad (13)$$

where

$$f(y, R) = \ln \frac{1 + \sqrt{1 - \frac{y}{R}}}{1 - \sqrt{1 - \frac{y}{R}}} - 2 \tan^{-1} \sqrt{1 - \frac{y}{R}} \\ - 0.572 \ln \frac{1 - \frac{y}{R} + 1.75 \sqrt{1 - \frac{y}{R}} + 1.53}{1 - \frac{y}{R} - 1.75 \sqrt{1 - \frac{y}{R}} + 1.53} \\ + 1.14 \tan^{-1} \frac{1.75 \sqrt{1 - \frac{y}{R}}}{1.53 - (1 - \frac{y}{R})} \quad (14)$$

Equation (13) supposedly agrees better with experimental data, however, the second term, $f(y, R)$, is very complex and inconvenient to use.

A limited comparison of the three logarithmic velocity distribution equations (8), (12) and (13) is presented by Knudsen and Katz(3). The few data which were plotted indicate good agreement with equation (8) at low Reynolds number and very good agreement with equation (13) at high Reynolds number. It is important to note that all three equations become invalid when y approaches zero.

A more general correlation, the so-called universal velocity distribution, employs the following dimensionless quantities,

$$u^+ = \frac{u}{u^*} = \frac{u}{\sqrt{\frac{g_c \tau_w}{\rho}}} \quad (15)$$

$$y^+ = y \frac{u^*}{\nu} = \frac{y}{\nu} \sqrt{\frac{g_c \tau_w}{\rho}} \quad (16)$$

Differentiating u^+ with respect to y^+ yields:

$$\frac{du}{dy} = u^* \frac{du^+}{dy} = \frac{g_c \tau_w}{\nu \rho} \frac{du^+}{dy^+} \quad (17)$$

$$\frac{d^2 u}{dy^2} = \frac{u^*^2}{\nu} \frac{d^2 u^+}{dy^+ dy} = \frac{g_c \tau_w}{\nu^2 \rho} \sqrt{\frac{g_c \tau_w}{\rho}} \frac{d^2 u^+}{dy^+^2} \quad (18)$$

Combining equations (17) and (18) with equation (9), in which viscous shear has been neglected, and integrating the resulting second order differential equation yields

$$\frac{dy^+}{du^+} = Ky^+ + C \quad (19)$$

Near the wall, the velocity gradient is very large and hence

$\frac{dy^+}{du^+}$ becomes very small, giving $C = 0$ for $y^+ = 0$. Integrating

a second time gives

$$u^+ = \frac{1}{K} \ln y^+ + C' \quad (20)$$

which is called the universal velocity distribution equation for turbulent flow. The constant of integration, C' , must be determined experimentally.

Equation (20) is only valid at a distance from the wall, hence, near the wall where the variation in shear stress can be neglected, a laminar sublayer is assumed to exist. In this region, where viscous shear is important, Newton's law of viscosity predicts

$$-g_c \tau_w = \mu \frac{du}{dy} = \rho u^*^2 \frac{du^+}{dy^+},$$

$$du^+ = dy^+$$

and thus, $u^+ = y^+ + C$. Since $u^+ = 0$ for $y^+ = 0$, the integration constant, C , vanishes, giving

$$u^+ = y^+ \quad (21)$$

Using the experimental results of Nikuradse(3), equation (20) was found to be valid for $y^+ > 30$. The limited data available for the regions near to the wall suggest that equation (21) might be applicable for $y^+ < 5$. In the region between this laminar sublayer and the turbulent core, the velocity distribution has been represented by an empirical equation of the form of equation (20).

The universal velocity distribution in a pipe can be represented by the following three equations(3),

$$u^+ = y^+ \quad y^+ < 5 \quad (21)$$

$$u^+ = 5.0 \ln y^+ - 3.05, \quad 5 < y^+ < 30 \quad (22)$$

$$u^+ = 2.5 \ln y^+ + 5.5, \quad 30 < y^+ \quad (23)$$

The constants as well as the applicable range were obtained using the experimental results of Nikuradse.

This set of equations, (21) to (23), is often used to predict the complete velocity profiles for fully developed turbulent flows in pipes or tubes.

In a more recent work by Deissler(7), slightly different constants were obtained. For air flows corresponding to Reynolds number of 8,000 to 220,000, Deissler obtained in the turbulent core, $y^+ > 26$,

$$u^+ = 2.78 \ln y^+ + 3.8 \quad (24)$$

However, it should be noted that Nikuradse's data cover a much wider range of Reynolds numbers, from 4,000 to 3,240,000.

Although the set of universal velocity distributions, equations (21), (22), (23) may be inconsistent with the physical situation, this approach yields a surprisingly good correlation of experimental data.

There is strong evidence(6) that the flow becomes laminar very close to the wall and that a separate turbulent central core exists. However, a gradual change from the one to the other would be anticipated. Therefore, the concept of three distinct zones would appear to be incorrect. The derived equation (20) also does not predict a zero velocity gradient at the center of the pipe. Finally, consistent deviations of the experimental results from equation (20) suggests that u^+ and y^+ cannot be the only dimensionless groups belonging in the universal relationship.

c. Improved Universal Velocity Distributions Near the Wall

In the region near to the wall, other correlations which appear to be equally satisfactory have been developed. Deissler(7) derived an equation for flow in the vicinity of the wall in which the effects of the magnitudes of u and y upon the turbulent shear have been taken into account.

The total shear stress defined as the sum of the viscous and the turbulent shear stresses is given by

$$\tau = \frac{\mu}{g_c} \frac{du}{dy} + \frac{\rho}{g_c} \epsilon \frac{du}{dy} \quad (25)$$

As an approximation, the following functional relation for ϵ , the coefficient of eddy diffusivity, was assumed:

$$\epsilon = f(u, y) \quad (26)$$

From dimensional analysis Deissler obtained

$$\epsilon = n^2 u y \quad (27)$$

where n is a constant of proportionality.

Equation (25) becomes

$$\tau = \left(\frac{\rho}{g_c} + \frac{\rho}{g_c} n^2 u y \right) \frac{du}{dy} \quad (28)$$

The dimensionless quantities, as defined by equations (15) to (17), substituted in equation (28), with shear stress approximated over the entire sublayer by the wall shear stress, τ_w , gives the following identity

$$1 = (1 + n^2 u^+ y^+) \frac{du^+}{dy^+} \quad (29)$$

Upon separating variables and integrating from the lower boundary condition, $u^+ = 0$, when $y^+ = 0$, Deissler obtained the solution,

$$y^+ = e^{\frac{(nu^+)^2}{2}} \int_0^{u^+} e^{-\frac{(nu^+)^2}{2}} du^+ \quad (30)$$

Equation (30) can be expressed in terms of the normal error function of nu^+ and the integral of the normal error function (both available in mathematical tables) to give

- 14 -

$$y^+ = \frac{1}{n} \frac{\int_0^{nu^+} e^{-\frac{(nu^+)^2}{2}} d(nu^+)}{\frac{1}{\sqrt{2\pi}} e^{-\frac{(nu^+)^2}{2}}} \quad (31)$$

Equation (31) has been found to fit the experimental data in the region, $y^+ < 26$.

Wasan et al(12) derived an equation for flow in the vicinity of a pipe wall based upon the equations of continuity and motion. The mean and fluctuating velocity components were expanded separately in Taylor series as functions of radial position and the equation of motion was integrated. It was shown that the velocity distribution function, in dimensionless form, can be expressed as

$$u^+ = y^+ + U_4^+ (y^+)^4 + U_5^+ (y^+)^5 \quad (32)$$

When the shear stress is assumed constant as Deissler did in deriving equation (31), it was found that U_4^+ and U_5^+ are universal constants. To determine the constants and the value of y^+ at which a smooth and continuous transition to the logarithmic distribution occurs, the values of u^+ and the first and second derivative of u^+ with respect to y^+ , obtained from equation (32), are matched with corresponding values obtained from equation (23). The transition was found to occur at $y^+ = 20$ and the velocity distribution for $y^+ < 20$ is as follows

$$u^+ = y^+ - 1.04 \cdot 10^{-4} (y^+)^4 + 3.03 \cdot 10^{-6} (y^+)^5 \quad (33)$$

Both equation (31) and (33) approach $u^+ = y^+$ for $y^+ < 5$ and so, they satisfy the condition of laminar flow close to the wall. Equation (33) was obtained matching equation (32) and (23) at $y^+ = 20$. In this region equation (23) is not valid and it can be expected that u^+ obtained from equation (33) will be too high.

d. Other Distributions in the Turbulent Core

To obtain equation (22), a constant shear stress was assumed across the pipe. Using the approach of von Karman, an alternative equation of the form of equation (12) was derived by Deissler(7).

$$u^+ = \frac{1}{K} \left[\ln \left(1 - \sqrt{1 - \frac{y^+}{R^+}} \right) + \sqrt{1 - \frac{y^+}{R^+}} + \frac{u_m}{u^*} \right] \quad (34)$$

Since equation (34) is expressed in terms of the maximum velocity, u_m , it is no longer a universal correlation. Furthermore, it can be seen that equations (12) and (34) essentially are identical.

Rothfus et al(8,9) from an examination of the available published data found that the relationship between u^+ and y^+ is dependent on the Reynolds number. Using this concept, they proposed a modification of the relationship between u^+ and y^+ which would result in a unique correlation of the steady component of the velocity. By examining u^+ , y^+

data, the necessary correction was made by multiplying one or both of the coordinates by a factor which would be unity at high Reynolds numbers and which would progressively depart from unity when the Reynolds number is decreased. This correction, the ratio of the bulk velocity to the maximum velocity, was applied and it was found that the modified coordinates,

$u^+ \frac{u_{av}}{u_m}$ and $y^+ \frac{u_m}{u_{av}}$, are represented by a single line over

the entire turbulent range tested, $3000 < Re < 3,240,000$.

However, in the vicinity of the wall further experimental work was reported to be necessary. Discrepancies can be expected in the laminar sublayer in particular if a true laminar sublayer exists.

The semi-logarithmic universal correlation given by equation (20) was extensively tested by Bogue and Metzner(10). They found that the data showed small but consistent deviations from the correlation. The deviations are primarily a function of radial position and to a lesser extent, of the friction factor (or more generally speaking, of the Reynolds number). A correlation of the following form was used,

$$u^+ - c(y, f) = 2.42 \ln y^+ + 5.57 \quad (35)$$

The correction term, $c(y, f)$ was determined by experiment and is given by the equation

$$c(y, f) = 0.05 \sqrt{\frac{8}{f}} \exp \left(\frac{-\left(\frac{y}{R} - 0.8\right)^2}{0.15} \right) \quad (35)$$

in which f = Fanning friction factor. Similar correlations have been suggested by Millikan(11), Reichardt(11) and Hinze(5), however, their correction terms only took into account the deviation as a function of radial position, and assumed no functional relationship with Reynolds number. The different correction functions are compared graphically by Bogue(11). Based on the data of Laufer and Nikuradse, significant improvements in the correlation using equation (35) were reported.

Gill and Scher(16) derived a velocity distribution based upon a modification of the Prandtl mixing length expression. Instead of assuming that $l = Ky$, the following mixing length expression was assumed,

$$l = Ky \left(1 - e^{-\phi \frac{y}{R}} \right) \quad (37)$$

where,

$$\phi = \frac{\frac{y_m^+}{22} - 60}{22} \quad (38)$$

Expression (37) purports to take into account the wall dampening effect upon the mixing length. For the case, y approaching R , equation (37) reduces to $l = Ky$.

Starting from equation (4), applying a linear variation of shear stress with position, and then using equation (37) for the mixing length, Gill and Scher showed that

$$u^+ = \int_0^{y^+} \frac{-l + \sqrt{l^2 + 4cd}}{2c} dy^+ \quad (39)$$

where,

$$c = K^2 y^+^2 (1 - e^{-\phi} \frac{y^+}{R^+})^2 \quad (40)$$

and

$$d = 1 - \frac{y^+}{R^+} \quad (41)$$

Equation (39) describes the velocity distribution from the wall to the center of the duct. A zero velocity gradient is obtained at the center of the tube and the Reynolds number effect upon the velocity distribution has been taken into account. Equation (39) still does not represent a true universal relationship in terms of the dimensionless groups, u^+ and y^+ , and graphically, the velocity distribution must be represented by a different curve for each value of the Reynolds number. Equation (39) has not been tested extensively for pipeflow, but it offers the great advantage of being valid from the wall to the center line.

Pai(13) developed a correlation for turbulent flow between parallel plates that is valid over the entire distance between the plates. It has subsequently been shown by Brodkey et al(14,15) that the correlation could be extended to flows in smooth tubes, to Newtonian as well as non-Newtonian fluids, and it would still be valid over the entire cross-section. For the flow of Newtonian fluids in a tube, the velocity distribution is represented by a three-term power series of the form

$$\frac{u}{u_m} = 1 + a_1 \left(\frac{r}{R}\right)^2 + a_2 \left(\frac{r}{R}\right)^{2M} \quad (42)$$

Integration of equation (42) yields an expression for the ratio of average to maximum velocity

$$\frac{u_{av}}{u_m} = 1 + \frac{1}{2} a_1 + \frac{1}{1+M} a_2 \quad (43)$$

In equation (42) and (43)

$$a_1 = \frac{S - M}{M - 1} \quad (44a)$$

$$a_2 = \frac{1 - S}{M - 1} \quad (44b)$$

By definition

$$S = \frac{\frac{Y_m^+}{2u_m^+}}{\frac{f}{64} Re} \quad (45)$$

With the aid of the following relation

$$y_m^+ = \sqrt{\frac{f}{64} Re} \quad (46)$$

S was computed in terms of Reynolds number,

$$S = 0.585 + 3.172(10^{-3}) Re^{0.833} \quad (47)$$

Equation (47) was found to be valid for $Re > 2,800$. The variable M was obtained from equation (43), by trial and error solution, and correlated in terms of Reynolds number

$$M = -0.617 + 8.211(10^{-3}) Re^{0.786} \quad (48)$$

Equation (48) was found to be valid for all Reynolds numbers.

The agreement with experimental data was evidently good but certain discrepancies at high Reynolds numbers, $Re > 100,000$ were reported.

2. The Development of Velocity Profiles in the Entrance Section of a Circular Duct

For laminar flow, relationships to predict entrance lengths and velocity profiles in the entrance section have been developed(3). These relationships agree well with experimental data. For turbulent flow, however, no reliable relationship is known. The entrance length could basically be defined in two ways: Most commonly, it is defined as the distance required for the complete velocity profile to reach its final value; or it could be taken as the distance required for the pressure gradient along the pipe to become uniform. In the present report, the first definition is applied unless otherwise stated.

Latzko(18) derived a relationship, based on a rounded entrance with an initially flat profile, to predict the entrance length as well as velocity profiles in the developing section for turbulent flow. However, the results were not satisfactory, with the predicted entrance lengths being 5 times shorter than what had been experimentally obtained(18). Using a rounded entrance, Nikuradse(4) obtained, for Reynolds numbers ranging from 4000 to 3,000,000, fully

developed flow at 25 to 40 diameters from the entrance. Deissler(7), also working with a rounded entrance, obtained fully developed flow at a location between 46 and 100 diameters for a Reynolds number of 46,000. Kirsten(18), working in the range of Reynolds numbers from 20,000 to 100,000, reported an entrance length of 40 diameters for a smooth entrance and 50 diameters for a sharp-edged entrance. Furthermore, he found that the entrance length decreased for a smooth entrance and increased for a sharp-edged entrance with increasing Reynolds number. However, Kirsten correlated u_{av}/u versus Reynolds number and found considerable scatter in his results, presumably from the error associated with obtaining the average velocity. Kirsten also compared velocity profiles in the entrance section with the Power Law Distribution. For a rounded entrance, the initial profiles were laminar, with an exponent close to 1, while with a sharp-edged entrance, the initial profiles had an exponent higher than that of fully developed flow. It should be noted that Kirsten obtained his flow by using an exhaust fan at the discharge end and thus had an entering stream of low turbulence level.

Deissler found, in contradiction to Kirsten, that the development of the velocity distribution was more rapid for the sharp-edged entrance than for the rounded entrance. With the sharp-edged entrance, fully developed flow was obtained after roughly 45 diameters and with the rounded entrance,

it was reported that the distribution was still developing at 100 diameters from the entrance. The difference between the entrance lengths experienced by Kirsten and Deissler, both working with rounded entrances, indicate a strong effect of the turbulence level in the entering stream upon the entrance length. Based upon the scarce experimental results mentioned, it seems apparent that there are at least three conditions that will determine the entrance length for turbulent flow in a smooth pipe:

1. entrance configuration
2. previous history of the entering stream or the turbulence level
3. Reynolds number based on the cross-section of the pipe.

The distance required for the local pressure gradient along the pipe to become steady is considerably less than that required for the development of the complete velocity profile. Pascucci(17) found that the development of the friction factor or shear stress is completed at

$$\frac{L}{D} = 3.80 \log_{10} Re - 2.14 \quad (49)$$

Latzko predicted(3)

$$\frac{L}{D} = 0.623 Re^{1/4} \quad (50)$$

For a Reynolds number of 50,000, equations (49) and (50) give an entrance length of 15.7 and 9.3 diameters, respectively, indicating that the pressure gradient, and thus the velocity profile adjacent to the wall, becomes established long before the velocity profile in the core. The latter was mentioned earlier in this report to be established at 40 to 100 diameters.

III. EXPERIMENTAL PROGRAM

The equipment used in this work has been described(1,2). However, a considerable number of improvements and additions were incorporated. These modifications were listed briefly in the Introduction section and the present physical setup is shown schematically in Figure 1. A further description of the equipment and its operation follows in the Equipment portion of this section.

Basically, this equipment provided a means of regulating the flow rate and the temperature of air with mean flows ranging from Reynolds numbers of 9,000 to 55,000 (based upon flow in the test section). Fixed locations along the pipe axis are available for measuring velocity profiles. The development of the velocity profiles, a matter of some importance in this work, was studied by means of a moving carriage placed within the tube. The experimental test program is described immediately following the equipment section.

1. Equipment and Its Operation

a. The Test Section

Air flows were studied within a vertically mounted aluminum tube 28.5 feet long, 6.255 inches in average inside diameter, and 0.203 inches in wall thickness. The tube was tapped at five fixed locations for velocity profile measurements as shown in Figure 1. The entrance and exit cones

diverged and converged, respectively, from a one inch diameter entrance to the 6.255 inch tube diameter and then to a two inch diameter exit.

Although the profiles measured at 41.5 pipe diameters down stream from the entrance were found to be symmetrical, considerable difficulty was experienced in designing an entrance section which produced symmetrical profiles at the tube inlet. To eliminate the distortion of the profile which results from the right angle tee immediately preceding the inlet cone, corner vanes were designed and installed(21, 22). These vanes partially remedied the flow distortion and reduced the pressure drop associated with the turn but, as can be seen in Figure 2, they were not completely successful. The final arrangement of vanes consisted of blades made from one quarter cross sections of 1.625 inch O.D. copper tubing, with a wall thickness of 0.04 inches. Five blades were used and they were spaced so that the distance between them increased in arithmetic progression, starting at the upper corner as shown in Figure 3.

To solve the problem of obtaining symmetrical flow at the tube inlet, the one-inch diameter pipe between the tee and the entrance cone was increased to 40 pipe diameters length. At this length, within the one-inch tube the flow of its own accord could be expected to become fully developed, and thus to produce a symmetrical velocity profile.

At the same time, it was found desirable to perfect

the connection from the entrance cone to the six-inch tube. This new connection is shown in Figure 4.

The final form of the entrance section, shown in Figure 5, gave symmetrical velocity profiles at all points along the axis of the aluminum tube as verified by the experimental data.

b. The Air Supply

Air was supplied by a Gardner-Denver Model 3CDL-5 Cyclo blower, a rotary lobe type of axial flow blower producing a continuous pulsation-free discharge. The blower was direct driven by a 20 hp, 3600 rpm induction motor, which had a maximum capacity of 240 SCFM at 12 psig. The compression chamber was so designed that lubrication was unnecessary, thus guaranteeing an oil-free air supply. The operation and maintenance of this unit is described in the Appendix section.

The blower intake was protected by an air filter. A relief valve was installed in the discharge line to prevent possible over pressure. One check valve was installed to protect the filter and another to prevent back-flow of bulk material into the blower at shutdown.

Because of the blower air discharge temperatures, between 200 and 300°F, an aftercooler was required. The final air temperatures were measured with an iron constantan thermocouple connected to a Brown single-point temperature recorder. By suitable manual control of the cooling water flow

rate, the aftercooler not only cooled the air but also maintained it at a constant reference temperature for all experimental runs.

The temperature recorder was checked with a calibrated mercury thermometer. At operating temperatures, the deviation was less than 0.3°F , and at steam and freezing point slightly less than 1°F . Due to the fact that the cooling water had to be controlled manually, the air temperature could only be guaranteed within $\pm 1^{\circ}\text{F}$. A startup period of about one hour was required to obtain a constant air temperature.

A moisture separator was installed downstream from the aftercooler to eliminate entrained water.

The air flow-rate was controlled by an orifice flow-meter of diameter of 1.544 inches, which gave sufficient control over the entire flow range. Two u-tube manometers were connected across the orifice, one with water as the manometer fluid for low pressure differentials and the other with mercury for higher differentials. Both manometers could be used for measurement of pressure differentials across the orifice or for gage pressure on the upstream side of the orifice.

The flow rate was set manually by means of a pneumatically operated 1-1/4 inch parabolic needle valve, Foxboro type F-8, located in the 2-inch recycle line. To obtain very low flow rates, it was necessary to open the globe valve in the bleed-off line.

In measuring air flow with the orifice meter, the geometry of the 2-1/2 inch air line from the blower to the entrance cone precluded having an adequate straight run upstream from the orifice. To eliminate the problem of a fluctuating orifice differential pressure which resulted, straightening vanes were designed and installed 48 inches upstream according to American Gas Association specifications(23). The fluctuations were thus reduced to negligible values for all flow rates encountered.

c. The Velocity Profile Probe Mount

A probe mount arrangement was available(1) to permit the positioning of probes along the tube diameter at right angles to the axis of the tube. The position of the probe could be read from a vernier scale with 0.01 inch subdivisions. At some of the probe locations, the orientation of the probe stem travel could be varied by 90 degrees. This allowed the measurement of two velocity profiles at right angles to each other.

Because a total-head pitot tube was employed to measure mean point velocity, the absolute pressure at the probe location and the difference between total pressure and static pressure at the same location were required. The pitot tube consisted of a 23-gauge hypodermic needle as shown in Figure 6. The static pressure was measured at the wall of the tube. A very fine hole, 0.031 inch diameter, was drilled

in a brass plug that had been machined to fit with the inner surface of the tube. This tap arrangement is shown in Figure 7. The static gauge pressure was read on a u-tube manometer using water as the manometer fluid. Pressure differentials were measured with a Flow Corporation Model MM3 Micromanometer. The micromanometer consisted of a u-tube type manometer operating on a nulling principle. It measured a maximum pressure difference of two inches of manometer fluid with a resolution of ± 0.0001 inch and an accuracy of ± 0.0002 inch of manometer fluid. In the present work, the manometer fluid employed was n-Butyl alcohol with a specific gravity of 0.8166 at 75°F.

The zero setting changed somewhat with time, and it was found necessary to measure and record the zero setting between each pressure differential measured and use the average value.

The barometric pressure was obtained with a standard barometer and was corrected for variations in the ambient temperature, an estimated accuracy of ± 0.2 mm Hg was obtained.

d. The Center-Line Velocity Travelling Carriage

A carriage arrangement with pitot tube and static pressure probe was designed to obtain measurements of the center-line velocity at any axial point along the entrance section of the aluminum tube. The carriage, as shown in Figure 9, consisted of a short piece of 7/8 inch pipe with six arms, mounted three on each end, to secure the central

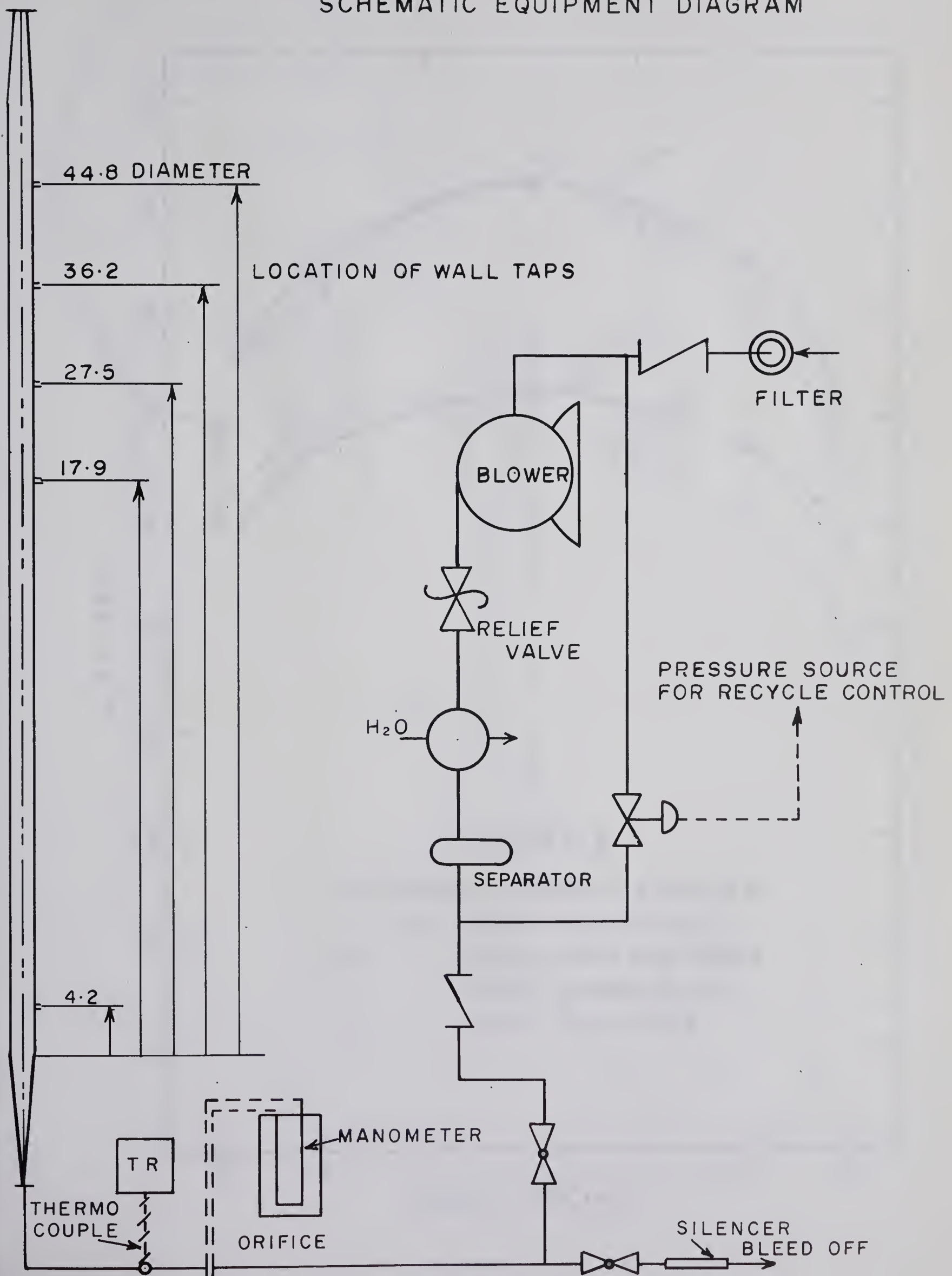
positioning of the carriage. The tip of each arm was fitted with a small teflon bearing surface to protect the surface of the test pipe and to make the carriage easier to move. To obtain the total head at the center-line of the tube, a hypodermic needle was mounted on the front end of the 7/8 inch pipe at the center of the carriage. A static pressure needle was mounted on one of the arms, one-third tube radius distant from the tube wall.

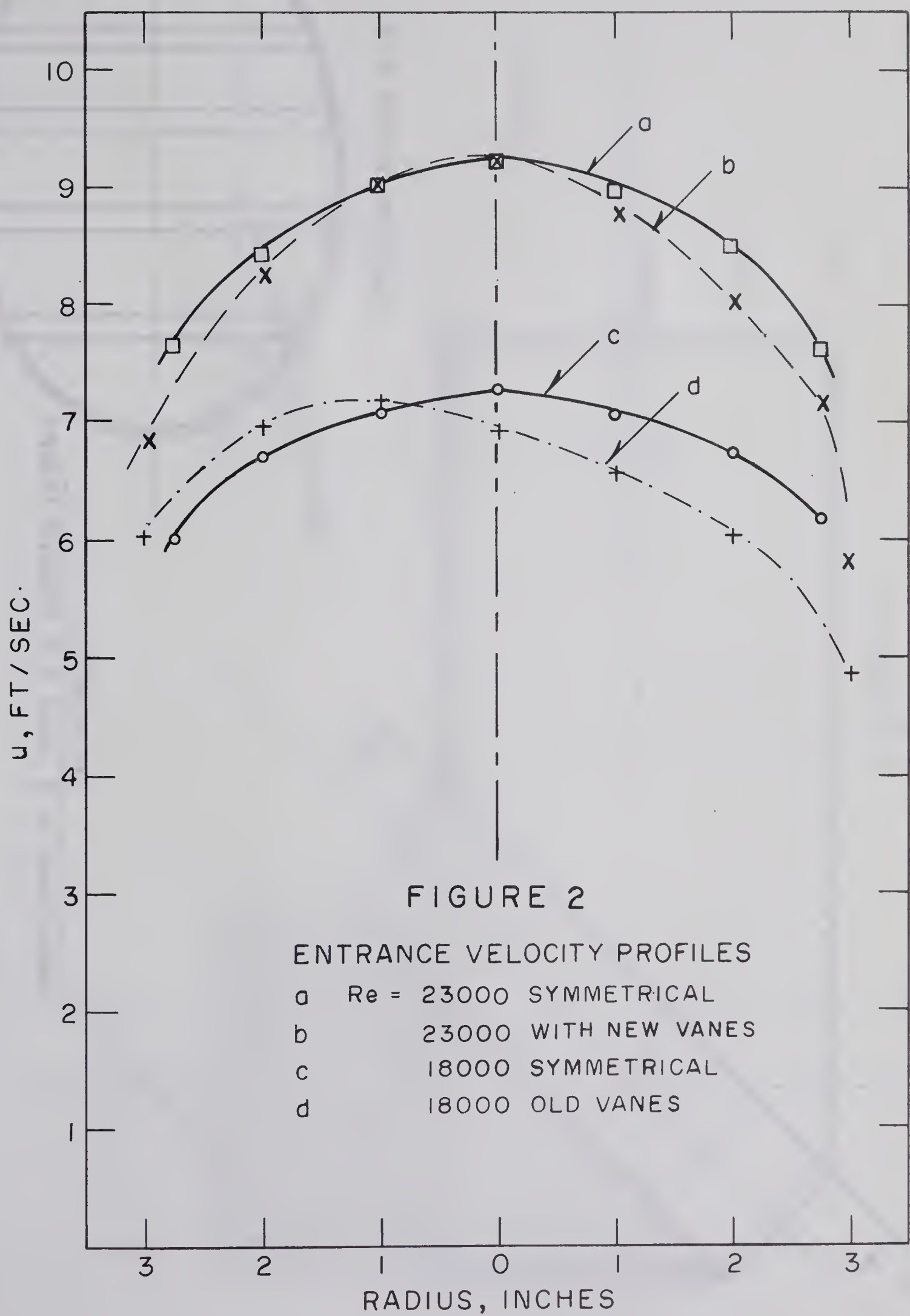
The carriage could be positioned along the tube axis by a steel cable connected to the carriage and which extended up and out of the tube through the upper cone. The leads from the total head and the static pressure probes consisted of 0.1 inch O.D. polyethylene tubing taped to the steel cable to ensure rigidity. The arrangement is shown in Figure 10.

e. The Measurement of Pressure Drop Along the Tube

Pressure drops along the tube were measured with two wall static pressure taps of the type shown in Figure 7. Positioned a known distance apart, the taps provided a means for obtaining pressure drop data between any two of the fixed probe mount locations.

FIGURE 1
SCHEMATIC EQUIPMENT DIAGRAM





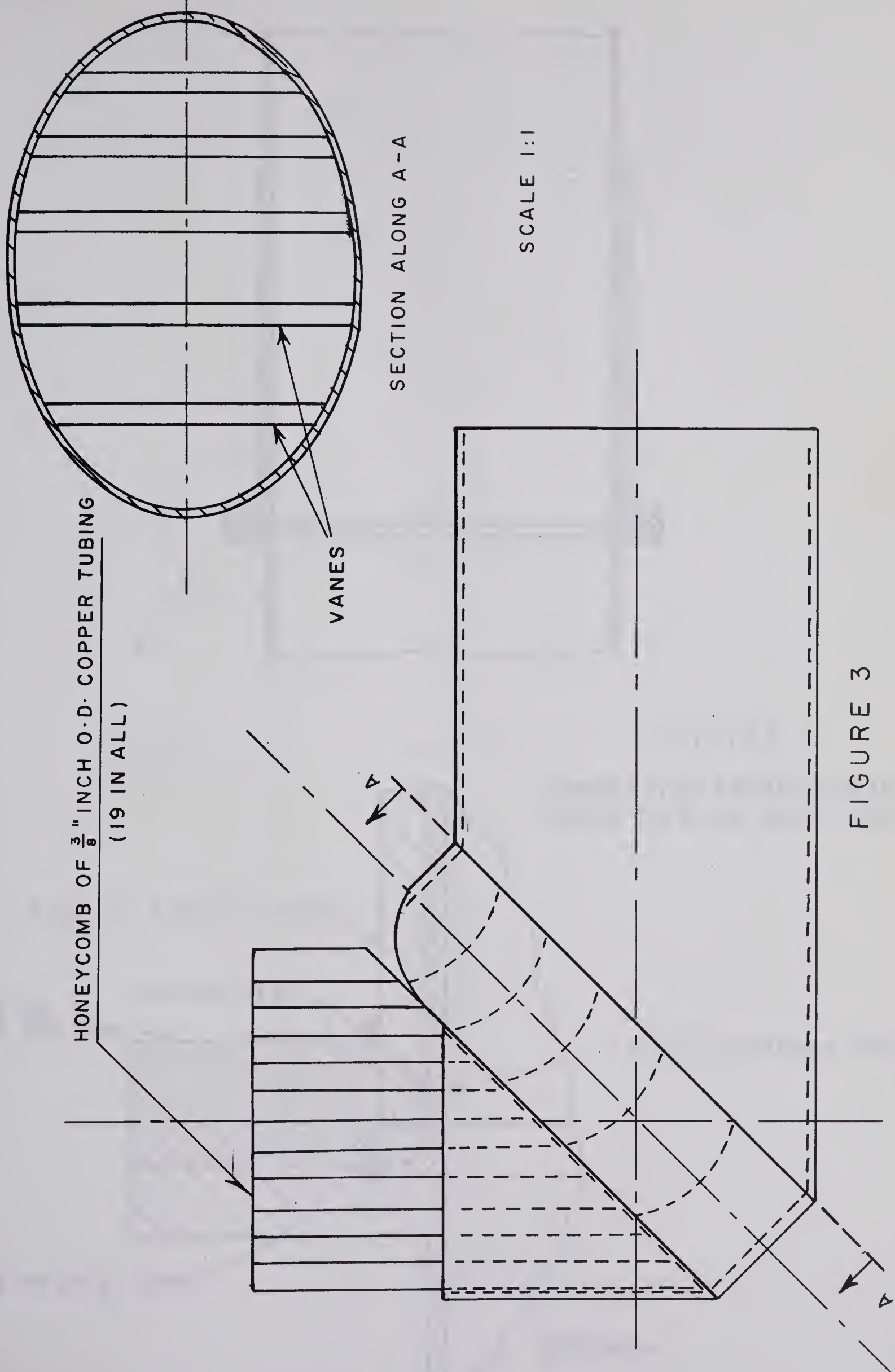


FIGURE 3
INLET ARRANGEMENT WITH VANES INSIDE TEE

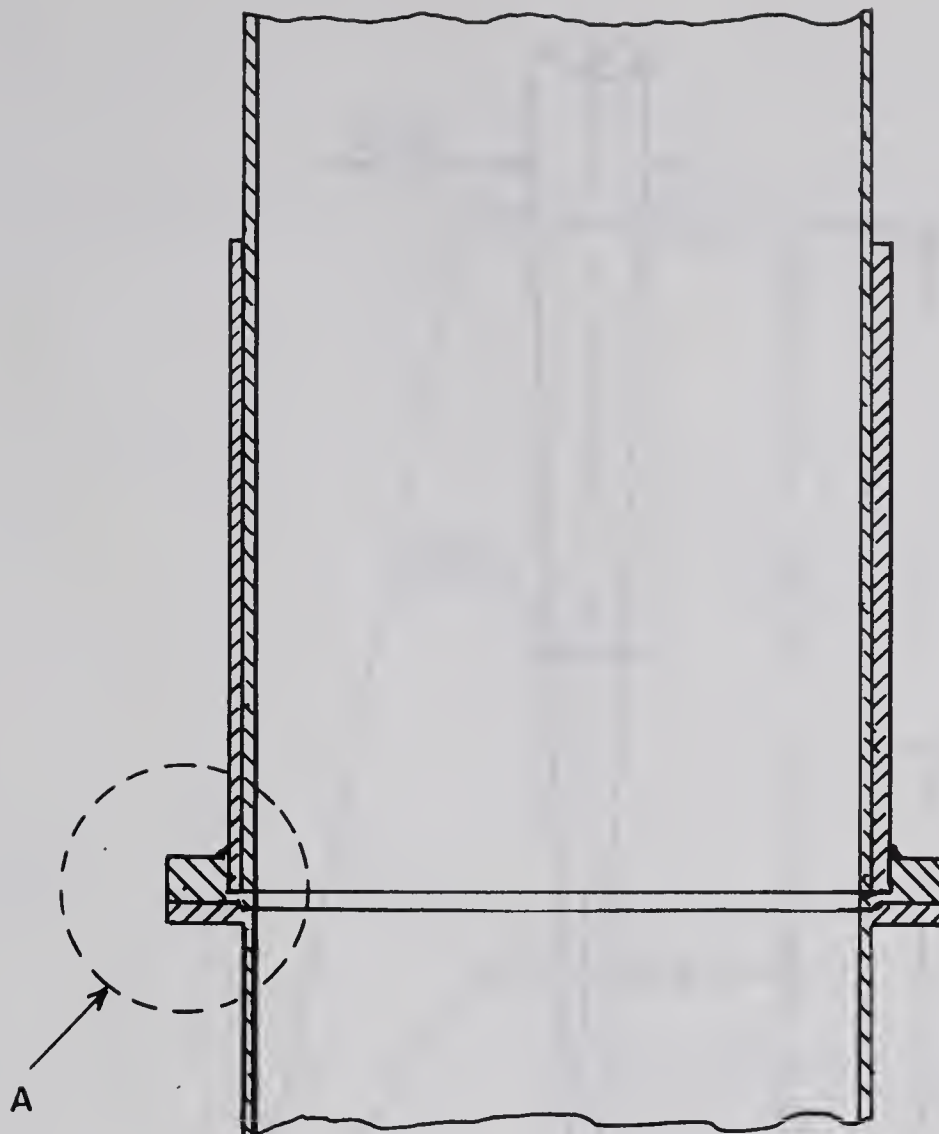
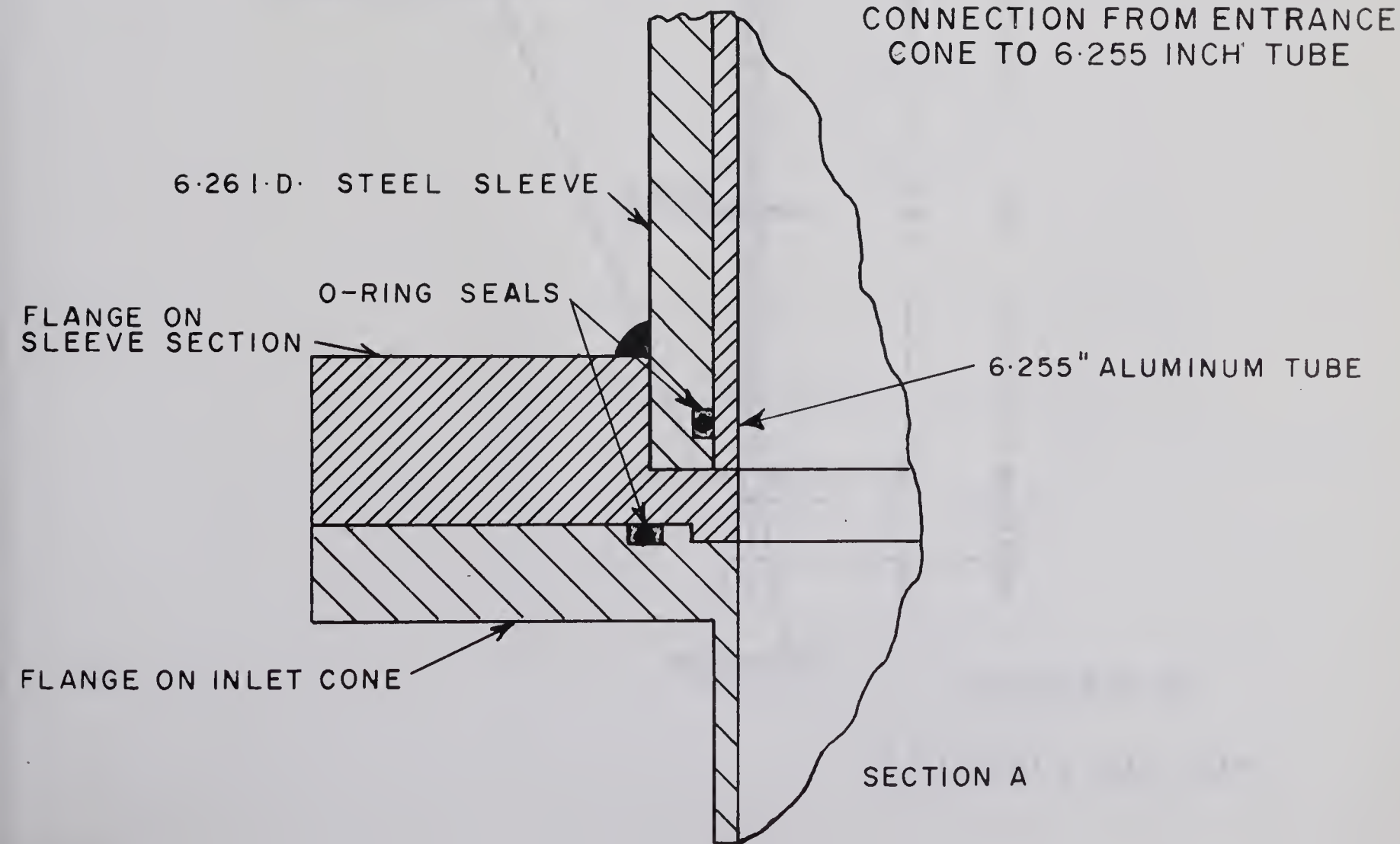


FIGURE 4

CONNECTION FROM ENTRANCE
CONE TO 6.255 INCH TUBE



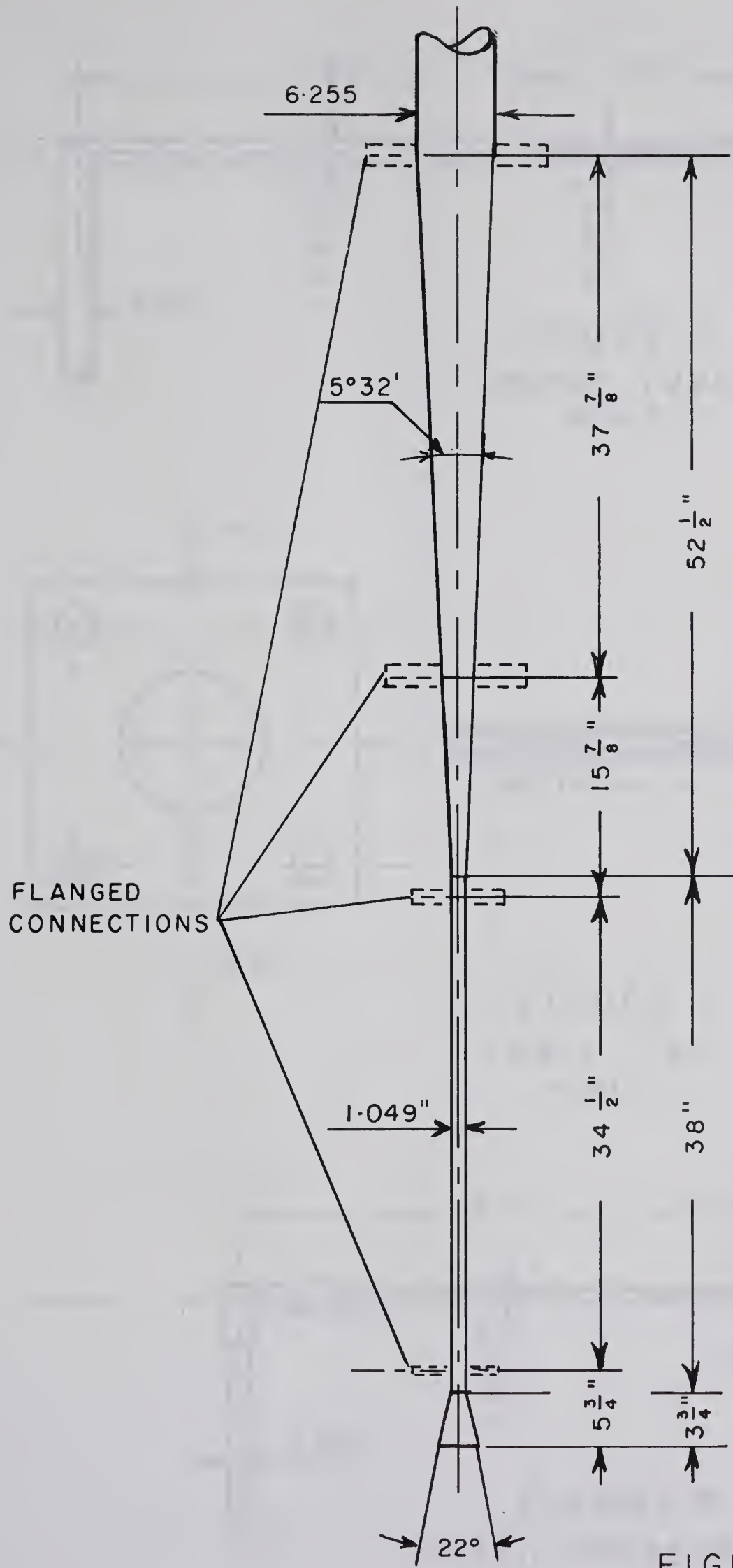


FIGURE 5
ENTRANCE SECTION

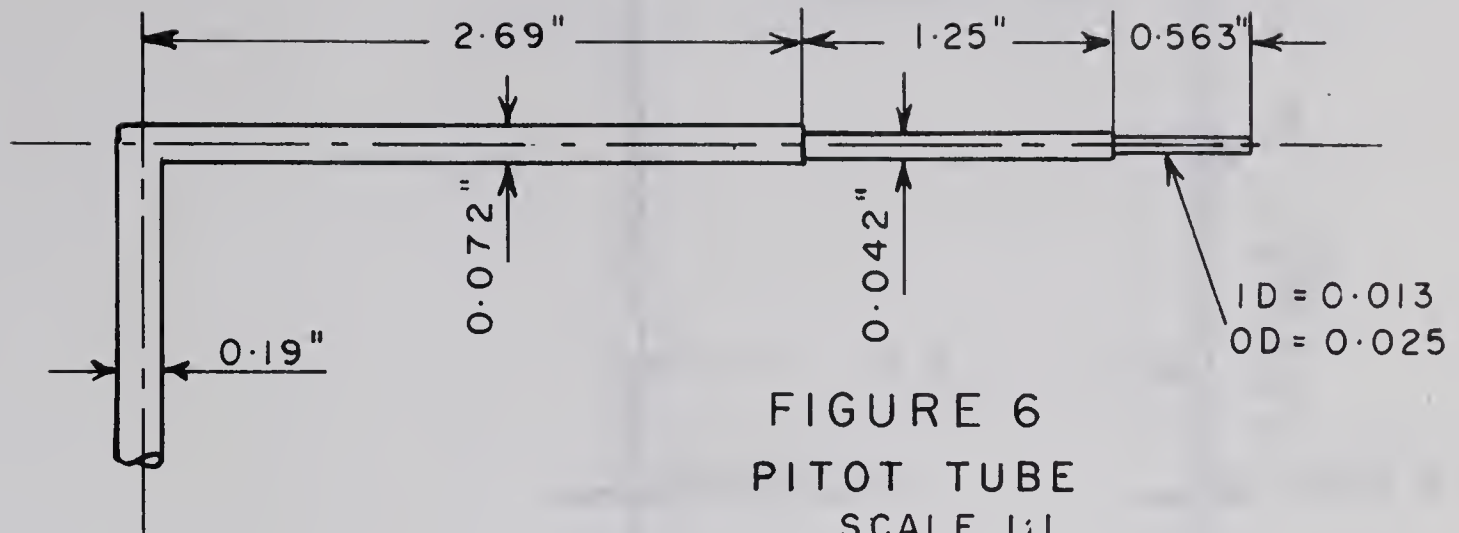


FIGURE 6
PITOT TUBE
SCALE 1:1

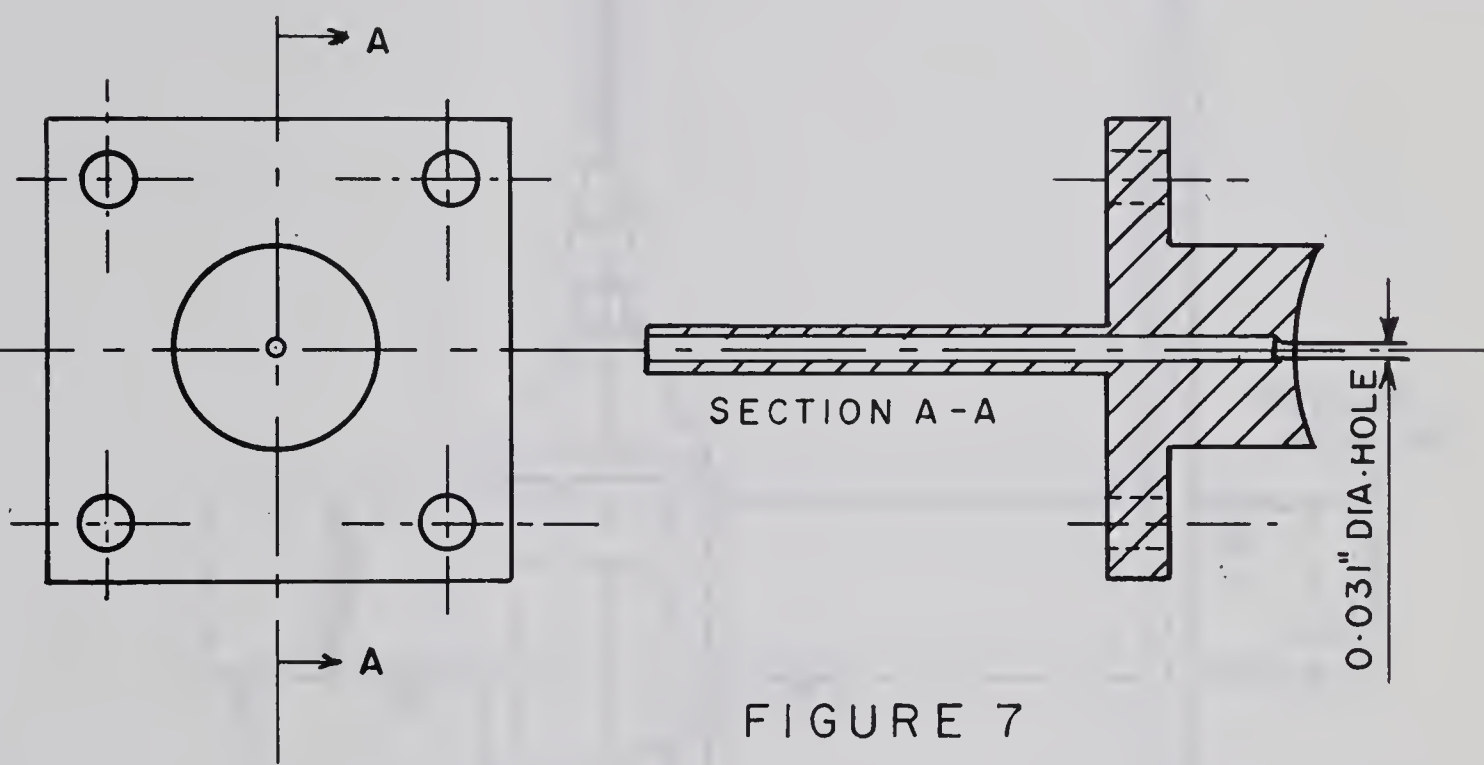


FIGURE 7
WALL TAP
SCALE 1:1

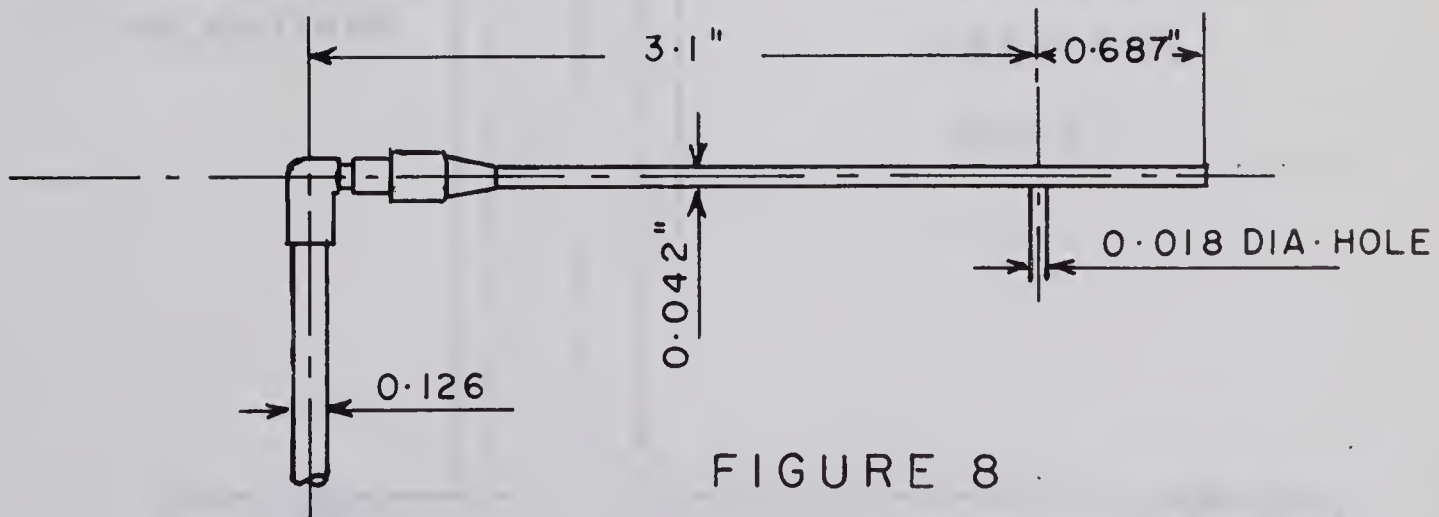
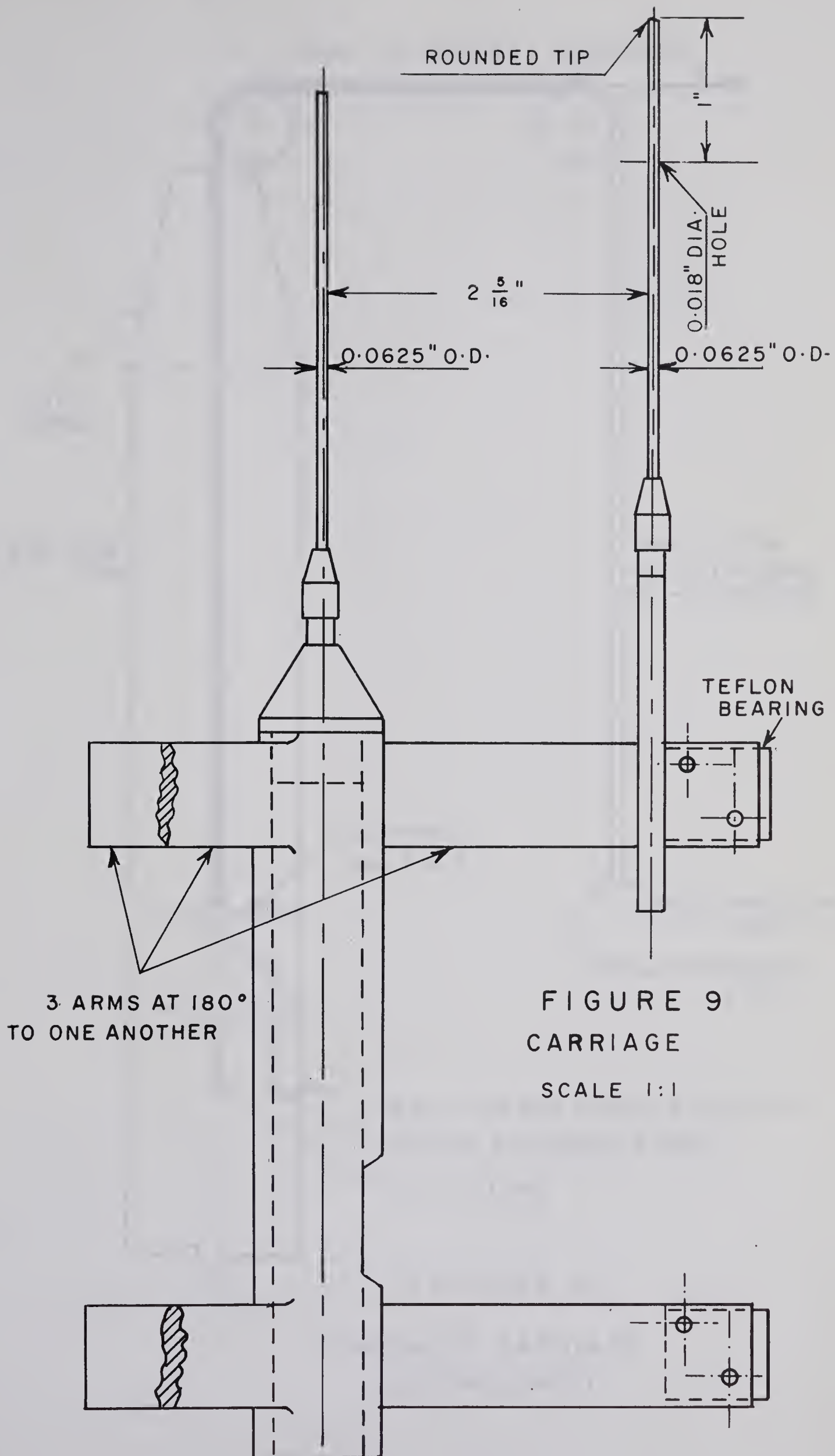


FIGURE 8
STATIC PRESSURE PROBE
SCALE 1:1



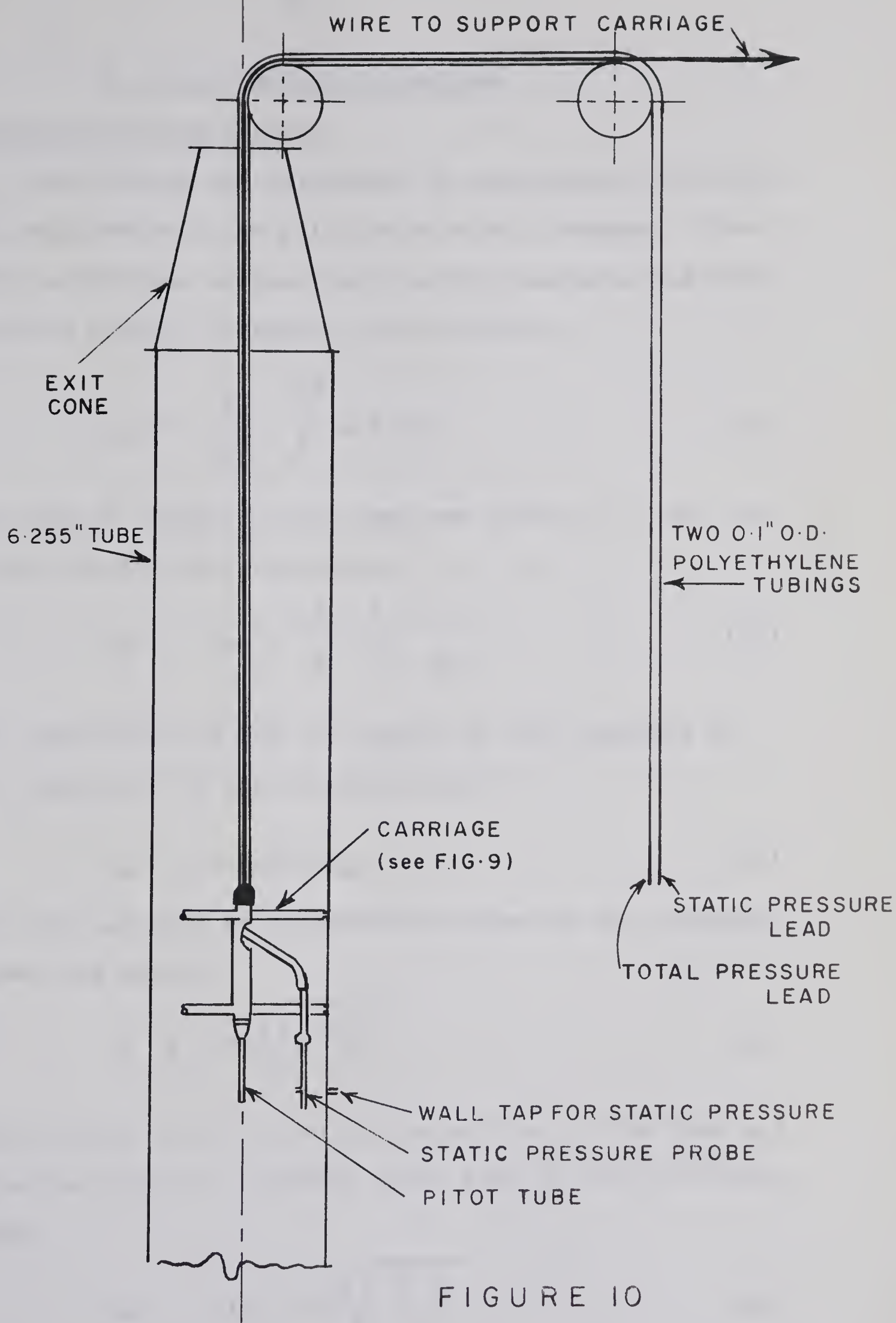


FIGURE 10
SCHEMATIC CARRIAGE
ARRANGEMENT

2. Experimental Procedures

a. Calibration of the Orifice

The orifice was calibrated by integrating velocity profiles obtained with the pitot tube as the standard. The mean point velocities across the tube were measured and then integrated to give an average or bulk velocity,

$$u_{av} = \frac{1}{\pi R^2} \int_0^R u 2\pi r dr \quad (51)$$

The flow rate in standard cubic feet per minute, Q_o , was obtained from the following equation,

$$Q_o = u_{av} F \frac{T_o}{T} \frac{P}{P_o} \frac{1}{60} \quad (52)$$

When the temperature of the air supply is held constant at $531.6^{\circ}R$, equation (52) may be simplified to

$$Q_o = 0.0167 P u_{av} \quad (53)$$

The flow rate can also be expressed in terms of the pressure drop across the orifice

$$Q = CFY \sqrt{\frac{2g_c \Delta P}{\rho}} \quad (54)$$

Upon substitution of the cross-sectional area of the tube and converting the units to standard cubic feet of air per minute, one obtains

$$Q_o = 31.73 CY \sqrt{\frac{\Delta P P}{T}} \quad (55)$$

An average value of the orifice coefficient was obtained by plotting Q_o from equation (53) versus Q_o/C from equation (55) and measuring the slope of the resulting straight line. Except for small deviations, the calibration points fell on a straight line passing through the origin. The flow coefficient, obtained by the method of least squares, was equal to 0.64 with a maximum deviation of 3%. The correlation is shown in Figure 11, and experimental data are given in Table 3. The expansion factors, Y , which were applied ranged from 0.97 to 1.0.

b. Measurement of Velocity Profiles

Complete velocity profiles were measured at a distance of 41 pipe diameters from the entrance, over a Reynolds number range of 9,000 to 56,000, using the pitot tube together with the wall static pressure tap. Values of the mean point velocities were obtained at positions as close as 0.0775 inch to the tube wall.

At Reynolds numbers less than 9,000, the impact pressure was too small to be measured accurately by the micro-manometer. The upper limit of the Reynolds number, 56,000, corresponded to the capacity output of the blower.

Two traverses were taken at right angles to each other at distances of 41 and also 4.2 diameters, downstream from the entrance, to ensure that the velocity profiles were symmetrical about the tube axis. These profiles are shown for $Re = 18,000$ at 41 diameters, and for $Re = 24,000$ at 4.2 diameters, downstream from the entrance in Figure 12. The corresponding

experimental data are given in Tables 5 and 6.

The velocity profiles corresponding to $Re = 13,000$ measured at 35.2 and repeated at 41 diameters were identical within the limitations of the experimental measurements, hence, it was concluded that the flow was fully developed at the 41 diameter position.

c. Measurement of Center-Line Velocity

To obtain a profile of axial velocity development using the travelling carriage already described, certain difficulties may be anticipated. The presence of the carriage could be expected to influence the static pressure in the tube. The static pressure was measured about four inches ahead of the main structure of the carriage. Initial tests comparing the static pressure obtained with the carriage static pressure probe and that of a wall tap, having the carriage a few inches further downstream from the location of the tap, showed no influence of the carriage. However, the velocity obtained with the carriage was consistently higher than that obtained with the traversing pitot tube when both were measured at the same location. Assuming that differences between the total pressures are minor compared to those between the static pressures and that the carriage values contain the error, it could be deduced that the static pressure obtained with the carriage read too low.

Experiments were then undertaken using the static

pressure taps along the tube wall together with the carriage pitot tube. The carriage was so positioned that the static pressure hole at the wall was two inches upstream from the center-line pitot tube. Center-line velocities measured in this way were noticeably lower, but these values were still higher than those obtained in the corresponding velocity profiles. It was thus concluded that the static pressure was affected by the presence of the carriage.

The results of carriage-measured center-line velocities obtained by using both the static pressure probe at the carriage and the static pressure taps at the tube wall are compared in Figure 13. The data are given in Tables 38 to 43.

d. Measurement of Friction Factors

The static pressure probes shown in Figure 8, spaced five feet apart at 44.8 and 35.2 diameters downstream from the entrance, were used to measure the pressure drop along the tube. Blasius friction factor were calculated assuming incompressible flow,

$$f = \frac{2g_c D}{\rho u_{av}^2} \left(- \frac{\Delta P}{\Delta x} \right) \quad (56)$$

The friction factors thus obtained disagreed greatly with the expected values(6). Furthermore, by interchanging the two probes, completely different values were obtained. It was then decided to use wall taps to measure pressure drop for

the calculation of friction factor. Although the wall taps were no more mechanically perfect, this arrangement was believed to be less sensitive to mechanical imperfection since the air velocity close to the wall was low.

The friction factors so obtained, given in Table 4, are plotted and compared to the Blasius friction factor correlation in Figure 14. The Blasius correlation, may be considered for all practical purposes to be identical to that of Moody(6), in the Reynolds number range investigated. The Blasius friction factor correlation is represented by

$$f = 0.316 Re^{-1/4} \quad (57)$$

The data so obtained were slightly higher than those given by equation (57). The type of deviation encountered did not seem to be caused by ordinary roughness but was more of the type caused by wall waviness. Prandtl and Tietjens(4) discuss the two types of roughness and also mention that a combination of roughness and waviness has been encountered with drawn metal tubes such as the aluminum tube involved in these tests.

The outside diameter of the tube was measured and found to vary slightly. The maximum variation, 3/32 inch, was found in the upper region of the test tube at approximately 45 diameter from the entrance while along the remainder of the tube, variations of less than 1/32 inch were encountered.

The data so obtained were fitted by the method of least squares and, assuming waviness to be present, are represented by

$$f = 0.377 Re^{-1/4} \quad (58)$$

However, since the maximum variation in diameter occurred downstream from the location where the fully developed velocity profiles were obtained, the Blasius friction factor correlation was used.

FIGURE II
CALIBRATION OF ORIFICE
PIPE DIAMETER = $2\frac{1}{2}$ "
ORIFICE DIAMETER = 1.544"
SQUARE EDGED ORIFICE

Q, SCFM

Slope = C = 0.64

$$31.73 \cdot y \sqrt{\frac{\Delta P \cdot P'}{T}}$$

300

200

100

100

200

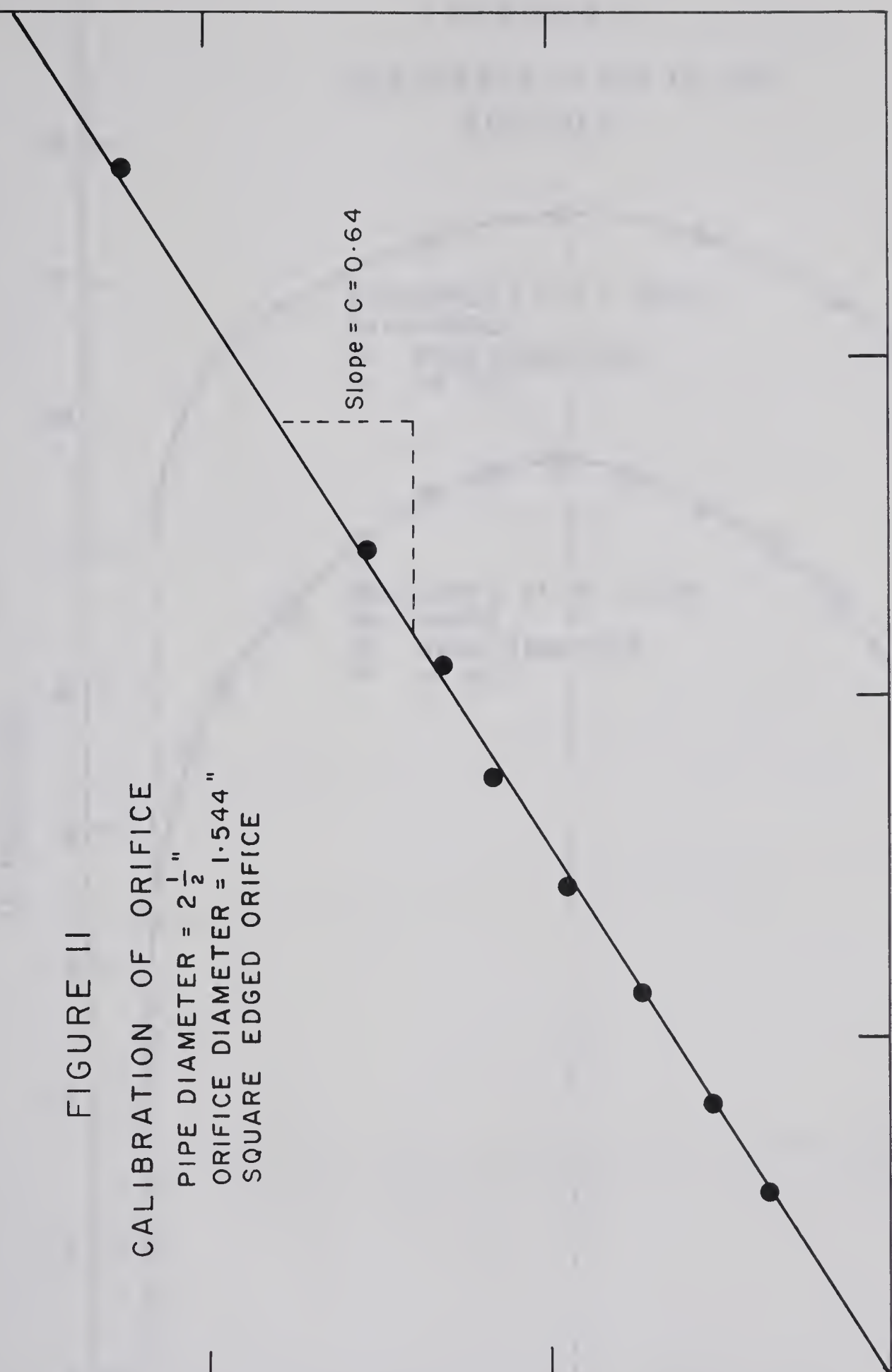
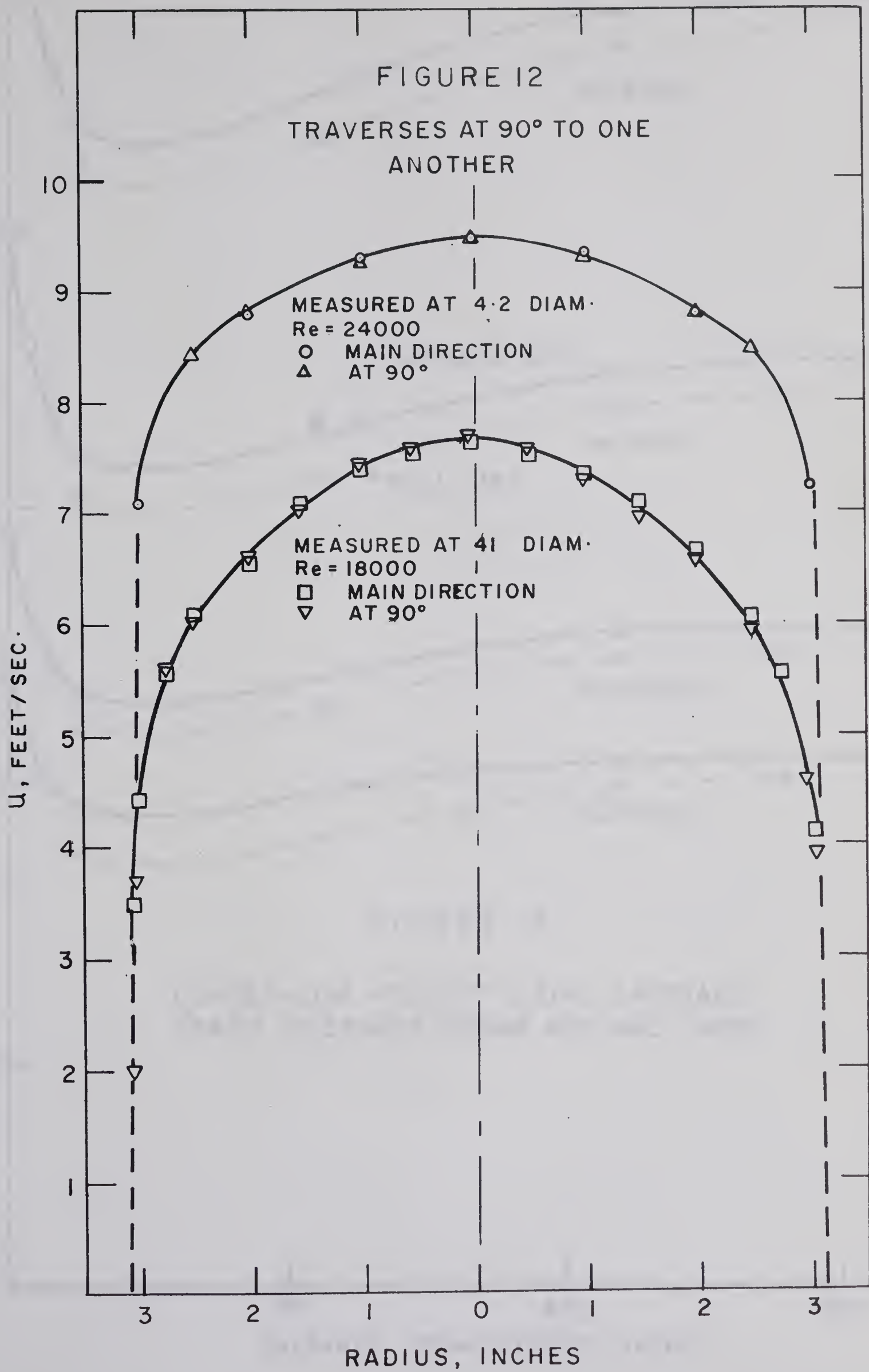


FIGURE 12

TRAVERSES AT 90° TO ONE
ANOTHER



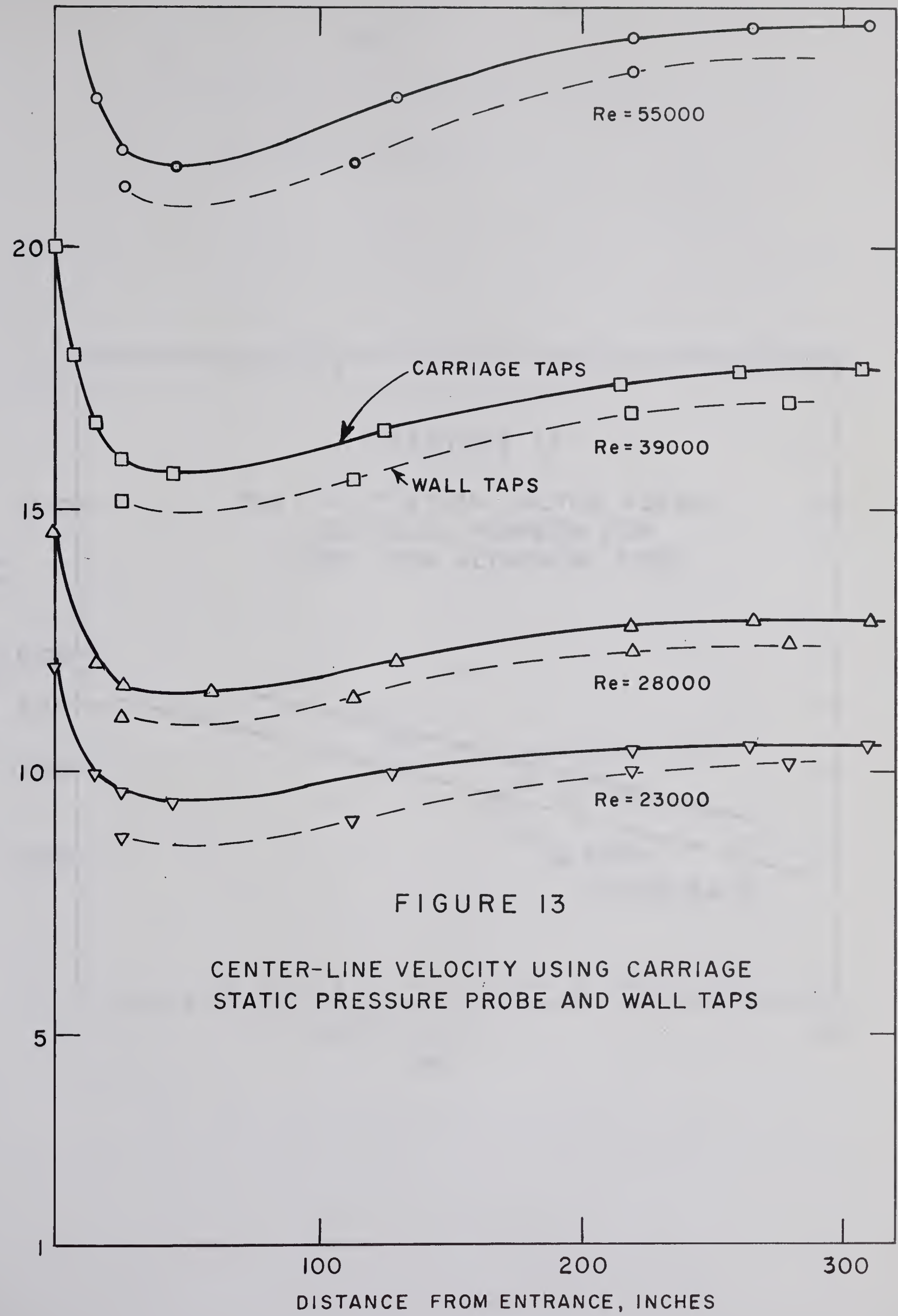
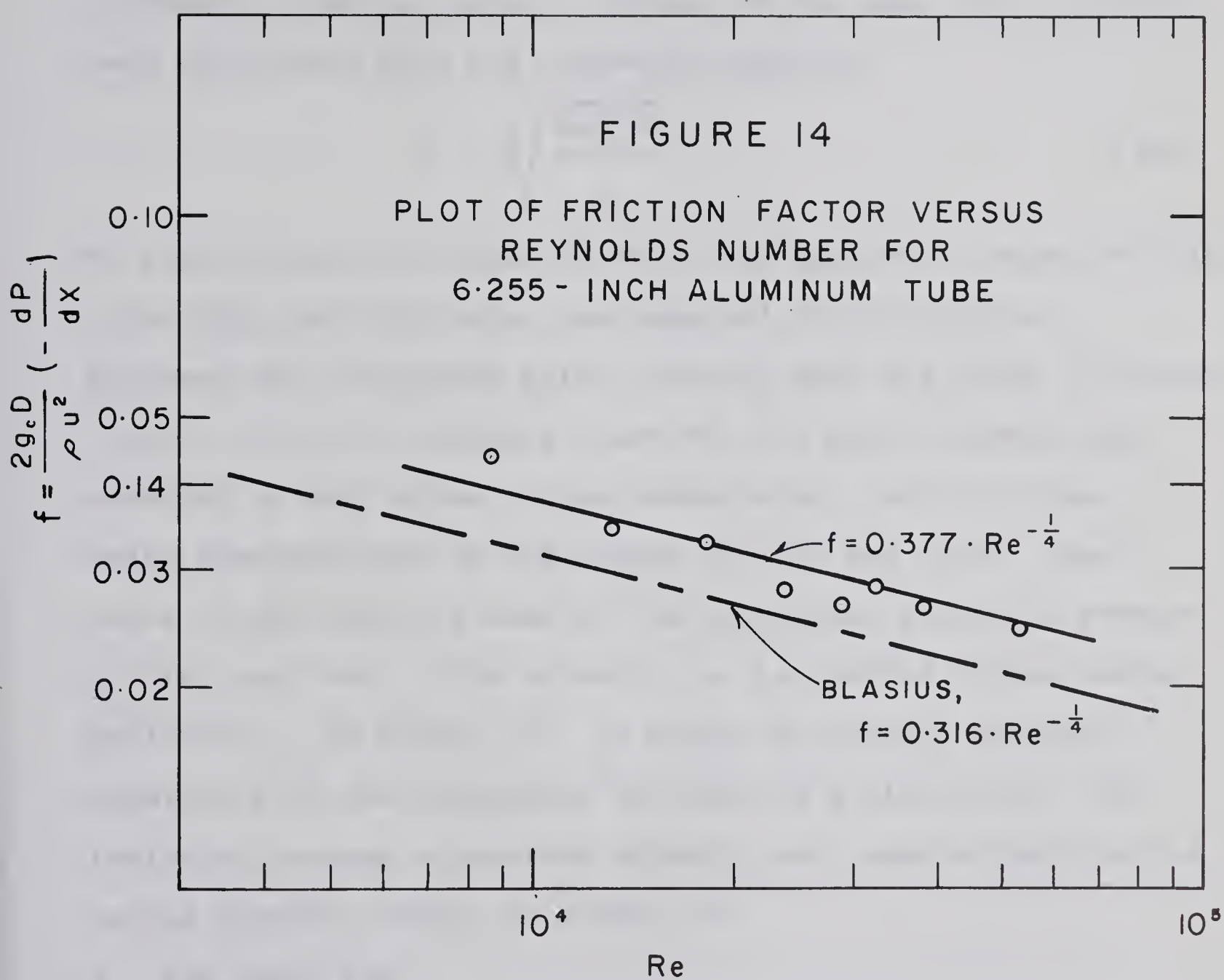


FIGURE 13

CENTER-LINE VELOCITY USING CARRIAGE
STATIC PRESSURE PROBE AND WALL TAPS



IV. EXPERIMENTAL RESULTS AND DISCUSSION

1. Fully Developed Flow

Velocity profiles were obtained at 41 diameters from the entrance (measured from the junction of the inlet cone and the 6.255 inches tube) for flow rates corresponding to 8 different Reynolds numbers. Values of the mean point velocity were calculated from the following equation:

$$u = \sqrt{\frac{2g_c \Delta P}{\rho}} \quad (59)$$

No pitot tube calibration constant was applied in equation (59) since the static pressure was measured at the tube wall.

Measured and calculated point velocity data are given in Tables 7 to 14. For all profiles measured, the point velocity was obtained on both sides of the center-line, the two values being distinguished in the Tables by "in" and "out". The value of the velocity used in the correlations was the average of "in" and "out". The velocity, u , is plotted versus radial position, r , in Figure 15. To obtain an average velocity, equation (51) was integrated by means of a planimeter. The ratios of average to maximum velocity was computed and plotted versus Reynolds number on Figure 16.

a. The Power Law

The point velocities were correlated in terms of the power law given by equation (1) and were found to correlate

well if the points measured close to the wall, at $y = 0.0775$, were omitted. The next value was obtained at $y = 0.1275$, and was found to be more reliable. The data given in Tables 15 to 18 correlated with an average deviation of 1.8% and of 3.4% when the point close to the wall was included. The power law exponents so obtained are shown in Table 19, and are plotted versus Reynolds number in Figure 17. Nunner(19) reported that the power law exponent could be expressed in terms of the friction factor

$$n = \sqrt{\frac{1}{f}} \quad (60)$$

Upon combining this with the Blasius friction factor of equation (57), the exponent can be related to the Reynolds number, giving

$$n = \sqrt{\frac{Re^{1/4}}{0.316}} \quad (61)$$

Equation (61) correlates the experimental data, as shown in Figure 17, reasonably well.

The dimensionless velocity raised to the n^{th} power, $(\frac{u}{u_m})^n$, was plotted versus $\frac{y}{R}$, using the value of n from equation (61). It was found that the data fell on a straight line

$$(\frac{u}{u_m})^n = C \left(\frac{y}{R}\right) \quad (62)$$

except for the center-line velocity. The average value of C was found by least squares to equal 1.145 and it varied by less than 2.2%. The results are shown in Figure 18. To avoid crowding of the data on the graph, the ordinates have been shifted for each run.

By integrating the Power Law, Schlichting(6) obtained an expression for the ratio of average to maximum velocity,

$$\frac{u_{av}}{u_m} = \frac{2n^2}{(n+1)(2n+1)} \quad (63)$$

Both equation (63) combined with equation (61), and equation (43) gave a velocity ratio slightly lower than the experimental values. The experimental results of Rothfus and Monrad(8), however, agree closely with those obtained in this work. The results given in Table 19 are shown and compared in Figure 16.

b. The Logarithmic Velocity Distribution

In the preceding theory, equations (8) and (12) were left with one constant, K, to be determined experimentally. It was also assumed to be a universal constant, that is to say, not dependent on Reynolds number. A value of $K = 0.40$ has been experimentally obtained by Nikuradse(6), but with the present data, considerably lower constants were obtained. By the method of least squares applied to all points measured, the following values of K were obtained:

$$K = 0.348, \quad \text{for equation (8)}$$

$$K = 0.311, \quad \text{for equation (12)}$$

For the individual runs, K varied between 0.28 and 0.38 with no consistent decrease or increase with increasing Reynolds number and with average deviations of more than 10%. The experimental data and calculated values are given in Tables 20 to 23. To avoid crowding the experimental results for Reynolds numbers of 56,045 and 18,176 only, together with equations (8) and (12), using the two experimental values of K and the value of 0.4 are shown in Figure 19. On the basis of the data obtained in the present investigation, the correlation of Prandtl, equation (8), was superior to that of von Karman, equation (12), but both were inferior to the simple Power Law distribution.

An equation similar to the von Karman equation can be obtained if we neglect to apply the second boundary condition, $u = u_m$ for $y = R$. Using this equation, in which there are two constants to be evaluated, a considerably better fit was achieved. However, one set of constants was needed for each value of Reynolds number.

The correlation proposed by Wang, equation (13), was not evaluated since it was too inconvenient for practical use.

c. The Universal Velocity Distribution

Equation (20) provides the most widely used basis for correlating point velocities in a duct, at a distance from the wall. The equation contains two constants which were

determined experimentally and found to be $K = 0.361$ and $C' = 4.00$ by the method of least squares. Equation (20), as obtained by Nikuradse, Deissler and in the present work are, respectively,

$$u^+ = 2.5 \ln y^+ + 5.5 \quad (23)$$

$$u^+ = 2.78 \ln y^+ + 3.8 \quad (24)$$

$$u^+ = 2.77 \ln y^+ + 4.0 \quad (64)$$

Based on Nikuradse's data, equation (23) was found to be valid for $y^+ > 30$, while Deissler reported equation (24) to be valid for $y^+ > 26$. The present work seems to agree with Deissler. The great difference in constants given that of equation (23) and those of (24) and (64) is believed to have been caused by the different range of Reynolds numbers over which they were obtained. Nikuradse worked with Reynolds numbers ranging from 4,000 to 3,240,000 while Deissler, and to an even greater extent the present investigator, worked over a considerably smaller range of Reynolds numbers. It is known that all of the points of a complete velocity profile do not fall on a straight line as given by equation (20), a true curve giving slightly higher velocities near the center line. This effect is confirmed on Figure 20. The present work and Deissler's did not include velocity profiles in the range of Reynolds number from 4,000 to 9,000, and thus the effect of higher point velocities than the equation (20) indicates was not present in the lower region, $y^+ < 200$. This effect could account

for a steeper slope and a shorter intersection obtained in equations (23) and (64). Equations (23) and (64) together with the experimental results are shown in Figure 20 and the corresponding data are given in Tables 24 to 27. Deissler's correlation was omitted from Figure 20 because it was practically identical to that of equation (24). For $y^+ > 26$, an average percent deviation of 1.28% and a maximum deviation of 3.96% were encountered for the 62 points which were measured. Equation (64) with one set of constants gave a better fit over the entire range of Reynolds numbers than the von Karman equation using a different set of constants for each individual Reynolds number.

By examining the constants obtained for equation (20) in the individual runs, it was found that they could vary greatly without causing much change in the computed velocity. Furthermore, it was noticed that for a decrease in slope the constant representing the intersection always increased and vice-versa. The maximum variation of K for any individual run was 10% while C' had a maximum deviation of more than 30%. This surprisingly high variation in the value of the constants only corresponded to a maximum variation of 4% in computed velocity. Errors in the constants attributed to possible errors in the experimental measurements giving the velocity profile will be analyzed in the appendix section. The results of the analysis clearly show that the value of the constant C' was

far more sensitive than the value of K to errors in the variables u^+ and y^+ .

To account for the observed deviations from equation (64), an equation of the form suggested by Bogue, equation (35) was assumed

$$u^+ - C \left(\frac{y}{R}, f \right) = A \ln y^+ + B \quad (65)$$

where

$$C \left(\frac{y}{R}, f \right) = C \sqrt{\frac{8}{f}} \exp \left(\frac{-(\frac{y}{R} - D)^2}{E} \right) \quad (66)$$

The constants A and B were obtained by the method of least squares while the constants C , D and E were determined by a trial-and-error procedure as shown in the Appendix. The criterion used for a best fit was the minimum of the sum of the absolute values of percent error. The constants which were obtained were slightly different from those of Bogue who selected the constants A and B in equation (65) so that this equation would, upon integration, yield the Moody friction factor correlation for smooth pipes and then curve fitted the remaining constants. The present work gave

$$u^+ - C \left(\frac{y}{R}, f \right) = 2.43 \ln y^+ + 5.24 \quad (67)$$

where

$$C \left(\frac{y}{R}, f \right) = 0.063 \sqrt{\frac{8}{f}} \exp \left(\frac{-(\frac{y}{R} - 0.77)^2}{0.17} \right) \quad (68)$$

On the basis of previous findings, equation (67) was assumed to be valid for $y^+ > 26$. An average percent deviation of 0.81% and a maximum deviation of 4.5% resulted.

However, by examining the data obtained in individual runs, it was found that the effect of Reynolds number on the velocity profiles was nearly insignificant, if at all observable. Thus, the empirical correction function, equation (68), was simplified as follows:

$$C \left(\frac{Y}{R}\right) = C' \exp \left(\frac{-(\frac{Y}{R} - D')^2}{E'} \right) \quad (69)$$

Using the same procedure as previously, the following correlation was obtained:

$$u^+ - C \left(\frac{Y}{R}\right) = 2.46 \ln y^+ + 5.11 \quad (70)$$

where

$$C \left(\frac{Y}{R}\right) = 1.07 \exp \left(\frac{-(\frac{Y}{R} - 0.77)^2}{0.16} \right) \quad (71)$$

The correction function given by equation (71) is of simpler form than equation (68) because it can be represented in the form of a single curve, a function of radial position y/R . Over the limited range investigated, Reynolds number from 9000 to 56,000, equation (70) was found to be comparable to equation (67). An average percent deviation of 0.82% and a maximum deviation of 4.26% were encountered. The correction function, equation (71), is shown in Figure 21. The experi-

mental data are given in Tables 24 to 27 and equation (70) is plotted in Figure 22.

d. The Velocity Distribution in the Vicinity of the Wall

The limited experimental data which were obtained in the region, $y^+ < 26$, showed considerable scatter as may be seen in Figure 20. With only 9 points, and a maximum of 2 points obtained in a given run, no conclusion may be drawn as to whether one correlation fits better than another. However, the points indicate that there is a changed physical situation for $y^+ < 25$. This change is caused by the wall which superimposes a viscous shear stress on the fluid near the wall. The experimental data reported here are insufficient to determine the exact limit where the viscous shear stress effect on the flow diminishes. To describe this situation more vividly, the empirical correlation, equation (22), together with that of Deissler, equation (31), and that of Wasan et al, equation (33), are shown for comparison in Figure 20.

Velocities computed from equation (22) together with (23), and from (31) together with (64), will not give continuous velocity profiles. Equation (33) was so derived that the resulting velocity profile would have a continuous transition to equation (23), however, it is unlikely that equation (23) is valid down to $y^+ = 20$. By using the approach of Wasan et al(12), matching equation (32) with equation (20), but using the constants obtained in the present work, the

following relation was found:

$$u^+ = y^+ - 1.403 (10^{-4}) (y^+)^4 + 4.55 (10^{-6}) (y^+)^5 \quad (65)$$

The transition was found to occur at $y^+ = 18$. As can be seen in Figure 20, the above equation agrees more closely with the equation (22), that has been experimentally verified in the region. The derivation of equation (65) is given in the Appendix section. The computed values are given in Table 28. Equation (65) possesses the advantages of providing a continuous transition to the equation valid in the turbulent core, of approaching laminar flow for $y^+ = 5$, and it is more convenient to use than the Deissler correlation, equation (31). However, experimental confirmation is lacking.

Gill and Scher's velocity distribution equation (39), based on a modified Prandtl mixing length theory was tested with the present data. The Legendre-Gauss quadrature formula(20) was used for the numerical integration. Details of the computational procedure are given in the Appendix section. The velocity computed from equation (39) resulted in a curved velocity profile with semilogarithmic coordinates as can be seen in Figure 23. The distribution which was obtained was consistently too low in the region close to the center line. The two constants which were employed, determined by Gill and Scher, were varied but no significant improvements were achieved. For computations, y_m^+ was obtained from the following relation:

$$y_m^+ = \frac{Re}{2} \sqrt{\frac{f}{8}} \quad (66)$$

The computed values are given in Tables 29 to 32. The correlation follows equation (21) and (22) closely in the region near the wall. In the region far away from the center line it is in fair agreement with experimental results and equation (64), however, approaching the center line the correlation is not very satisfactory. Computed values are given in the Appendix section following the computational procedure. Experimental data and computed values are plotted in Figure 23 for Reynolds numbers of 13,120 and 56,050.

The Pai power series correlation, given by equation (42), was found to be superior to the other correlations valid from the wall to the center line. By means of the Brodkey correlation(15) for the variables used in the Pai type equation, S and M, the velocity profiles shown in Figure 24 were obtained. The large deviations for points measured close to the wall were random and thus believed to have been caused primarily by inaccuracies in measuring the velocity and not by an inconsistency in the correlation. Points which were obtained in the turbulent core, $y^+ > 26$, showed an average deviation of only 0.9% and a maximum deviation of 4.5%. This was considerably better than what was obtained with equation (64), and comparable to the results obtained with the Bogue universal velocity distribution, equation (35). Furthermore, for the

Pai power series correlation no constants were curve-fitted to the present experimental data. Brodkey(15) reported certain discrepancies at high Reynolds number. In the range tested, $9,000 < Re < 56,000$, no such trend was observed. For decreasing Reynolds numbers, both the experimental data and equation (42) converge to the laminar velocity distribution, as can be seen in Figure 24.

The von Karman correlation was re-arranged in terms of u/u_m versus y/R and plotted in Figure 24. Dividing equation (12) by u_m gave

$$\frac{u}{u_m} = 1 + \frac{1}{K} \frac{u^*}{u_m} \left[\ln \left(1 - \sqrt{1 - \frac{y}{R}} \right) + \sqrt{1 - \frac{y}{R}} \right] \quad (67)$$

where

$$u^* = u_{av} \sqrt{\frac{f}{8}} \quad (68)$$

and

$$\frac{u_{av}}{u_m} = \frac{2n^2}{(n+1)(2n+1)} \quad (63)$$

Equations (68) and (63) were substituted into equation (67)

$$\frac{u}{u_m} = 1 + \frac{1}{K} \frac{2n^2}{(n+1)(2n+1)} \sqrt{\frac{f}{8}} \left[\ln \left(1 - \sqrt{1 - \frac{y}{R}} \right) + \sqrt{1 - \frac{y}{R}} \right] \quad (69)$$

The power law exponent, n , is related to the Reynolds number via equation (61), the Blasius friction factor via equation (57) and finally the constant K was determined for each individual run by the method of least squares. The correlation represented the velocity profiles very well, and provides an interesting comparison to the Pai correlation. At low Reynolds number, the curvatures seemed to approach each other. At higher Reynolds number they differ considerably for y/R between 0.2 and 0.5 and the experimental data tend to fall between the two curves. Good agreement between experimental results and equation (69) could only be obtained by using a different K for each individual run. The K -value varied by more than 10% with varying Reynolds number, but no consistency could be observed.

This type of a correlation, equation (69), could only be useful if K proved to be a universal constant, independent of Reynolds number, and the value of K could be determined accurately. In the present work the average value of K was 0.31. Data calculated for the Pai power series and for equation (69) are given in the Appendix section in Tables 33 to 36.

2. The Entrance Section

Velocity profiles were obtained at 4.2 diameters downstream from the entrance for flow rates corresponding to

those measured at 41 diameters. The entrance velocity profiles are shown in Figure 25, and the corresponding values are given in Table 37. The dimensionless velocity, u/u_m , was plotted versus y/R in Figure 26 for Reynolds number 18,000, 29,000 and 38,000 and both 4.2 and 41 diameter locations. Upon examining the two sets of profiles shown in Figure 26, it can be seen that the velocity profiles obtained near the entrance are fuller, i.e. flatter near the center line, than those obtained at 41 and also that both sets of velocity profiles become fuller with increasing Reynolds number. The velocity profiles in Figure 26 represent the limiting conditions for the test unit and the evaluation of the change from the one to the other was one of the aims in this work.

To provide a comparison of the velocity distributions, the entrance profiles were tested with the universal velocity distribution correlation, equation (20). The constants, K and C' , were obtained by the method of least squares giving the equation

$$u^+ = 1.68 \ln y^+ + 9.77 \quad (70)$$

This correlation together with the experimental points are shown in Figure 27. All of the points measured were included and except for the data obtained at the lowest flow rate, $Re = 8,900$, the data correlated reasonably well with an average deviation of 1.39% and a maximum deviation of 4.44%.

The question arises whether a set of profiles at any fixed location with varying Reynolds number, could be plotted on a single curve. Since the universal velocity distribution makes no distinction between different fully developed profiles in turbulent flow, this approach was attempted, however, the question could not be solved with the limited data available.

Equation (70) intersects the correlation for fully developed flow at $y^+ = 200$. The slope of the equation, 1.68, indicates much flatter profiles than for fully developed flow. For a pipe with an entrance giving constant velocity across the diameter (plug flow), a velocity profile would yield a horizontal line in terms of the universal velocity distribution correlation. If the velocity profiles at various locations between the entrance and the location where the flow becomes fully developed would correlate in terms of straight lines on a $u^+ - y^+$ plot, their slopes should vary between 2.77 and zero. In this way, the universal velocity distribution could be used for correlating data in the entrance section of a pipe. However, it is apparent that a correction factor of the type suggested by Rothfus et al(8,9) would be necessary in a "universal" correlation because the intersection for flat profiles would increase with increasing Reynolds number, as can be inferred from the definition of u^+ , $u_{av}^+ = \sqrt{\frac{8}{f}}$.

The preceding comments are largely conjectural because of the limited data, however, they might provide an

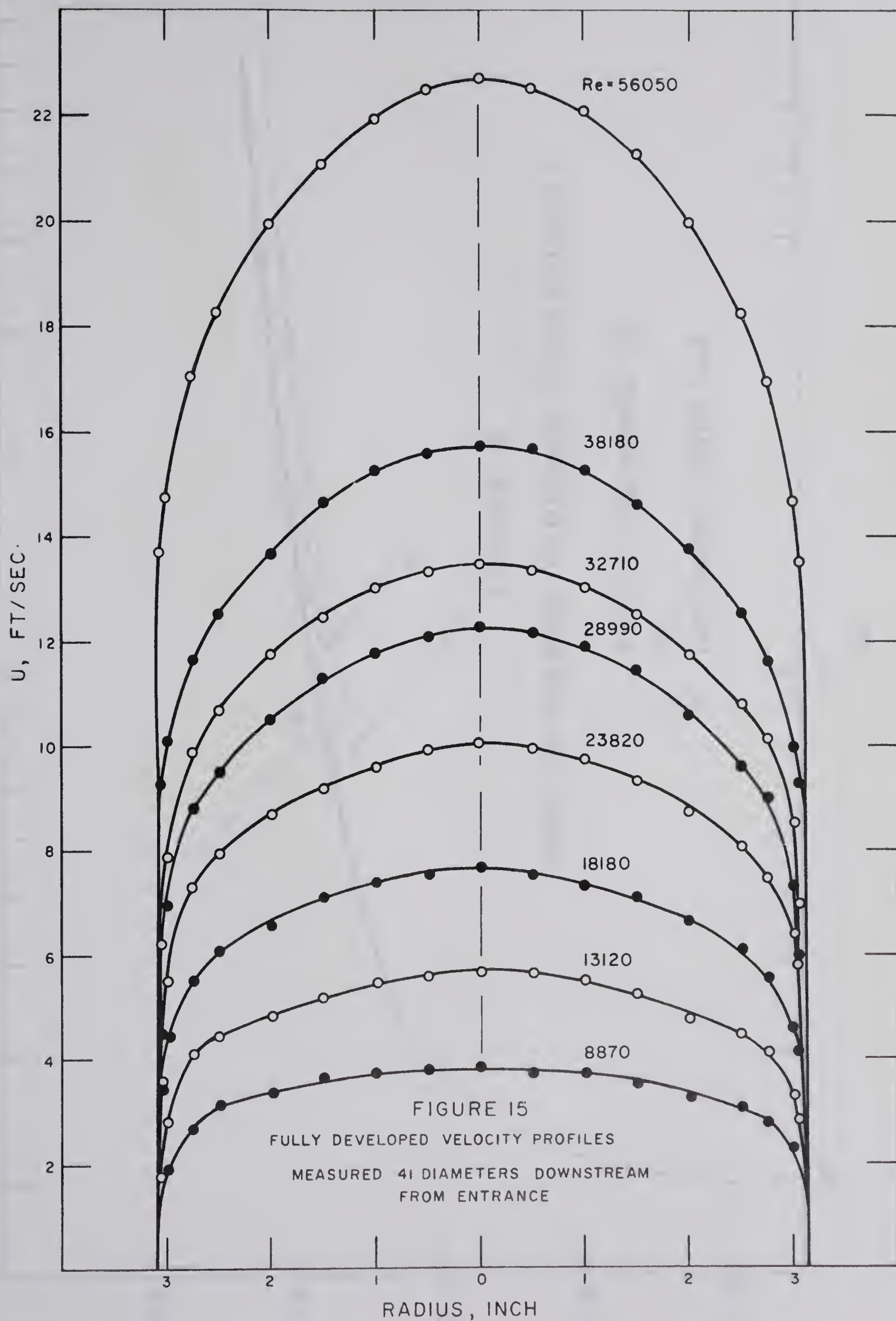
empirical way of examining and comparing the development of velocity profiles in quantitative terms, and consistent with the concept of fully developed profiles.

The original center line velocities measured with the carriage, using the carriage static pressure probe, did not yield the correct absolute value of the velocity as stated earlier in the "Experimental Procedure" section. However, the deviations between these values and the more correct values were found to be constant for one particular flow rate, thus making the center-line velocity dimensionless by dividing the value measured at any position along the tube axis by the one measured in the fully developed region, a representation of the center-line development was obtained. The center-line velocity, shown in Figure 28, was measured for 8 different flow rates, from $Re = 8,800$ to 55,000. All of the axial velocity profiles which were obtained are given in Tables 38 to 43, while the data for the two lower flow rates were excluded from Figure 28. At low flow rates, the measured change in impact pressure was small as compared to the accuracy of the micro-manometer and the results so obtained showed great scatter. The data shown in Figure 28 covers a small range of Reynolds numbers, 18,300 to 55,000, and the effect of Reynolds number could only be distinguished for averaged center-line velocity values of two and two runs together. Inspite of a very high center-line velocity at the entrance, as revealed

by Figure 28, a consequence of jetting of the fluid from the one-inch line, the velocity profile after a short distance downstream had assumed the more normal shape shown in Figure 25. However, this jet entering the 6.255 inches tube, from a one-inch pipe with a high turbulence level, enables the flow to attain a more developed velocity profile in a shorter distance downstream than, for example, a rounded entrance such as that used by Deissler(3). This would explain the relatively short entrance length encountered in the present investigation. Defining the entrance length, L/D , as the distance required for the center-line velocity to reach within 1.0% of the constant, fully developed value, it was found that

$$\frac{L}{D} \approx 40, \quad 9000 \leq Re \leq 55,000 \quad (71)$$

From Figure 28 it can also be seen that the entrance length increases with increasing Reynolds number. However, no functional relationship could be derived because of the restricted data available.



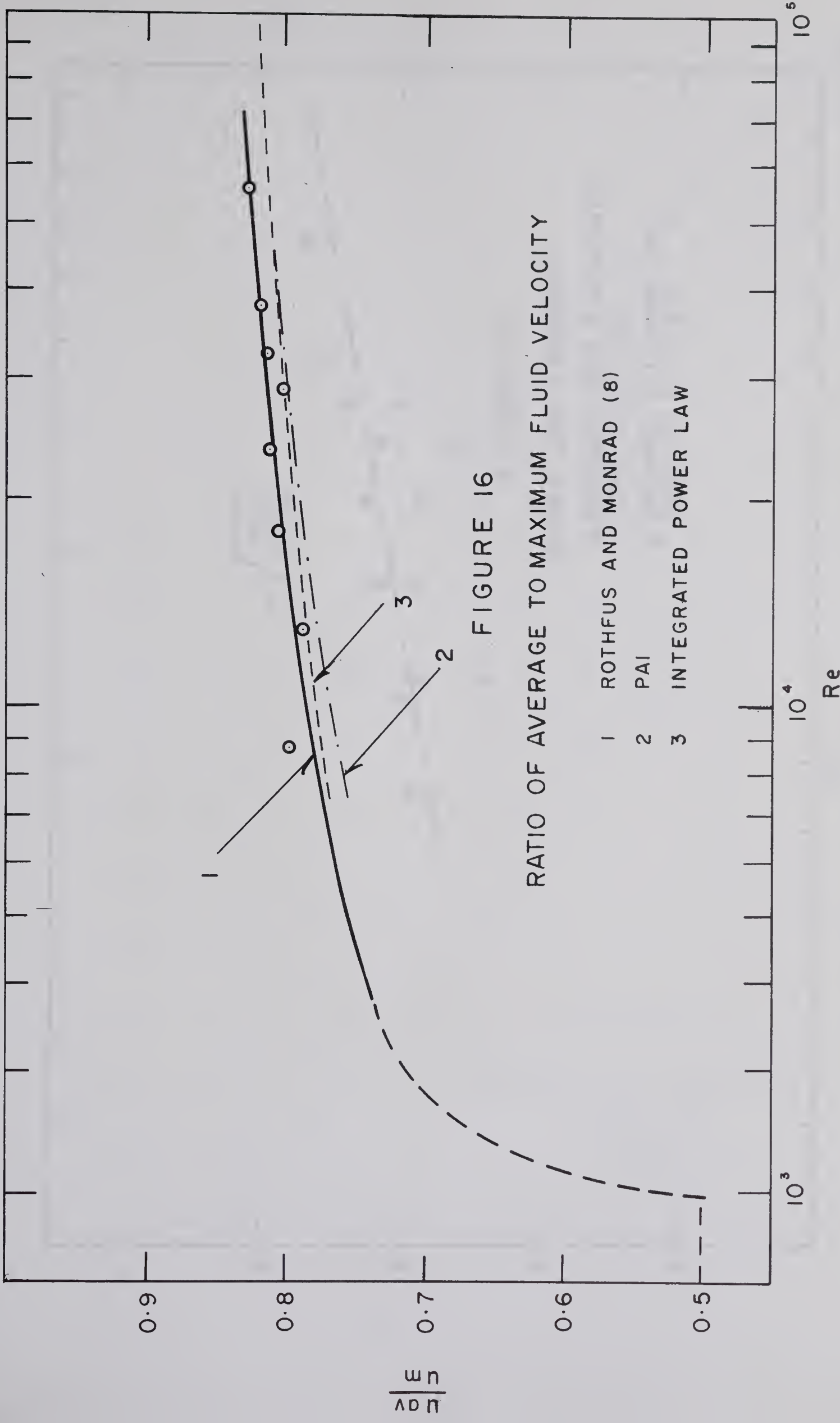
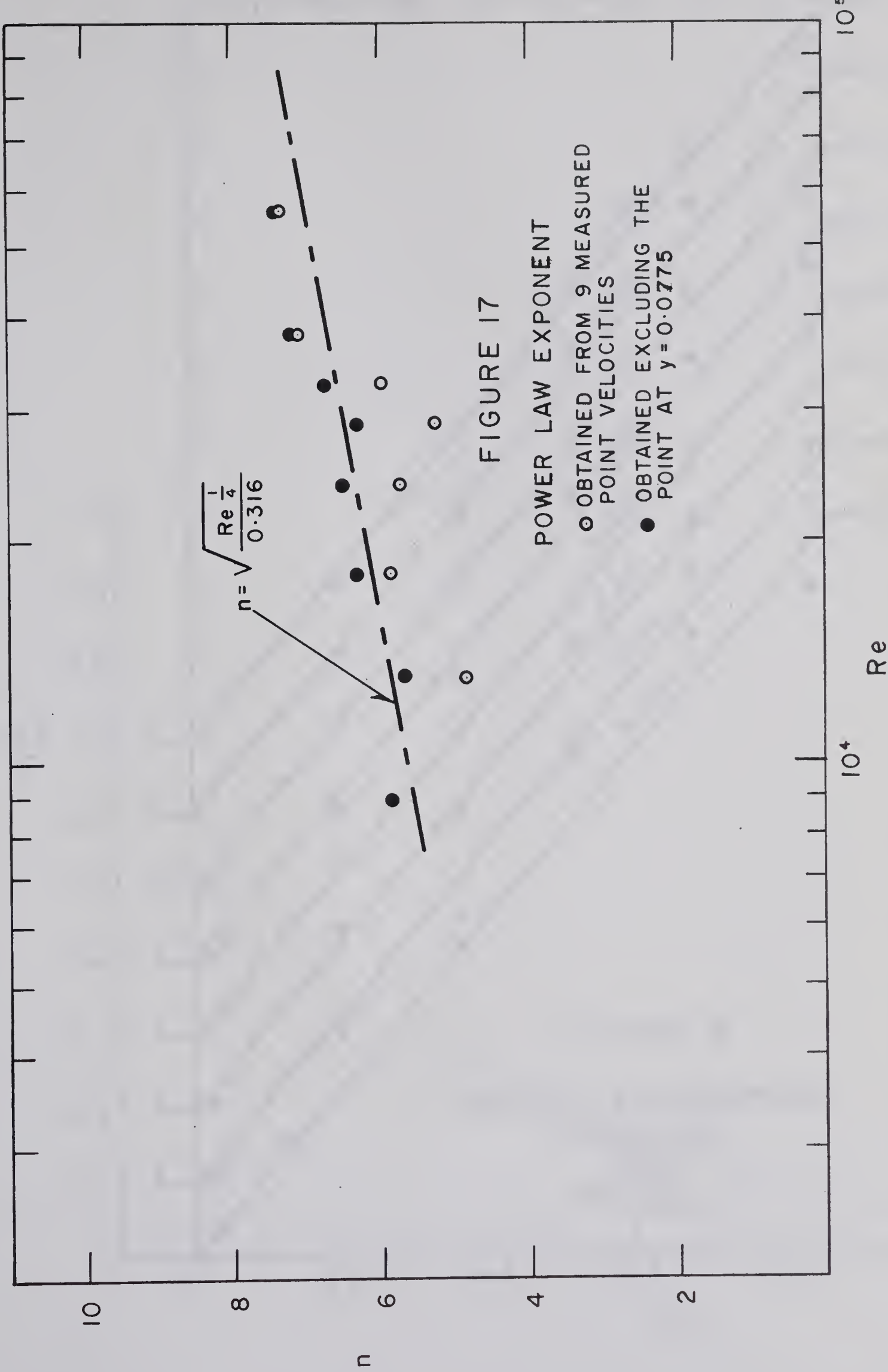
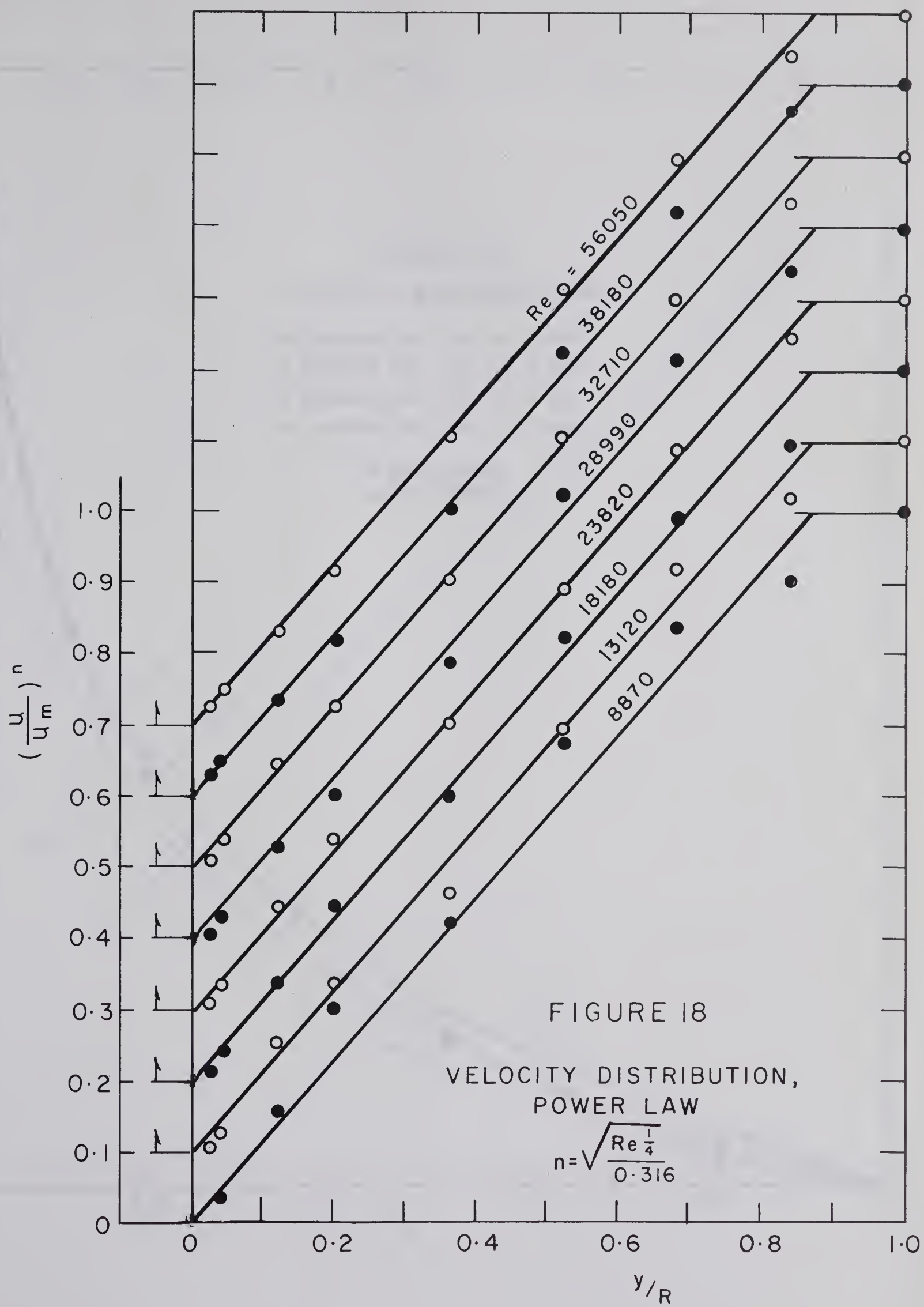
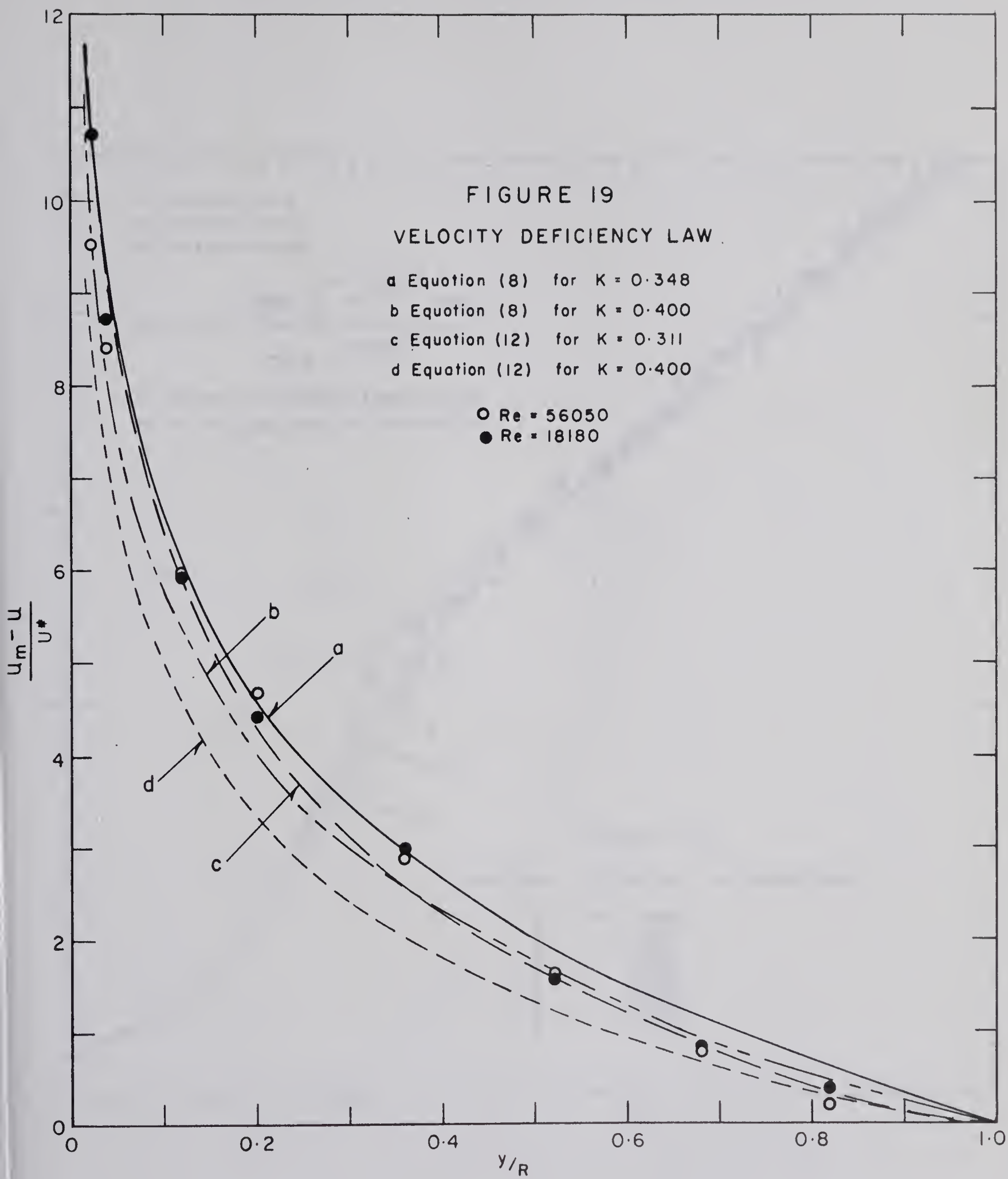


FIGURE 16
RATIO OF AVERAGE TO MAXIMUM FLUID VELOCITY

- 1 ROTHFUS AND MONRAD (8)
- 2 PAI
- 3 INTEGRATED POWER LAW







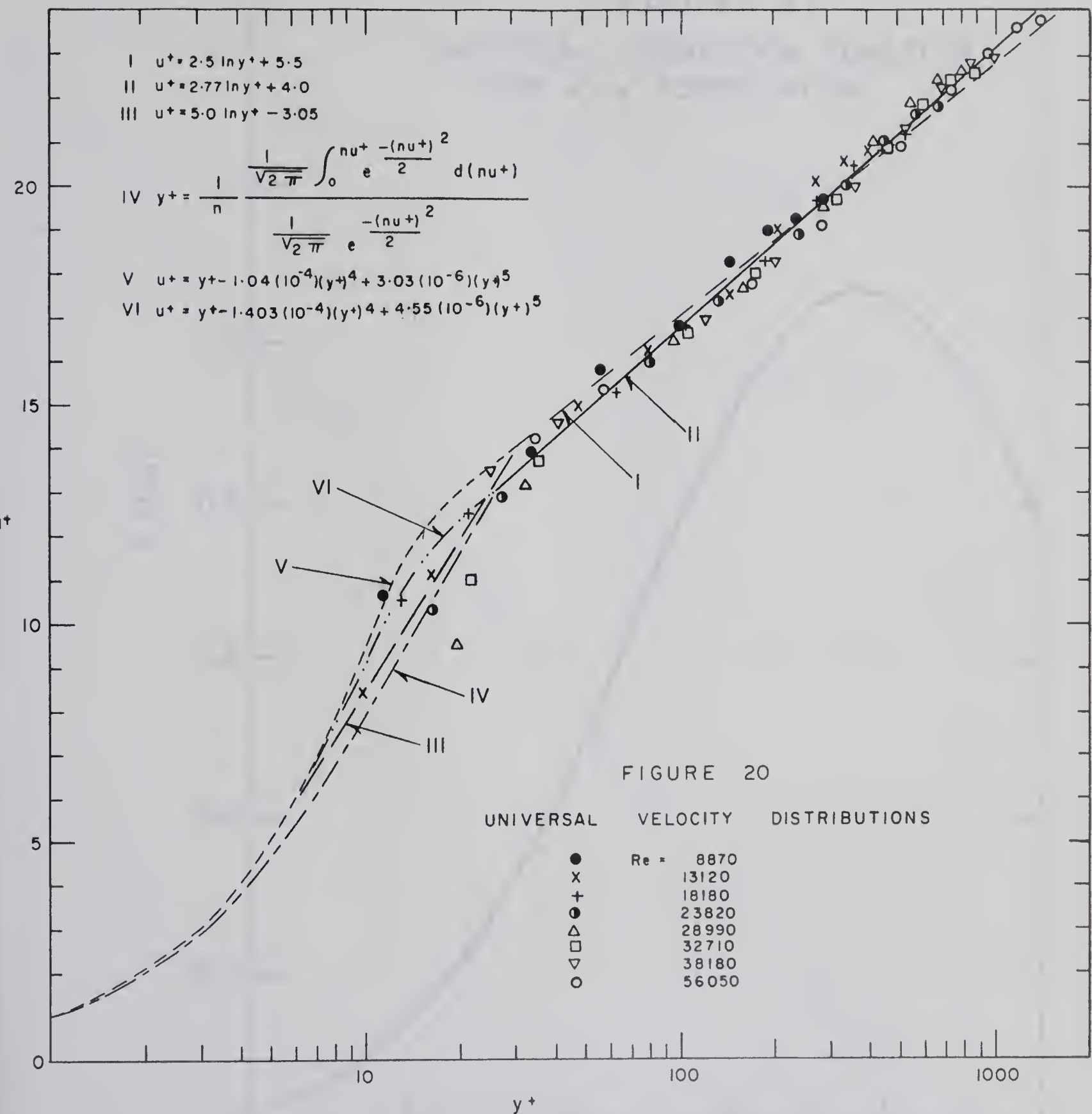
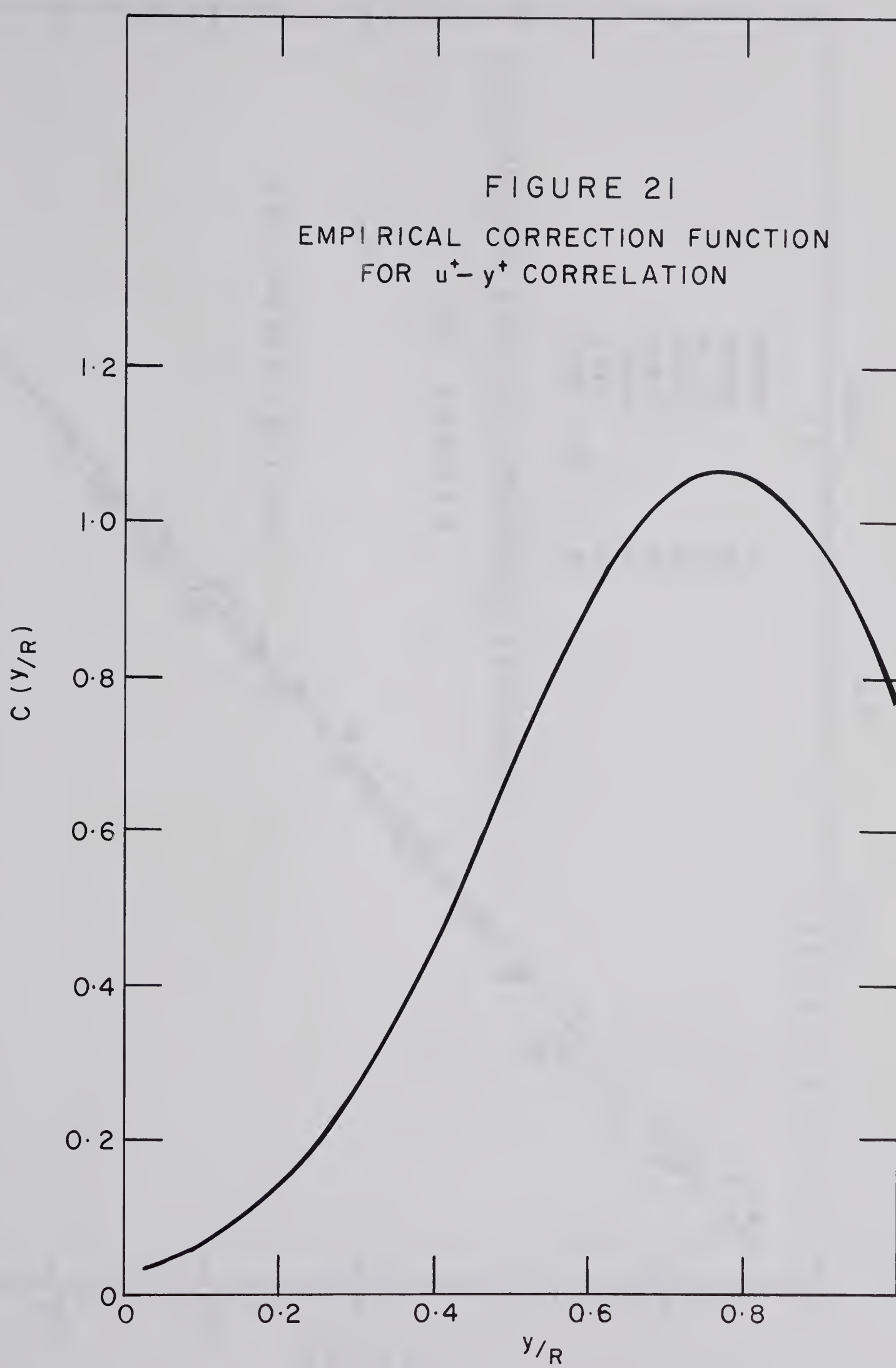


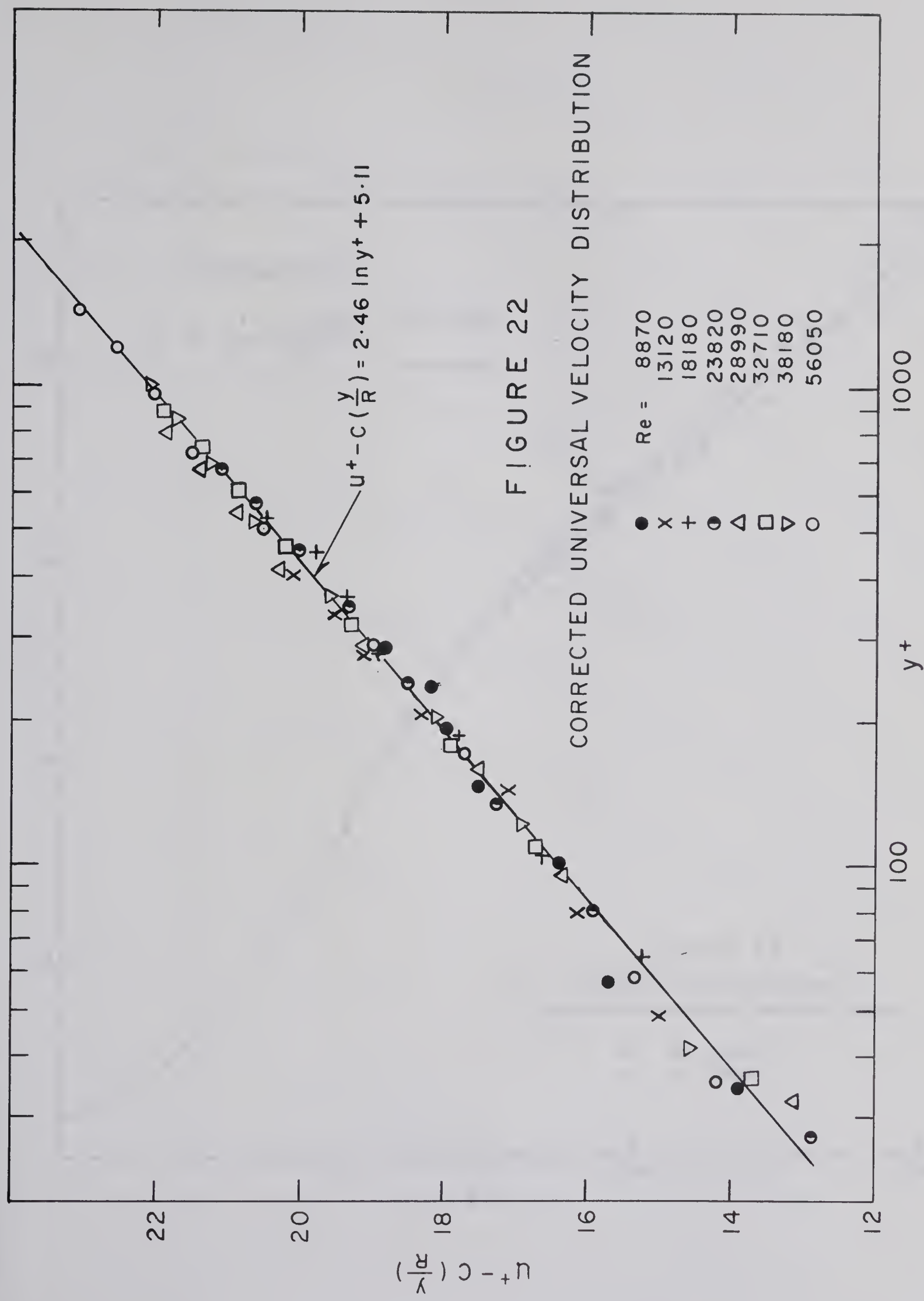
FIGURE 20

UNIVERSAL VELOCITY DISTRIBUTIONS

\bullet $Re = 8870$
 \times 13120
 \oplus 18180
 \bullet 23820
 \triangle 28990
 \square 32710
 ∇ 38180
 \circ 56050

FIGURE 21
EMPIRICAL CORRECTION FUNCTION
FOR $u^+ - y^+$ CORRELATION





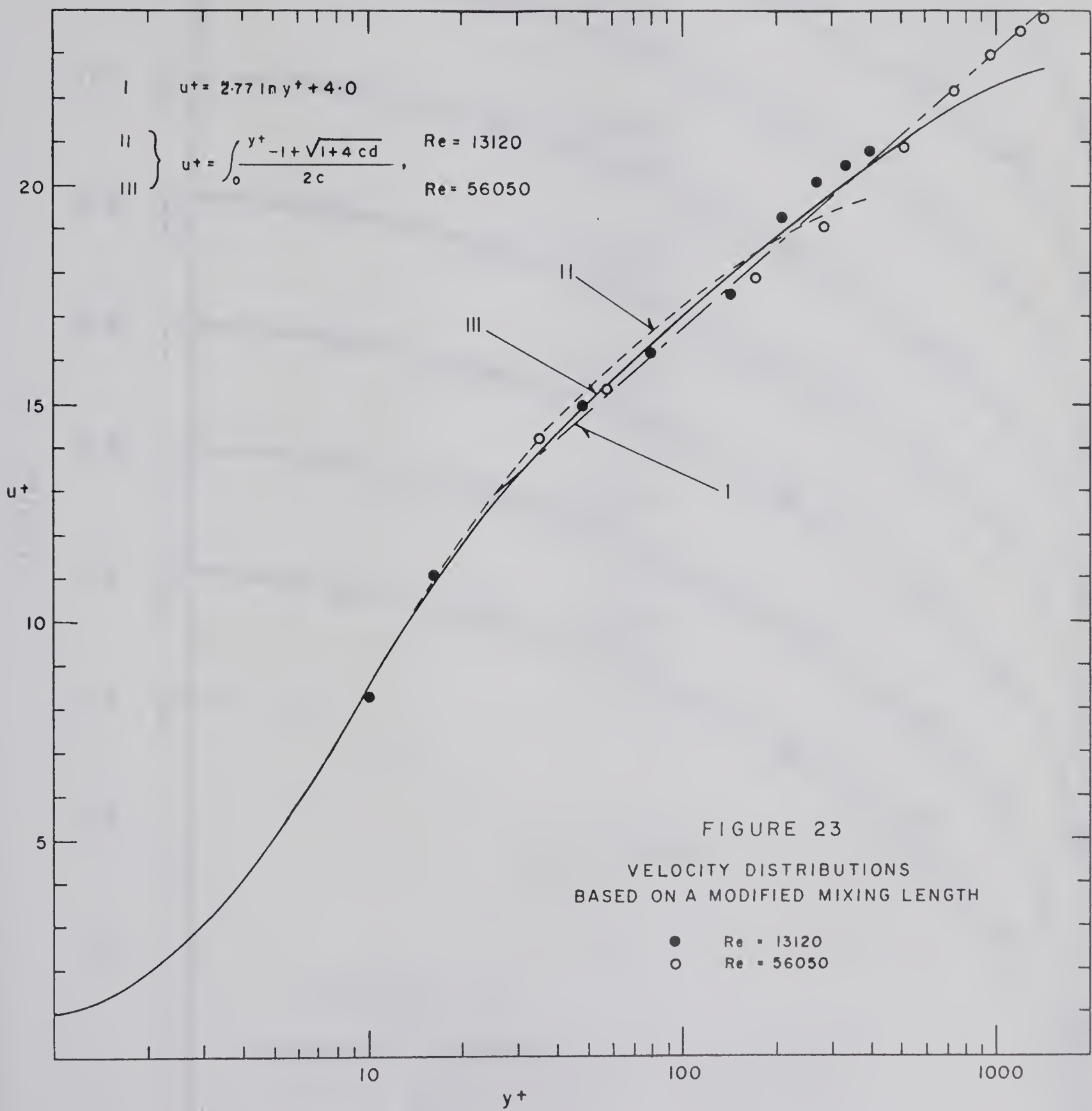


FIGURE 23
VELOCITY DISTRIBUTIONS
BASED ON A MODIFIED MIXING LENGTH

● $Re = 13120$
○ $Re = 56050$

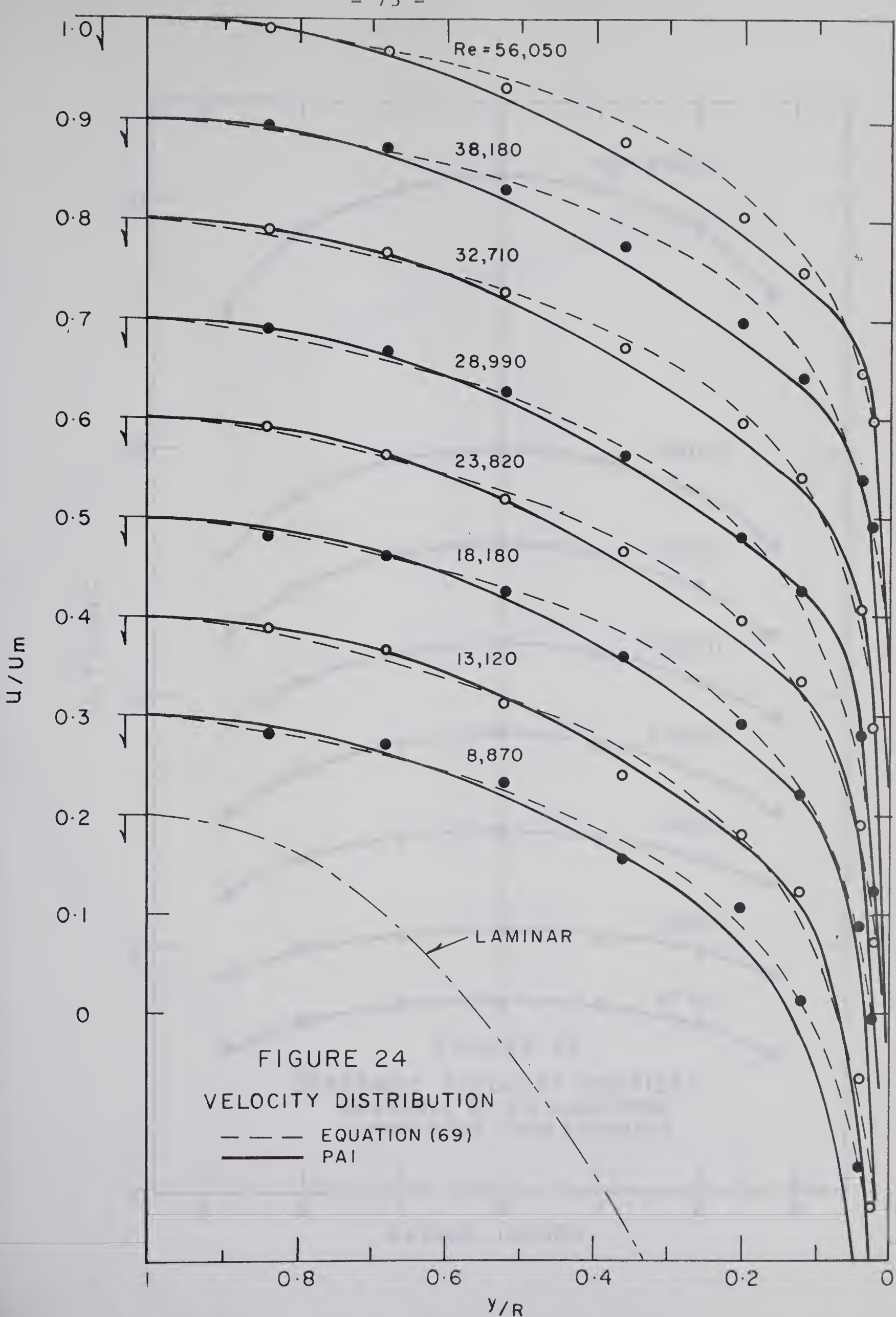
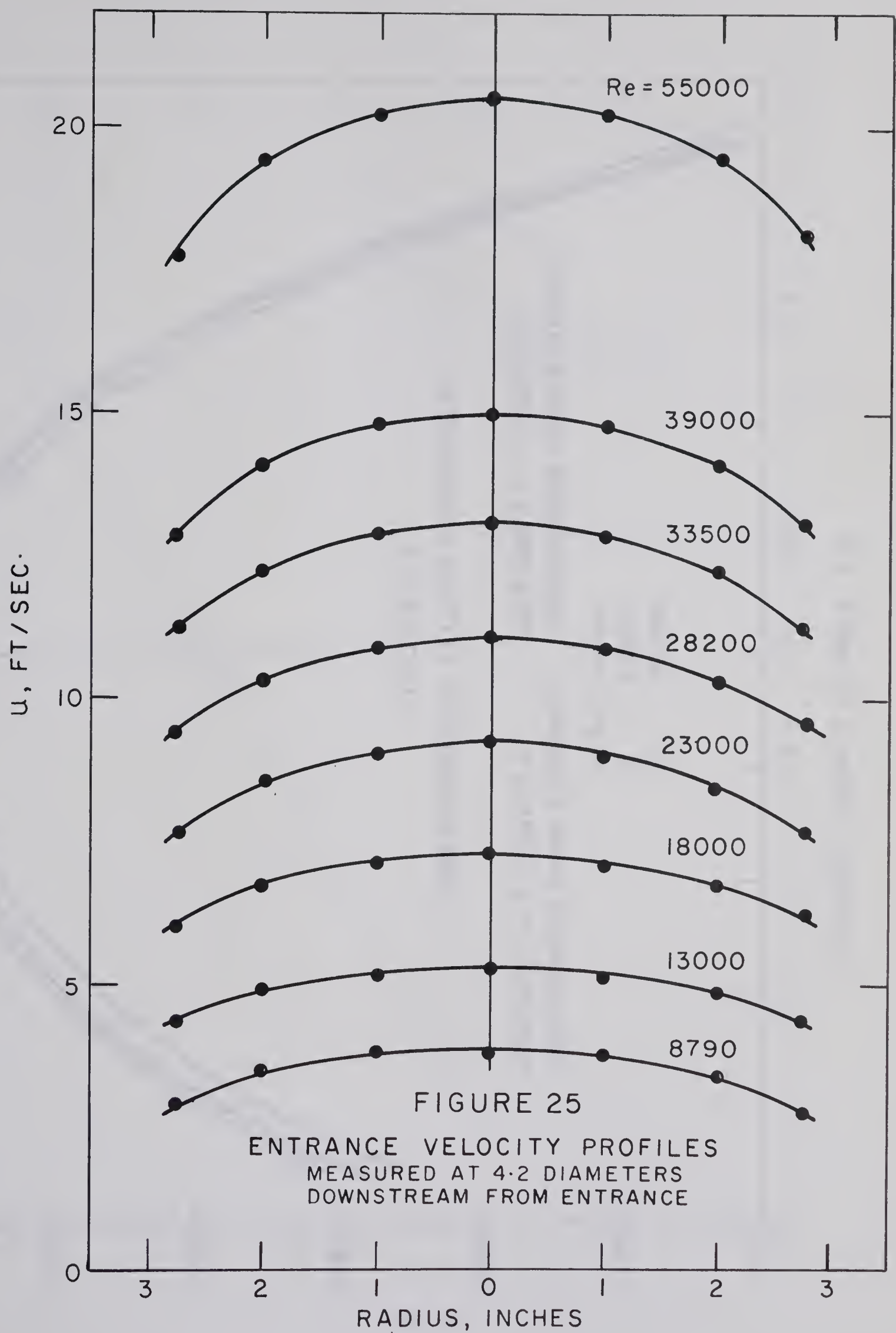
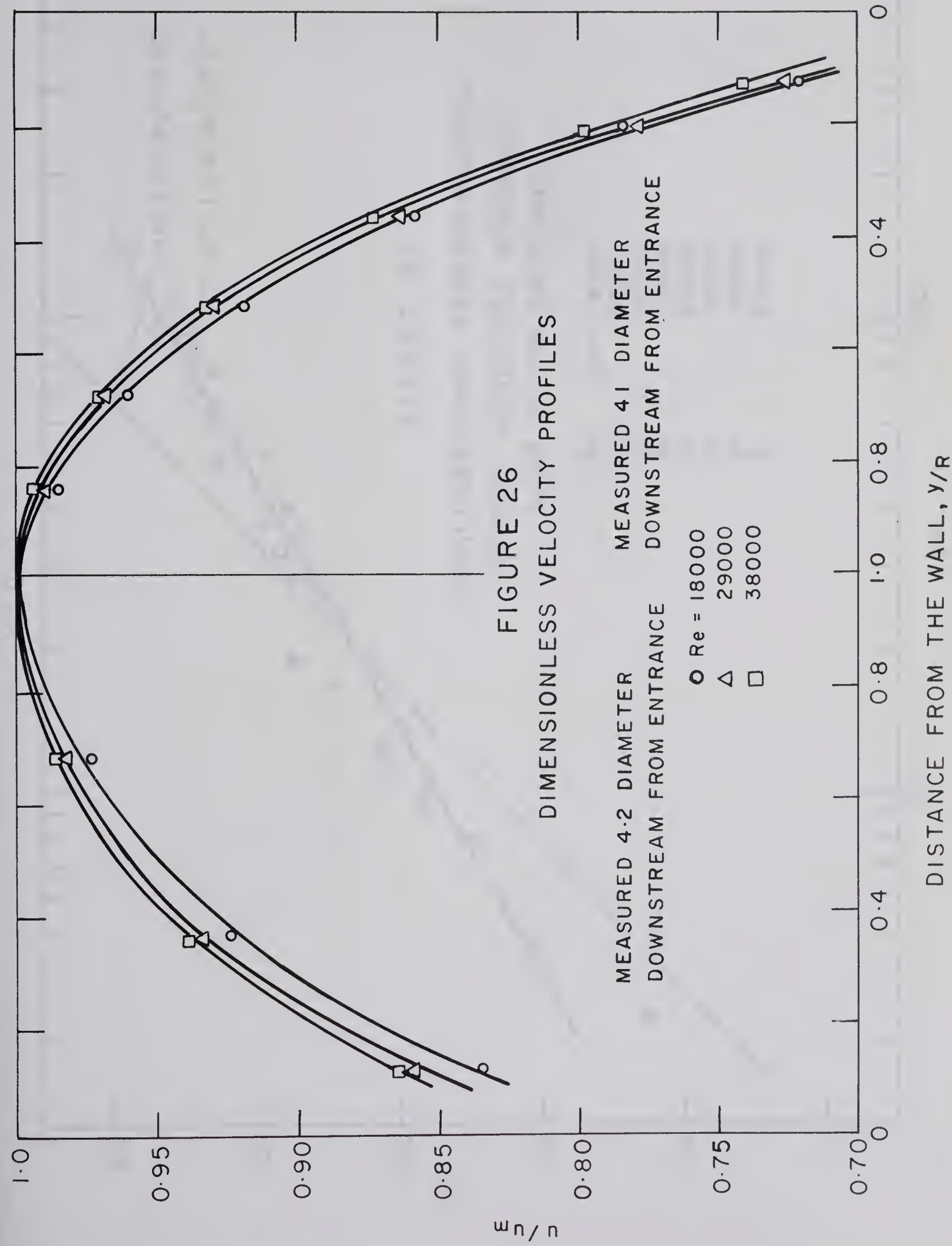


FIGURE 24
VELOCITY DISTRIBUTION

— — — EQUATION (69)
— PAI





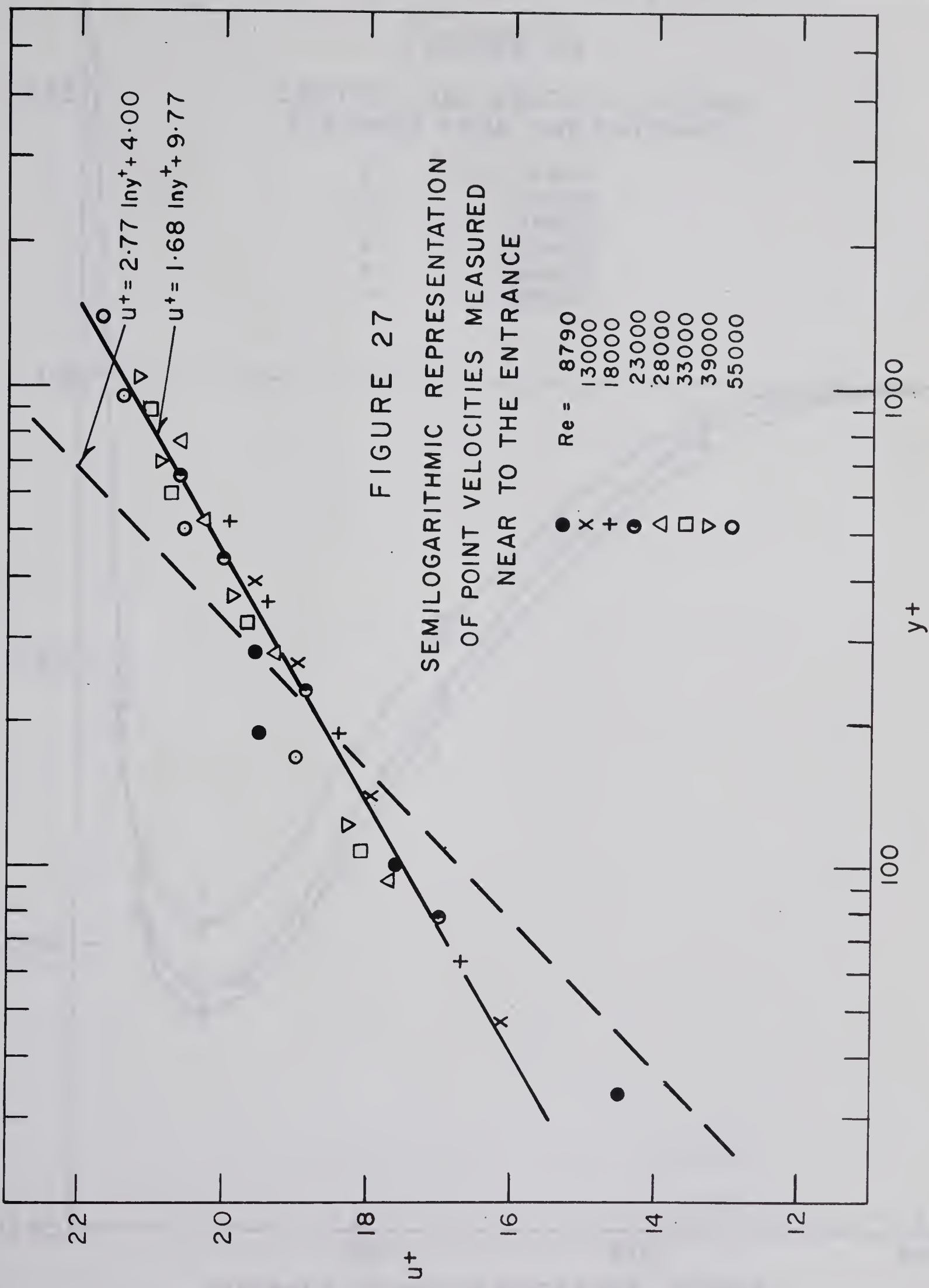
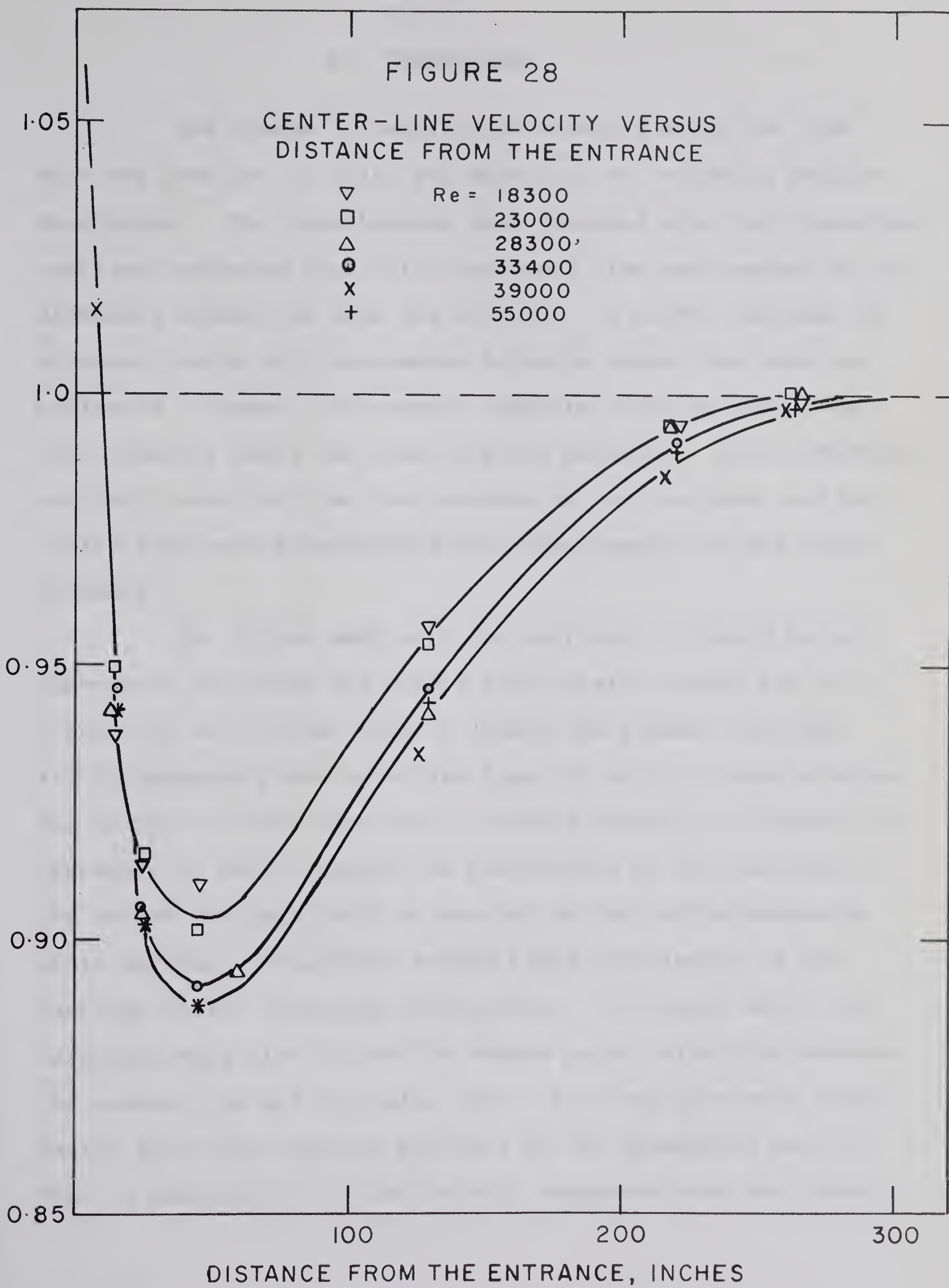


FIGURE 28

CENTER-LINE VELOCITY VERSUS
DISTANCE FROM THE ENTRANCE

▽ $Re = 18300$
□ 23000
△ 28300
○ 33400
X 39000
+ 55000

U/U_{FD}



V. CONCLUSIONS

The change in center-line velocity along the tube axis was used as the basis for measuring the velocity profile development. The experimental data obtained with the travelling carriage indicated that fully developed flow was reached at 40 diameters downstream from the entrance. A slight increase in entrance length with increasing Reynolds number was also experienced. However, no correct absolute value of the center-line velocity along the tube axis was obtained. This uncertainty partially resulted from the presence of the carriage, and partially from errors associated with measurements of the static pressure.

For future work with the carriage, it would be advantageous to extend the probes additionally beyond the carriage, and at the same time to change the present carriage static pressure probe to a disc type(24) static pressure probe. The aluminum 6-inch tube was not always perfectly circular and therefore it would improve the positioning of the carriage if its teflon bearings could be mounted to the carriage-arms on small springs. This would secure rigid positioning of the carriage at all locations in the tube. In further work, the carriage could also be used to obtain point velocities between the center line and the wall, and in this way give more information about the velocity profiles in the developing section. This is believed to be particularly important near the inlet.

A set of 8 velocity profiles under fully developed conditions were measured in the 6.255 in. I.D. aluminum test tube at 41 diameters from the entrance. Various velocity profile relationships were tested and found to correlate the experimental data more or less accurately. Over the range of Reynolds numbers tested, $Re = 9,000$ to $56,000$, an equation based on a derivation of Pai was found to correlate the obtained velocity profiles very well:

$$\frac{u}{u_m} = 1 + a_1 \left(\frac{r}{R}\right)^2 + a_2 \left(\frac{r}{R}\right)^{2M} \quad (42)$$

This equation is more complicated than the logarithmic type of distribution, but it is of an easy form assuming a computer is available. The equation has the great advantage of being valid from the wall to the center line. The improved universal velocity distribution correlation suggested by Bogue, and simplified slightly in the present investigation, was comparable to the Pai correlation, but has the disadvantage of not being valid near the wall. The form of the improved universal velocity distribution which was obtained in the range of Reynolds numbers from 9,000 to 56,000 was

$$u^+ - c \left(\frac{y}{R}\right) = 2.46 \ln y^+ + 5.11 \quad (70)$$

where

$$c \left(\frac{y}{R}\right) = 1.07 \exp \left(\frac{-\left(\frac{y}{R} - 0.77\right)^2}{0.16} \right) \quad (71)$$

However, this velocity distribution could be joined in a continuous manner with one of the equations derived for the region near the wall, if such an extension were desirable.

The data obtained close to the wall were not satisfactory, and the only evident conclusion was that for $y^+ < 25$ viscous effects become significant making the universal velocity distribution no longer valid. This is in agreement with Deissler who found the universal velocity distribution to be valid for $y^+ > 26$. The different equations suggested for the wall region, $y^+ < 26$, still remain to be tested experimentally. However, the present experimental equipment does not provide the accuracy needed in measuring point velocity close to the wall.

The pressure drop data for friction factor calculations were obtained in the upper region of the tube. These results gave slightly higher friction factors than the Blasius friction factor correlation for smooth pipes would predict. However, the region where the pressure drop data were obtained was found to deviate locally from a circular cross-section, and thus the obtained friction factors were questionable. Further investigation of pressure drop along other sections of the tube might clarify the uncertainty regarding the true value of the friction factor. A survey of pressure drop along the tube is restricted by the length of the tube and furthermore by the developing shear stress in the region near the inlet. At low rates, the measurement of pressure drop along the tube becomes greatly restricted by the decreasing accuracy of the micromanometer.

NOMENCLATURE

a_1, a_2	Variables in the Pai correlation
A, B	Constants in the Universal Velocity Distribution
c, d	Variables in the Gill and Scher correlation
C, C'	Constants of integration
$c(y, f), c(y)$	Bogue correction functions
D	Diameter of the tube, in.
F	Cross section of the tube, in ²
f	Blasius friction factor
g_c	Dimensional conversion factor, $1b_m ft/1b_f sec^2$
Δh	Pressure difference, in.
K	Universal constant
l	Mixing length
L	Entrance length, in.
M	Variable in the Pai correlation
n	Power law exponent
n	Constant of proportionality
P	Absolute pressure, lb/ft ²
P_o	Absolute pressure at standard conditions (760 mm Hg and 273°K)
ΔP	Dynamic or impact pressure, lb/ft ²
Q	Flow rate, ft ³ /sec.
Q_o	Flow rate at standard conditions, SCFM
r	Radius, in.
R	Radius of tube, in.
Re	Reynolds number

S	Variable in the Pai correlation
T	Temperature, °R or °K
T ₀	Standard temperature, 273°K
u	Point velocity, ft/sec.
u _{av}	Average or bulk velocity, ft/sec.
u _m	Maximum velocity, ft/sec.
u _{FD}	Fully developed center-line velocity, ft/sec.
u ⁺	Dimensionless velocity
u*	Friction velocity, ft/sec
u ₄ ⁺ , u ₅ ⁺	Universal constants in the Wasan correlation
x	Distance downstream from entrance of tube, in.
y	Distance from the wall, in.
y ⁺	Dimensionless distance from the wall
Y	Expansion factor
€	Coefficient of eddy diffusivity, ft ² /sec.
μ	Dynamic viscosity, lb/ft.sec.
ν	Kinematic viscosity, ft ² /sec.
ρ	Density, lb/ft ³
τ	Shear stress, lb/ft ²
τ _L	Shear stress produced by viscosity, lb/ft ²
τ _T	Shear stress produced by turbulence, lb/ft ²
τ _W	Shear stress at the wall, lb/ft ²
∅	Variable in the Gill and Scher correlation

BIBLIOGRAPHY

1. Bowers, B., "Flow of Gas-Solid Mixtures in Vertical Circular Ducts, I: Calibration and Use of Air Velocity Measuring Devices", M.Sc. thesis, University of Alberta, Edmonton, Alberta, 1963.
2. Sandall, O., "Flow of Gas-Solids Mixtures in a Vertical Circular Duct: II The Aerodynamic Characteristics of the Test Unit", M.Sc. thesis, University of Alberta, Edmonton, Alberta, 1963.
3. Knudsen, J.G., and Katz, D.L., "Fluid Dynamics and Heat Transfer", McGraw-Hill Book Company Inc., New York, N.Y., 1958.
4. Prandtl, L., and Tietjens, O.G., "Applied Hydro- and Aeromechanics", Dover Publications Inc., New York, N.Y., 1957.
5. Hinze, J.O., "Turbulence", McGraw-Hill Book Company Inc., New York, N.Y., Ch. 7, 1959.
6. Schlichting, H., "Boundary Layer Theory", McGraw-Hill Book Company Inc., New York, N.Y., Ch. 19 and 20, 1962.
7. Deissler, R.G., "Analytical and Experimental Investigation of Adiabatic Turbulent Flow in Smooth Tubes", NACA-TN-2138, 1950.
8. Rothfus, R.R., and Monrad, C.C., "Correlation of Turbulent Velocities for Tubes and Parallel Plates", Ind. and Eng. Chem., 47, 1144, 1955.
9. Rothfus, R.R., Archer, D.M., Klimas, I.C. and Sikchi, K.G., "Simplified Flow Calculations for Tubes and Parallel Plates", A.I.Ch.E. Journal, 3, 208, 1957.
10. Bogue, D.C., and Metzner, A.B., "Velocity Profiles in Turbulent Pipe Flow", I & EC Fundamentals, 2, 147, 1963.
11. Bogue, D.C., "Velocity Profiles in Turbulent Non-Newtonian Pipe Flow", Ph.D. Thesis, University of Delaware, Newark, Del., 1960.

12. Wasan, D.T., Tien, C.L., and Wilke, C.R., "Theoretical Correlation of Velocity and Eddy Viscosity for Flow Close to a Pipe Wall", *A.I.Ch.E. Journal*, 9, 567, 1963.
13. Pai, S.I., "On Turbulent Flow Between Parallel Plates", *J. Appl. Mech.*, 20, 109, 1953.
14. Brodkey, R.S., Jon Lee, and Chase, R.C., "A Generalized Velocity Distribution for Non-Newtonian Fluids", *A.I.Ch.E. Journal*, 7, 392, 1961.
15. Brodkey, R.S., "Limitations on a Generalized Velocity Distribution", *A.I.Ch.E. Journal*, 9, 448, 1963.
16. Gill, W.N., and Scher, M., "A Modification of the Momentum Transport Hypothesis", *A.I.Ch.E. Journal*, 7, 61, 1961.
17. Deissler, R.G., "Turbulent Heat Transfer and Friction in the Entrance Regions of Smooth Passages", *Trans. A.S.M.E.*, 77, 1221, 1955.
18. Kirsten, H., "Experimentelle Untersuchungen der Entwicklung der Geschwindigkeitsverteilung der Turbulenten Rohrstroemung", Thesis, Leipzig, 1927.
19. Nunner, W., "Waermeuebergang und Druckabfall in Rauhen Rohren", *VDI - Forschungsheft* No. 455, 1956.
20. Lapidus, L., "Digital Computation for Chemical Engineers", McGraw-Hill Book Company Inc., New York, N.Y., Ch. 2, 1962.
21. Dimmock, N.A., "Cascade Corners for Ducts of Circular Cross-Section", *British Chemical Engineering*, 302 June, 1957.
22. Anonymous, "Methods for Producing Uniform Gas Flow in Processing Equipment", *British Chemical Engineering*, 359, July, 1957.
23. American Gas Association, "Orifice Metering of Natural Gas - Gas Measurement Committee Report No. 3", New York, N.Y., January, 1956.
24. Bradshaw, P., "Experimental Fluid Mechanics", Oxford Permagon Press, 1964.

A P P E N D I X A
EXPERIMENTAL AND CALCULATED DATA

1. Point Velocity Calculations from Pitot Tube Measurements

The standard equation to calculate velocity from measured impact pressure is:

$$u = \sqrt{\frac{2g_c \Delta P}{\rho_{air}}}$$

where

u = air velocity, ft/sec

g_c = 32.17, $lb_m ft/lb_f sec^2$

ΔP = impact pressure, lb/ft^2

ρ_{air} = air density, lb/ft^3

The air density was obtained by assuming the ideal gas law holds

$$\rho_{air} = \rho_{air_0} \frac{T_0}{T} \frac{P}{P_0}$$

where

ρ_{air_0} = 0.0808 lb/ft^3 *

T_0 = $273^{\circ}K$

P_0 = 760 mm Hg

T = $296^{\circ}K$

and $\rho_{air} = 0.98387 (10^{-4}) P$

* Perry, J.H., "Chemical Engineers' Handbook", McGraw-Hill Book Company Inc., New York, N.Y., Fourth Edition, 1963.

The impact pressure was measured in inches of alcohol

$$\Delta P = \rho_{alc} \frac{\Delta h}{12}$$

where

Δh = length of column, in. alc.

ρ_{alc} = density of alcohol, lb/ft^3

Density of the n-Butyl alcohol*

$$\rho_{alc} = 0.8176 - 0.0004 (t^{\circ}F - 50), gr/cm^3$$

At $75^{\circ}F$

$$\rho_{alc} = 0.8076 gr/cm^3 = 50.4185 lb/ft^3$$

At a flowing air temperature of $22^{\circ}C$ and a micromanometer temperature of $75^{\circ}F$

$$u = \sqrt{2.75 (10^6) \frac{\Delta h}{P}}$$

where

Δh = length of column, in. alc.

P = pressure at probe location, mm Hg

The above relation was used for all velocity calculations.

* Flow Corporation, Model MM3 Micromanometer Notes and Instructions, Bulletin No. 19, March 1961.

2. Flow Rate Calculations from Orifice Pressure Drop Measurements

The standard equation to calculate flow rate is

$$Q = CFY \sqrt{\frac{2g_c \Delta P}{\rho_{air}}}$$

Substituting the internal cross section of the orifice,

$$F = \frac{\pi 6.255^2}{(4)(144)}, \text{ ft}^2$$

and the air density

$$\rho_{air} = 0.98387 (10^{-4}) P$$

the standard equation becomes

$$Q = 0.7612 CY \sqrt{\frac{\Delta PT}{P}}$$

Expressed in terms of standard cubic feet per minute,

$$Q_o = 31.73 CY \sqrt{\frac{\Delta PP}{T}}$$

where

Q_o = flow rate, SCFM

C = flow coefficient, dimensionless

Y = expansion factor, dimensionless

ΔP = pressure difference across orifice, mm Hg

P = pressure on upstream side of orifice, mm Hg

T = temperature, °R

3. Friction Factor Calculations from Pressure Drop Measurements

The friction factor for incompressible flow is obtained from the Blasius equation,

$$f = \frac{2g_c}{\rho_{air}} \frac{D}{u_{av}^2} \left(- \frac{dP}{dx} \right)$$

where

$$\left(- \frac{dP}{dx} \right) \approx \frac{\rho_{alc}}{\Delta x} \Delta h = \frac{50.4}{(6)(12)} \Delta h$$

and

$$D = 6.255 \text{ in.}$$

Upon substitution, the friction factor equation becomes

$$f = 28.12 \frac{\Delta h}{\rho_{air} u_{av}^2}$$

where

f = Blasius friction factor, dimensionless

Δh = length of alcohol column, in.

ρ_{air} = air density, lb/ft^3

u_{av} = average velocity, ft/sec

TABLE 1

Entrance Velocity Profiles - Old Vanes

Point of measurement	4.2 diameter
Barometric pressure	708.0 mm Hg
Flowing temperature	531.6 °R
Pressure at probe location	709.3 mm Hg
Orifice pressure	723.1 mm Hg
Orifice pressure difference	9.64 mm Hg
Reynolds number	18,000

Probe Position (in.)		Δh (in. alc.)	u (ft/sec)
0.00		0.0123	6.92
1.00	in	0.0132	7.17
2.00	in	0.0125	6.97
3.00	in	0.0094	6.05
1.00	out	0.0111	6.56
2.00	out	0.0094	6.05
3.00	out	0.0061	4.87

TABLE 2
Entrance Velocity Profiles - New Vanes

Point of measurement	4.2 diameter
Barometric pressure	693.4 mm Hg
Flowing temperature	531.6°R
Pressure at probe location	695.5 mm Hg
Orifice pressure	715.2 mm Hg
Orifice pressure difference	15.3 mm Hg
Reynolds number	23,000

Probe Position (in.)		Δh (in. alc.)	u (ft/sec)
0.00		0.0216	9.25
1.00	in	0.0194	8.77
2.00	in	0.0163	8.04
2.75	in	0.0131	7.20
3.00	in	0.0085	5.81
1.00	out	0.0206	9.04
2.00	out	0.0173	8.28
3.00	out	0.0119	6.86

TABLE 3
Calibration of Orifice

Re	Q_O SCFM	Q_O/C SCFM	C
8,874	35.588	54.944	0.6477
13,117	52.607	81.067	0.6489
18,176	72.898	113.554	0.6420
23,816	95.516	144.288	0.6620
28,987	116.255	176.394	0.6591
32,711	131.191	209.238	0.6270
38,181	153.128	243.383	0.6292
56,045	224.773	355.982	0.6314

TABLE 4
Friction Factor

Re	Δh (in. alc.)	ρ (lbs/ft ³)	u_{av} (ft/sec)	f
8,874	0.0010	0.06835	3.058	0.04399
13,117	0.0017	0.06881	4.49	0.03446
18,176	0.0031	0.06917	6.19	0.03289
23,816	0.0045	0.06883	8.15	0.02767
28,987	0.0063	0.06953	9.82	0.02642
32,711	0.0085	0.07011	10.99	0.02822
38,181	0.0109	0.06972	12.90	0.02641
53,696	0.0197	0.07015	18.03	0.02429

TABLE 5
Traverse at Right Angle

Pt. of measurement 41 diameter
 Baro. press. 702.6 mm Hg
 Flowing temp. 531.6°R
 Press at probe loc. 703.8 mm Hg
 Orifice pressure 718.5 mm Hg
 Orifice press. diff. 9.56 mm Hg
 Reynolds number 18,000

Probe Position (in)	Main Position			At 90°		
	Δh (in. alc.)	u ($\frac{\text{ft}}{\text{sec}}$)	u(av) ($\frac{\text{ft}}{\text{sec}}$)	Δh (in. alc.)	u ($\frac{\text{ft}}{\text{sec}}$)	u(av) ($\frac{\text{ft}}{\text{sec}}$)
0.00	0.0150	7.66	7.66	0.0151	7.68	7.68
0.50 in	0.0145	7.53	7.52	0.0147	7.58	7.59
1.00 in	0.0140	7.40	7.36	0.0142	7.45	7.38
1.50 in	0.0129	7.10	7.09	0.0128	7.07	7.01
2.00 in	0.0110	6.56	6.59	0.0112	6.61	6.58
2.50 in	0.0094	6.06	6.06	0.0092	5.99	5.95
2.75 in	0.0078	5.52	5.52	0.0080	5.59	5.54
3.00 in	0.0050	4.42	4.51	0.0035	3.70	4.20
3.05 in	0.0031	3.48	3.79	0.0010	1.98	2.52
0.50 out	0.0144	7.50		0.0147	7.59	
1.00 out	0.0137	7.32		0.0136	7.30	
1.50 out	0.0128	7.07		0.0123	6.94	
2.00 out	0.0112	6.61		0.0109	6.54	
2.50 out	0.0094	6.06		0.0089	5.91	
2.75 out	0.0078	5.52		0.0077	5.49	
3.00 out	0.0054	4.59		0.0056	4.69	
3.05 out	0.0043	4.10		0.0040	3.96	

TABLE 6
Traverse at Right Angle

Pt. of measurement	4.2 diameter
Baro. press.	705.8 mm Hg
Flowing temp.	531.6°R
Press. at probe loc.	708.1 mm Hg
Orifice press.	754.2 mm Hg
Orifice press. diff.	16.1 mm Hg
Reynolds number	24,000

Probe Position (in.)	Main Position			At 90°		
	Δh	u	u(av)	Δh	u	u(av)
	(in. alc.)	($\frac{ft}{sec}$)	($\frac{ft}{sec}$)	(in. alc.)	($\frac{ft}{sec}$)	($\frac{ft}{sec}$)
0.00	0.0230	9.45	9.45	0.0231	9.47	9.47
1.00 in	0.0221	9.27	9.29	0.219	9.22	9.24
2.00 in	0.0198	8.77	8.77	0.0198	8.77	8.77
2.50 in	-	-	-	0.0182	8.41	8.44
3.00 in	0.0129	7.08	7.15	-	-	-
1.00 out	0.0223	9.31		0.0221	9.26	
2.00 out	0.0198	8.77		0.0198	8.77	
2.50 out	-	-		0.0185	8.47	
3.00 out	0.0134	7.21		-	-	

TABLE 7
Fully Developed Velocity Profile

Pt. of Measurement	41 diameter
Baro. press	695.5 mm Hg
Flowing temp.	531.6°R
Press. at Probe loc.	695.5 mm Hg
Density	0.06835 lbs/ft ³
Orifice press	699.0 mm Hg
Orifice press diff.	2.28 mm Hg
Expansion factor	1.0

Probe Position (in.)	Δh (in. alc.)	u ($\frac{\text{ft}}{\text{sec}}$)	$u(\text{av})$ ($\frac{\text{ft}}{\text{sec}}$)	u_r ($\frac{\text{ft.in.}}{\text{sec}}$)	$\frac{u}{u_m}$
0.00		0.0037	3.82	3.82	1.0000
0.50	in	0.0036	3.77	3.75	0.9817
1.00	in	0.0035	3.72	3.70	0.9686
1.50	in	0.0033	3.61	3.56	0.9319
2.00	in	0.0028	3.33	3.27	0.8560
2.50	in	0.0025	3.14	3.08	0.8063
2.75	in	0.0018	2.67	2.72	0.7120
3.00	in	0.0009	1.89	2.08	0.5445
0.50	out	0.0035	3.72		
1.00	out	0.0034	3.67		
1.50	out	0.0031	3.50		
2.00	out	0.0026	3.21		
2.50	out	0.0023	3.02		
2.75	out	0.0019	2.74		
3.00	out	0.0013	2.27		

Average velocity	3.085 ft/sec
Flow rate	35.588 SCFM
Flow coefficient	0.6477
Reynolds number	8,874
Ratio of av. to max. vel.	0.80
Friction factor	0.04399

TABLE 8
Fully Developed Velocity Profile

Pt. of measurement	41 diameters
Baro. press.	699.6 mm Hg
Flowing temp.	531.6°R
Press. at probe loc.	700.2 mm Hg
Density	0.06881 lbs/ft ³
Orifice press.	707.3 mm Hg
Orifice press. diff.	4.93 mm Hg
Expansion factor	.79

Probe Position (in.)	Δh (in. alc.)	u ($\frac{ft}{sec}$)	$u(av)$ ($\frac{ft}{sec}$)	u_r ($\frac{ft.in.}{sec}$)	$\frac{u}{u_m}$
0.00		0.0082	5.68	5.68	0.0
0.50	in	0.0080	5.60	5.60	2.800
1.00	in	0.0076	5.47	5.49	5.490
1.50	in	0.0068	5.17	5.19	7.785
2.00	in	0.0059	4.81	4.77	9.540
2.50	in	0.0050	4.43	4.43	11.075
2.75	in	0.0043	4.11	4.11	11.3025
3.00	in	0.0020	2.80	3.03	9.090
3.05	in	0.0008	1.77	2.29	6.9845
0.50	out	0.0080	5.60		
1.00	out	0.0077	5.50		
1.50	out	0.0069	5.21		
2.00	out	0.0057	4.73		
2.50	out	0.0050	4.43		
2.75	out	0.0043	4.11		
3.00	out	0.0027	3.26		
3.05	out	0.0020	2.80		
Average velocity				4.49 ft/sec	
Flow rate				52.607 SCFM	
Flow coefficient				0.6489	
Reynolds number				13,117	
Ratio of av. to max. velocity				0.79	
Friction factor				0.03446	

TABLE 9
Fully Developed Velocity Profile

Pt. of measurement	41 diameter
Baro. press.	702.6 mm Hg
Flowing temp.	531.6°R
Press. of probe loc.	703.8 mm Hg
Density	0.06917 lbs/ft ³
Orifice press	718.5 mm Hg
Orifice press. diff.	9.56 mm Hg
Expansion factor	0.9955

Probe Position (in.)	Δh (in. alc.)	u ($\frac{\text{ft}}{\text{sec}}$)	$u(\text{av})$ ($\frac{\text{ft}}{\text{sec}}$)	u_r ($\frac{\text{ft.in.}}{\text{sec}}$)	$\frac{u}{u_m}$
0.00		0.0150	7.66	7.66	0.0
0.50	in	0.0145	7.53	7.52	3.760
1.00	in	0.0140	7.40	7.36	7.360
1.50	in	0.0129	7.10	7.09	10.635
2.00	in	0.0110	6.56	6.59	13.180
2.50	in	0.0094	6.06	6.06	15.150
2.75	in	0.0078	5.52	5.52	15.180
3.00	in	0.0050	4.42	4.51	13.530
3.05	in	0.0031	3.48	3.79	11.5595
					0.4948
0.50	out	0.0144	7.50		
1.00	out	0.0137	7.32		
1.50	out	0.0128	7.07		
2.00	out	0.0112	6.61		
2.50	out	0.0094	6.06		
2.75	out	0.0078	5.52		
3.00	out	0.0054	4.59		
3.05	out	0.0043	4.10		
Average velocity					
6.19 ft/sec					
Flow rate					
72.898 SCFM					
Flow coefficient					
0.6420					
Reynolds number					
18,176					
Ratio of Av. to max. velocity					
0.808					
Friction factor					
0.03289					

TABLE 10
Fully Developed Velocity Profile

Pt. of measurement	41 diameter
Baro. press.	698.2 mm Hg
Flowing temp.	531.6°R
Press. at probe loc.	700.4 mm Hg
Density	0.06883 lbs/ft ³
Orifice press.	722.7 mm Hg
Orifice press. diff.	15.44 mm Hg
Expansion factor	0.9925

Probe Position (in.)	Δh (in. alc.)	u ($\frac{\text{ft}}{\text{sec}}$)	$u(\text{av})$ ($\frac{\text{ft}}{\text{sec}}$)	u_r ($\frac{\text{ft.in.}}{\text{sec}}$)	$\frac{u}{u_m}$
0.00		0.0256	10.03	10.03	1.0000
0.50	in	0.0250	9.91	9.94	0.9910
1.00	in	0.0234	9.59	9.65	0.9621
1.50	in	0.0213	9.15	9.22	0.9192
2.00	in	0.0193	8.70	8.69	0.8664
2.50	in	0.0161	7.95	7.99	0.7966
2.75	in	0.0136	7.31	7.36	0.7338
3.00	in	0.0077	5.50	5.92	0.5902
3.05	in	0.0032	3.55	4.74	0.4726
0.50	out	0.0253	9.97		
1.00	out	0.0240	9.71		
1.50	out	0.0220	9.29		
2.00	out	0.0192	8.68		
2.50	out	0.0164	8.02		
2.75	out	0.0140	7.41		
3.00	out	0.0102	6.33		
3.05	out	0.0090	5.93		

Average velocity	8.15 ft/sec
Flow rate	95.516 SCFM
Flow coefficient	0.6620
Reynolds number	23,816
Ratio of average to max. velocity	0.813
Friction factor	0.02767

TABLE 11
Fully Developed Velocity Profile

Pt. of measurement	41 diameter
Baro. press.	704.3 mm Hg
Flowing temp.	531.6°R
Press. at probe loc.	707.5 mm Hg
Density	0.06953 lbs/ft ³
Orifice press.	740.0 mm Hg
Orifice press. diff.	22.65 mm Hg.
Expansion factor	0.99

Probe Position (in.)	Δh (in. alc.)	u ($\frac{\text{ft}}{\text{sec}}$)	$u(\text{av})$ ($\frac{\text{ft}}{\text{sec}}$)	u_r ($\frac{\text{ft.in.}}{\text{sec}}$)	$\frac{u}{u_m}$
0.00		0.0384	12.22	12.22	0.000
0.50	in	0.0375	12.07	12.10	6.050
1.00	in	0.0356	11.76	11.83	11.830
1.50	in	0.0327	11.27	11.35	17.025
2.00	in	0.0283	10.49	10.54	21.080
2.50	in	0.0231	9.48	9.53	23.825
2.75	in	0.0199	8.79	8.88	24.420
3.00	in	0.0124	6.94	7.11	21.330
3.05	in	0.0052	4.50	5.14	15.677
0.50	out	0.0378	12.12		
1.00	out	0.0364	11.89		
1.50	out	0.0336	11.43		
2.00	out	0.0288	10.58		
2.50	out	0.0236	9.58		
2.75	out	0.0207	8.97		
3.00	out	0.0139	7.27		
3.05	out	0.0086	5.78		

Average velocity	9.82 ft/sec
Flow rate	116.255 SCFM
Flow coefficient	0.6591
Reynolds number	28,987
Ratio of average to max. velocity	0.804
Friction factor	0.02642

TABLE 12

Fully Developed Velocity Profile

Pt. of measurement	41 diameter
Baro. press.	709.0 mm Hg
Flowing temp.	531.6°R
Press. at probe loc.	713.4 mm Hg
Density	0.07011
Orifice press.	760.0 mm Hg
Orifice press. diff.	31.25 mm Hg
Expansion factor	0.9865

Probe Position (in.)	Δh (in. alc.)	u ($\frac{ft}{sec}$)	$u(av)$ ($\frac{ft}{sec}$)	u_r ($\frac{ft.in.}{sec}$)	$\frac{u}{u_m}$
0.00		0.0471	13.47	13.47	1.0000
0.50	in	0.0461	13.33	13.33	0.9896
1.00	in	0.0440	13.02	13.02	0.9666
1.50	in	0.0403	12.46	12.47	0.9258
2.00	in	0.0359	11.76	11.73	0.8708
2.50	in	0.0296	10.68	10.73	0.7966
2.75	in	0.0253	9.88	9.98	0.7409
3.00	in	0.0161	7.88	8.19	0.6080
3.05	in	0.0100	6.21	6.58	0.4885
0.50	out	0.0461	13.33		
1.00	out	0.0439	13.01		
1.50	out	0.0404	12.48		
2.00	out	0.0355	11.70		
2.50	out	0.0301	10.77		
2.75	out	0.0264	10.08		
3.00	out	0.0187	8.49		
3.05	out	0.0125	6.94		

Average velocity	10.99 ft/sec
Flow rate	131.191 SCFM
Flow coefficient	0.6270
Reynolds number	32,711
Ratio of average to max. velocity	0.02822
Friction factor	0.816

TABLE 13

Fully Developed Velocity Profile

Pt. of measurement	41 diameter
Baro. press.	703.0 mm Hg
Flowing temp.	531.6°R
Press. at probe loc.	709.4 mm Hg
Density	0.06972 lbs/ft ³
Orifice press.	774.0 mm Hg
Orifice press. diff.	41.9 mm Hg
Expansion factor	0.982

Probe Position (in.)	Δh (in. alc.)	u ($\frac{\text{ft}}{\text{sec}}$)	$u(\text{av})$ ($\frac{\text{ft}}{\text{sec}}$)	u_r ($\frac{\text{ft.in.}}{\text{sec}}$)	$\frac{u}{u_m}$
0.00		0.0636	15.70	15.70	1.0000
0.50	in	0.0625	15.57	15.61	0.9943
1.00	in	0.0599	15.24	15.24	0.9707
1.50	in	0.0550	14.64	14.62	0.9312
2.00	in	0.0482	13.67	13.71	0.8732
2.50	in	0.0405	12.53	12.52	0.7975
2.75	in	0.0350	11.65	11.63	0.7408
3.00	in	0.0262	10.08	10.02	0.6382
3.05	in	0.0222	9.28	9.28	0.5911
0.50	out	0.0631	15.64		
1.00	out	0.0599	15.24		
1.50	out	0.0549	14.59		
2.00	out	0.0488	13.75		
2.50	out	0.0404	12.51		
2.75	out	0.0347	11.60		
3.00	out	0.0256	9.96		
3.05	out	0.0222	9.28		

Average velocity	12.90 ft/sec
Flow rate	153.128 SCFM
Flow coefficient	0.6292
Reynolds number	38,181
Ratio of average to max. velocity	0.822
Friction factor	0.02641

TABLE 14

Fully Developed Velocity Profile

Pt. of measurement	41 diameter
Baro. press.	699.0 mm Hg
Flowing temp.	531.6°R
Press. at probe loc.	713.0 mm Hg
Density	0.07009 lbs/ft ³
Orifice press.	952.0 mm Hg
Orifice press. diff.	74.0 mm Hg
Expansion factor	0.9745

Probe Position (in.)	Δh (in. alc.)	u ($\frac{ft}{sec}$)	u(av) ($\frac{ft}{sec}$)	ur ($\frac{ft.in}{sec}$)	$\frac{u}{u_m}$
0.00		0.1337	22.71	22.71	1.0000
0.50	in	0.1311	22.49	22.51	0.9912
1.00	in	0.1243	21.90	21.98	0.9679
1.50	in	0.1151	21.07	21.17	0.9322
2.00	in	0.1034	19.97	19.97	0.8793
2.50	in	0.0867	18.28	18.25	0.8036
2.75	in	0.0755	17.06	17.00	0.7486
3.00	in	0.0663	14.73	14.68	0.6464
3.05	in	0.0487	13.71	13.61	0.5993
0.50	out	0.1315	22.52		
1.00	out	0.1262	22.06		
1.50	out	0.1173	21.27		
2.00	out	0.1034	19.97		
2.50	out	0.0861	18.22		
2.75	out	0.0744	16.94		
3.00	out	0.0654	14.62		
3.05	out	0.0473	13.51		

Average velocity	18.84 ft/sec
Flow rate	224.773 SCFM
Flow coefficient	0.6314
Reynolds number	56,045
Ratio of average to max. velocity	0.830

4. Power Law Distribution

The power law distribution is of the following form:

$$\frac{u}{u_m} = \left(\frac{y}{R}\right)^{1/n} \quad (1)$$

The experimental data were correlated by using three sets of n-values. The first two sets were obtained by the method of least squares, as follows:

$$i) \quad n = \frac{\sum_{1}^{9} \left(\frac{y}{R}\right)^2}{\sum_{1}^{9} \left[\ln \left(\frac{y}{R}\right) \ln \left(\frac{u}{u_m}\right) \right]}$$

$$ii) \quad n = \frac{\sum_{1}^{8} \left(\frac{y}{R}\right)^2}{\sum_{1}^{8} \left[\ln \left(\frac{y}{R}\right) \ln \left(\frac{u}{u_m}\right) \right]}$$

The third set of n-values was obtained from equation (61).

$$iii) \quad n = \sqrt{\frac{1}{f}} = \sqrt{\frac{Re^{1/4}}{0.316}}$$

Experimental data and calculated values are given in Tables 15 to 18.

TABLE 15

Power Law Distribution

Equation 1
(9 points)

Point No.	Re	$\frac{y}{R}$	$\frac{u}{u_m}$	$\frac{u}{u_m}$ %	$\frac{u}{u_m}$ deviation	$\frac{u}{u_m}$ %	$\frac{u}{u_m}$ deviation	$\frac{u}{u_m}$ %	$\frac{u}{u_m}$ deviation
1	8,874	1	1.0000	1.0000	0	1.0000	0	1.0000	0
2		0.8401	0.9817	0.9817	-1.1184	0.9691	-1.2885	0.9691	-1.2885
3		0.6803	0.9686	0.9686	-3.3234	0.9329	-3.6907	0.9329	-3.6907
4		0.5204	0.9319	0.9319	-4.0047	0.8883	-4.6222	0.8883	-4.6222
5		0.3605	0.8560	0.8560	-1.8358	0.8319	-2.8204	0.8319	-2.8204
6		0.2006	0.8063	0.8063	-5.7002	0.7484	-7.1852	0.7484	-7.1852
7		0.1207	0.7120	0.7120	-2.0740	0.6828	-4.0936	0.6828	-4.0936
8		0.0408	0.5445	0.5445	6.4240	0.5614	3.1127	0.5614	3.1127

1	13,117	1	1.0000	1.0000	0	1.0000	0	1.0000	0
2		0.8401	0.9859	0.9648	-2.1399	0.9697	-1.6457	0.9705	-1.5616
3		0.6803	0.9665	0.9238	-4.4143	0.9342	-3.3439	0.9359	-3.1611
4		0.5204	0.9137	0.8743	-4.3113	0.8910	-2.4872	0.8938	-2.1743
5		0.3605	0.8398	0.8107	-3.4614	0.8350	-0.5715	0.8392	-0.0726
6		0.2006	0.7799	0.7187	-7.8523	0.7528	-3.4718	0.7588	-2.7082
7		0.1207	0.7236	0.6474	10.5349	0.6882	-4.8954	0.6943	-3.9039
8		0.0408	0.5335	0.5179	-2.9163	0.5681	6.4908	0.5771	8.1750
9		0.0248	0.4032	0.4675	15.9569	0.4675	0.5293	0.5293	31.3979

n = 4.86260

n = 5.65799

n = 5.81950

TABLE 16

Power Law Distribution

Point No.	Re	$\frac{Y}{R}$	Measured	Equation 1 (all 9 points)			Equation 1 (8 points)			Equation 1 (n from eq. 61)		
				$\frac{u}{u_m}$	% deviation	$\frac{u}{u_m}$	% deviation	$\frac{u}{u_m}$	% deviation	$\frac{u}{u_m}$	% deviation	$\frac{u}{u_m}$
18,176	1	1.0000	1.0000	1.0000	0	1.0000	0	1.0000	0	1.0000	0	1.0000
	2	0.8401	0.9817	0.9706	-1.330	0.9729	-0.8974	0.9717	-0.0221	0.9726	-1.8573	0.9726
	3	0.6803	0.9608	0.9361	-2.5702	0.9410	-2.0563	0.9384	-2.3286	0.9404	-2.2544	0.9404
	4	0.5204	0.9256	0.8941	-3.4046	0.9021	-2.5390	0.8979	-2.9980	0.9011	-1.9724	0.9011
	5	0.3605	0.8603	0.8396	-2.4105	0.8513	-1.0411	0.8451	-1.7681	0.8498	-1.9128	0.8498
	6	0.2006	0.7911	0.7593	-4.0186	0.7762	-1.8893	0.7672	-3.0219	0.7740	-2.8399	0.7740
	7	0.1207	0.7206	0.6960	-3.4151	0.7164	-0.5851	0.7055	-2.0928	0.7137	-2.7335	0.7137
	8	0.0408	0.5888	0.5779	-1.8484	0.6037	2.5354	0.5899	0.1918	0.6004	1.7218	0.6004
	9	0.0248	0.4948	0.5306	7.2450	0.5434	0.5434	0.5434	0.8253	0.5545	1.3374	0.5545
23,816	1	1.0000	1.0000	1.0000	0	1.0000	0	1.0000	0	1.0000	0	1.0000
	2	0.8401	0.9910	0.9700	-2.1172	0.9734	-1.7715	0.9726	-1.8573	0.9726	-1.8573	0.9726
	3	0.6803	0.9621	0.9349	-2.8257	0.9422	-2.0652	0.9404	-2.2544	0.9404	-2.2544	0.9404
	4	0.5204	0.9192	0.8922	-2.9418	0.9040	-1.6504	0.9011	-1.9724	0.9011	-1.9724	0.9011
	5	0.3605	0.8664	0.8367	-3.4239	0.8542	-1.4092	0.8498	-1.9128	0.8498	-1.9128	0.8498
	6	0.2006	0.7966	0.7553	-5.1861	0.7802	-2.0532	0.7740	-2.8399	0.7740	-2.8399	0.7740
	7	0.1207	0.7338	0.6911	-5.8132	0.7214	-1.6956	0.7137	-2.7335	0.7137	-2.7335	0.7137
	8	0.0408	0.5902	0.5718	-3.1112	0.6101	3.3686	0.6004	1.7218	0.6004	1.7218	0.6004
	9	0.0248	0.4726	0.5242	10.9190							

TABLE 17

Power Law Distribution

Re	Point No.	Measured $\frac{Y}{R}$	Equation 1 (all 9 points)			Equation 1 (8 points)			Equation 1 (n from eq. 61)		
			u	$\frac{u}{u_m}$	% deviation	u	$\frac{u}{u_m}$	% deviation	u	$\frac{u}{u_m}$	% deviation
29,987	1	1.0000	1.0000	0	0	1.0000	0	0	1.0000	0	0
	2	0.8401	0.9902	0.9673	-2.3136	0.9726	-1.7789	0.9832	0.9418	0.9034	-1.7118
	3	0.6803	0.9681	0.9291	-4.0274	0.9404	-2.8622	0.9427	0.9047	0.8532	-2.7153
	4	0.5204	0.9288	0.8828	-4.9538	0.9010	-2.9889	0.9047	0.8600	0.8244	-2.7401
	5	0.3605	0.8625	0.8230	-4.5740	0.8498	-1.4745	0.8532	0.7739	0.7676	-1.0796
	6	0.2006	0.7799	0.7359	-5.6383	0.7739	-0.7676	0.7788	0.7137	0.7939	-0.1406
	7	0.1207	0.7267	0.6679	-8.0887	0.7137	-1.7939	0.7196	0.6003	3.1735	-0.9763
	8	0.0408	0.5818	0.5430	-6.6658	0.6003	3.1735	0.6078	0.5392	17.4025	4.4758
	9	0.0248	0.4206	0.4938	17.4025	0.5625	0.5625	0.5625	10.3839	33.7438	16.1515
32,711	1	1.0000	1.0000	0	0	1.0000	0	0	1.0000	0	0
	2	0.8401	0.9896	0.9713	-1.8481	0.9746	-1.5176	0.9736	0.9447	0.9234	-1.6122
	3	0.6803	0.9666	0.9377	-2.9929	0.9447	-2.2693	0.9427	0.8600	0.2347	-2.4767
	4	0.5204	0.9258	0.8966	-3.1515	0.9080	-1.9234	0.9047	0.8433	0.2347	-2.2761
	5	0.3605	0.8708	0.8433	-3.1597	0.8600	-1.2347	0.8552	0.7646	0.9936	-1.7889
	6	0.2006	0.7966	0.7646	-4.0148	0.7887	-0.9936	0.7817	0.7024	0.2489	-1.8669
	7	0.1207	0.7409	0.7024	-5.1960	0.7316	-1.2489	0.7232	0.5860	0.6233	-2.3938
	8	0.0408	0.6080	0.5860	-3.6199	0.6233	2.5157	0.6124	0.4885	10.3839	0.7228
	9	0.0248	0.4248	0.5392	10.3839	0.5625	0.5625	0.5625	10.3839	33.7438	16.1515

TABLE 18

Power Law Distribution

TABLE 19
Power Law Exponent-Velocity Ratio

Re	Measured n	Equation (61)		Equation (63)		Equation (43)	
		$\frac{u_{av}}{u_m}$	n	$\frac{u_{av}}{u_m}$	n	$\frac{u_{av}}{u_m}$	n
8,874	5.863	0.800		5.542		0.777	0.766
13,117	4.863	0.790		5.820		0.786	0.779
18,176	5.834	0.808		6.062		0.793	0.789
23,816	5.724	0.813		6.270		0.799	0.796
28,987	5.239	0.804		6.426		0.803	0.801
32,711	5.986	0.816		6.524		0.805	0.804
38,181	7.124	0.822		6.651		0.809	0.807
56,045	7.337	0.830		6.978		0.816	0.816

5. Semilogarithmic Velocity Distribution

$$i) \frac{u_m - u}{u^*} = \frac{1}{K} \ln \left(\frac{Y}{R} \right) \quad (8)$$

$$ii) \frac{u_m - u}{u^*} = \frac{1}{K} \left[\ln \left(1 - \sqrt{1 - \frac{Y}{R}} \right) + \sqrt{1 - \frac{Y}{R}} \right] \quad (12)$$

The constant, K , was assumed to be universal and was calculated by the method of least squares for each of the two equations.

for equation 8

$$K = \frac{\sum_{1}^n \left(\ln \left(\frac{Y}{R} \right) \right)^2}{\sum_{1}^n \left[\frac{u_m - u}{u^*} \left(\ln \left(\frac{Y}{R} \right) \right) \right]}$$

for equation 12

$$K = \frac{\sum_{1}^n \left[\ln \left(1 - \sqrt{1 - \frac{Y}{R}} \right) + \sqrt{1 - \frac{Y}{R}} \right]^2}{\sum_{1}^n \left[\frac{u_m - u}{u^*} \left(\ln \left(1 - \sqrt{1 - \frac{Y}{R}} \right) + \sqrt{1 - \frac{Y}{R}} \right) \right]}$$

Experimental data and calculated values are given in Tables 20 to 23.

TABLE 20

Semilogarithmic Velocity Distribution

Re	$\frac{Y}{R}$	u	Measured		Equation (8)		Equation (12)		Equation (8)		Equation (12)	
			$\frac{u_m - u}{u^*}$	$\frac{u_m - u}{u^*}$	$K = 0.348$	$K = 0.311$	$K = 0.40$	$K = 0.40$	$\frac{u_m - u}{u^*}$	$\frac{u_m - u}{u^*}$	$K = 0.40$	$K = 0.40$
8,874	1.0000	3.82	0.0000	0.0000	0.5008	0.3562	0.4356	0.4356	0.0000	0.0000	0.2769	0.2769
	0.8401	3.75	0.3588	0.5008	1.1073	0.8618	0.9631	0.9631	0.0000	0.0000	0.6699	0.6699
	0.6803	3.70	0.6151	1.1073	1.8775	1.5658	1.6329	1.6329	1.2171	1.2171	2.0205	2.0205
	0.5204	3.56	1.3328	2.8193	2.9327	2.5993	2.5507	2.5507	3.3777	3.3777	4.5956	4.5956
	0.3605	3.27	3.7932	4.6177	4.3454	4.0161	5.2861	5.2861	7.2562	7.2562	8.4907	8.4907
	0.2006	3.08	5.6386	6.0780	5.9123	5.9123	7.9977	7.9977	9.2423	9.2423	10.9233	10.9233
	0.1207	2.72	8.9192	9.1957	9.3351	7.9977	7.9977	7.9977	7.9977	7.9977	7.9977	7.9977
	0.0408	2.08										
13,117	1.0000	5.68	0.0000	0.0000	0.5008	0.3562	0.4356	0.4356	0.0000	0.0000	0.2769	0.2769
	0.8401	5.60	0.2933	0.5008	1.1073	0.8618	0.9631	0.9631	0.0000	0.0000	0.6699	0.6699
	0.6803	5.49	0.6965	1.7963	1.8775	1.5658	1.6329	1.6329	1.2171	1.2171	2.0205	2.0205
	0.5204	5.19	3.3360	2.9327	2.5993	2.5507	2.5507	2.5507	3.3777	3.3777	4.5956	4.5956
	0.3605	4.77	4.5824	4.6177	4.3454	4.0161	5.2861	5.2861	7.2562	7.2562	8.4907	8.4907
	0.2006	4.43	5.7555	6.0780	5.9123	5.9123	7.9977	7.9977	7.9977	7.9977	7.9977	7.9977
	0.1207	4.11	9.7147	9.1957	9.3351	9.3351	10.9233	10.9233	10.9233	10.9233	10.9233	10.9233
	0.0408	3.03										
	0.0248	2.29										

TABLE 21

Semilogarithmic Velocity Distribution

Re	$\frac{Y}{R}$	u	$\frac{u_m - u}{u^*}$	$\frac{u_m - u}{u^*}$	$\frac{u_m - u}{u^*}$	$\frac{u_m - u}{u^*}$	$\frac{u_m - u}{u^*}$
			Measured	Equation (8) $K = 0.348$	Equation (12) $K = 0.311$	Equation (8) $K = 0.40$	Equation (12) $K = 0.40$
18,176	1.0000	7.66	0.0000	0.0000	0.0000	0.0000	0.0000
	0.8401	7.52	0.3878	0.5008	0.3562	0.4356	0.2769
	0.6803	7.36	0.8309	1.1073	0.8618	0.9631	0.6699
	0.5204	7.09	1.5788	1.8775	1.5658	1.6329	1.2171
	0.3605	6.59	2.9637	2.9327	2.5993	2.5507	2.0205
	0.2006	6.06	4.4317	4.6177	4.3454	4.0161	3.3777
	0.1207	5.52	5.9274	6.0780	5.9123	5.2861	4.5956
	0.0408	4.51	8.7249	9.1957	9.3351	7.9977	7.2562
	0.0248	3.79	10.7191	10.6268	10.9233	9.2423	8.4907
23,816	1.0000	10.03	0.0000	0.0000	0.0000	0.0000	0.0000
	0.8401	9.94	0.1958	0.5008	0.3562	0.4356	0.2769
	0.6803	9.65	0.8269	1.1073	0.8618	0.9631	0.6699
	0.5204	9.22	1.7625	1.8775	1.5658	1.6329	1.2171
	0.3605	8.69	2.9158	2.9327	2.5993	2.5507	2.0205
	0.2006	7.99	4.4390	4.6177	4.3454	4.0161	3.3777
	0.1207	7.36	5.8098	6.0780	5.9123	5.2861	4.5956
	0.0408	5.92	8.9432	9.1957	9.3351	7.9977	7.2562
	0.0248	4.74	11.5109	10.6268	10.9233	9.2423	8.4907

TABLE 22

Semilogarithmic Velocity Distribution

Re	$\frac{y}{R}$	u	Measured		Equation (8)	Equation (12)	Equation (8)	Equation (12)	Equation (8)	Equation (12)
			$u_m - u$	u^*	$K = 0.348$	$K = 0.311$	$K = 0.40$	$K = 0.40$	$K = 0.40$	$K = 0.40$
28,987	1.0000	12.22	0.0000	0.0000	0.0000	0.0000	0.0000	0.0000	0.0000	0.0000
	0.8401	12.10	0.2221	0.5008	0.3562	0.4356	0.3562	0.4356	0.2769	0.2769
	0.6803	11.83	0.7218	1.1073	0.8618	0.9631	0.8618	0.9631	0.6699	0.6699
	0.5204	11.35	1.6102	1.8775	1.5658	1.6329	1.5658	1.6329	1.2171	1.2171
	0.3605	10.54	3.1094	2.9327	2.5993	2.5507	2.5993	2.5507	2.0205	2.0205
	0.2006	9.53	4.9787	4.6177	4.3454	4.0161	4.3454	4.0161	3.3777	3.3777
	0.1207	8.88	6.1818	6.0780	5.9123	5.2861	5.9123	5.2861	4.5956	4.5956
	0.0408	7.11	9.4577	9.1957	9.3351	7.9977	9.3351	7.9977	7.2562	7.2562
	0.0248	5.14	13.1038	10.6268	10.9233	9.2423	10.9233	9.2423	8.4907	8.4907
32,711	1.0000	13.47	0.0000	0.0000	0.0000	0.0000	0.0000	0.0000	0.0000	0.0000
	0.8401	13.33	0.2351	0.5008	0.3562	0.4356	0.3562	0.4356	0.2769	0.2769
	0.6803	13.02	0.7555	1.1073	0.8618	0.9631	0.8618	0.9631	0.6699	0.6699
	0.5204	12.47	1.6790	1.8775	1.5658	1.6329	1.5658	1.6329	1.2171	1.2171
	0.3605	11.75	2.9214	2.9327	2.5993	2.5507	2.5993	2.5507	2.0205	2.0205
	0.2006	10.73	4.6004	4.6177	4.3454	4.0161	4.3454	4.0161	3.3777	3.3777
	0.1207	9.98	5.8596	6.0780	5.9123	5.2861	5.9123	5.2861	4.5956	4.5956
	0.0408	8.19	8.8649	9.1957	9.3351	7.9977	9.3351	7.9977	7.2562	7.2562
	0.0248	6.53	11.5680	10.6268	10.9233	9.2423	10.9233	9.2423	8.4907	8.4907

TABLE 23

Semi-logarithmic Velocity Distribution

Re	$\frac{Y}{R}$	u	Measured		Equation (8)	Equation (12)	Equation (8)	Equation (12)	Equation (8)	Equation (12)
			$\frac{u_m - u}{u^*}$	$\frac{u_m - u}{u^*}$	$K = 0.348$	$K = 0.311$	$K = 0.40$	$K = 0.40$	$K = 0.40$	$K = 0.40$
38,181	1.0000	15.70	0.0000	0.0000	0.0000	0.0000	0.0000	0.0000	0.0000	0.0000
	0.8401	15.61	0.1312	0.5008	0.3562	0.4356	0.4356	0.4356	0.4356	0.2769
	0.6803	15.24	0.6708	1.1073	0.8618	0.9631	0.9631	0.9631	0.9631	0.6699
	0.5204	14.62	1.5749	1.8775	1.5658	1.6329	1.6329	1.6329	1.6329	1.2171
	0.3605	13.71	2.9020	2.9327	2.5993	2.5507	2.5507	2.5507	2.5507	2.0205
	0.2006	12.52	4.6373	4.6177	4.3454	4.0161	4.0161	4.0161	4.0161	3.3777
	0.1207	11.63	5.9352	6.0780	5.9123	5.2861	5.2861	5.2861	5.2861	4.5956
	0.0408	10.02	8.2831	9.1957	9.3351	7.9977	7.9977	7.9977	7.9977	7.2562
	0.0243	9.28	9.3622	10.6268	10.9233	9.2423	9.2423	9.2423	9.2423	8.4907
56,045	1.0000	22.71	0.0000	0.0000	0.0000	0.0000	0.0000	0.0000	0.0000	0.0000
	0.8401	22.51	0.2095	0.5008	0.3562	0.4356	0.4356	0.4356	0.4356	0.2769
	0.6803	21.98	0.7647	1.1073	0.8618	0.9631	0.9631	0.9631	0.9631	0.6699
	0.5204	21.17	1.6133	1.8775	1.5658	1.6329	1.6329	1.6329	1.6329	1.2171
	0.3605	19.97	2.8704	2.9327	2.5993	2.5507	2.5507	2.5507	2.5507	2.0205
	0.2006	18.25	4.6722	4.6177	4.3454	4.0161	4.0161	4.0161	4.0161	3.3777
	0.1207	17.00	5.9817	6.0780	5.9123	5.2861	5.2861	5.2861	5.2861	4.5956
	0.0408	14.68	8.4121	9.1957	9.3351	7.9977	7.9977	7.9977	7.9977	7.2562
	0.0243	13.61	9.5330	10.6268	10.9233	9.2423	9.2423	9.2423	9.2423	8.4907

6. Universal Velocity Distribution

$$i) \quad u^+ = A \ln y^+ + B \quad (64)$$

The constants A and B were assumed to be universal and were obtained by the method of least squares

$$A = \frac{\sum_{1}^n u^+ \ln y^+ - \frac{1}{n} \sum_{1}^n u^+ \sum_{1}^n \ln y^+}{\sum_{1}^n (\ln y^+)^2 - \frac{1}{n} \left(\sum_{1}^n \ln y^+ \right)^2}$$

$$B = \frac{1}{n} \sum_{1}^n u^+ - \frac{A}{n} \sum_{1}^n \ln y^+$$

$$ii) \quad u^+ - C \left(\frac{Y}{R} \right) = A' \ln y^+ + B' \quad (70)$$

The constants A' and B' were obtained as above, while the correction function, $C(y/R)$, was determined by a simple trial-and-error procedure. The criterion used for a best fit was the minimum of the sum of the absolute values of percent error.

$$A' = \left[\frac{1}{n} \sum_{1}^n C \left(\frac{Y}{R} \right) \sum_{1}^n \ln y^+ + \sum_{1}^n u^+ \ln y^+ - \frac{1}{n} \sum_{1}^n u^+ \sum_{1}^n \ln y^+ \right. \\ \left. - \sum_{1}^n C \left(\frac{Y}{R} \right) \ln y^+ \right] / \left[\sum_{1}^n (\ln y^+)^2 - \frac{1}{n} \left(\sum_{1}^n \ln y^+ \right)^2 \right]$$

$$B' = \frac{1}{n} \left(\sum_{l=1}^n u^+ - \sum_{l=1}^n c \left(\frac{y}{R} \right) - A \sum_{l=1}^n \ln y^+ \right)$$

n = 62 = measured points.

TABLE 24

Universal Velocity Distribution

Re	u (ft/sec)	y (in.)	Equation (64)		Equation (70)	
			u ⁺	y ⁺	u ⁺ - C(Y/R)	% Deviation
8,874	2.080	0.1275	10.662	11.539	-1.3262	-0.4473
	2.720	0.3775	13.943	34.165	-3.9612	-3.7517
	3.080	0.6275	15.788	56.790	0.1236	0.6595
	3.270	1.1275	16.762	102.041	-2.4721	-0.6723
	3.560	1.6275	18.249	147.293	-2.2573	0.5897
	3.700	2.1275	18.966	192.544	-0.5248	2.0567
	3.750	2.6275	19.223	237.795	0.1118	1.0038
	3.820	3.1275	19.581	283.046		
13,117	2.290	0.0775	8.395	9.874	-2.4142	-2.2873
	3.030	0.1275	11.108	16.244	-0.8127	-1.2462
	4.110	0.3775	15.067	48.095	14.9902	1.3820
	4.430	0.6275	16.240	79.945	17.1113	-1.4891
	4.770	1.1275	17.486	143.647	18.3013	-3.1923
	5.190	1.6275	19.026	207.348	19.1085	-2.2513
	5.490	2.1275	20.126	271.050	19.4916	-0.3382
	5.600	2.6275	20.529	334.751	20.0537	-1.3152
	5.680	3.1275	20.822	398.453		-0.9734

TABLE 25

Universal Velocity Distribution

Re	u (ft/sec)	$\frac{y}{R}$ (in.)	u^+	$\frac{u^+}{\sqrt{y}}$	Equation (64)		Equation (70)	
					% Deviation	% Deviation	% Deviation	% Deviation
18,176	3.790	0.0775	10.498	13.135	1.3281	0.8876	0.6686	-0.2655
	4.510	0.1275	12.492	21.610				
	5.520	0.3775	15.289	63.982				
	6.060	0.6275	16.785	106.355				
	6.590	1.1275	18.253	191.099				
	7.090	1.6275	19.638	275.844				
	7.360	2.1275	20.386	360.589				
	7.520	2.6275	20.829	445.334				
	7.660	3.1275	21.217	530.078				
				20.4479				
23,816	4.740	0.0775	10.314	16.639	2.0458	3.2210	0.8175	-0.0499
	5.920	0.1275	12.882	27.374				
	7.360	0.3775	16.015	81.050				
	7.990	0.6275	17.386	134.725				
	8.690	1.1275	18.909	242.076				
	9.220	1.6275	20.062	349.427				
	9.650	2.1275	20.998	456.778				
	9.940	2.6275	21.629	564.128				
	10.030	3.1275	21.825	671.479				
				21.0562				

TABLE 26

Universal Velocity Distribution

Re	u (ft/sec)	Y (in.)	u ⁺	Y ⁺	u ⁺ - C($\frac{Y}{R}$)		% Deviation	Equation (70)
					Equation (64)	% Deviation		
28,987	5.140	0.0775	9.513	19.761	3.5047	4.2597	4.2597	4.2597
	7.110	0.1275	13.159	32.510	1.1318	-0.0299		
	8.880	0.3775	16.435	96.254	2.1989	0.6092		
	9.530	0.6275	17.638	159.999	17.4973	-0.4361		
	10.540	1.1275	19.508	287.488	19.1325	-1.6466		
	11.350	1.6275	21.007	414.977	20.2820	-2.2547		
	11.830	2.1275	21.895	542.466	20.8778	-1.2202		
	12.100	2.6275	22.395	669.955	21.3574	-1.8300		
	12.220	3.1275	22.617	797.444	21.8483	-0.6648		
	6.580	0.0775	11.048	21.965	13.7121	1.1800		
	8.190	0.1275	13.751	36.136	16.6793	0.9411		
	9.980	0.3775	16.756	106.992	17.8742	1.6838		
	10.730	0.6275	18.015	177.848	319.559	1.3190		
32,711	11.730	1.1275	19.694	461.270	20.2118	0.0798	0.0015	0.0015
	12.470	1.6275	20.937	21.860	602.981	20.8426		
	13.020	2.1275	22.381	744.692	21.3429	-0.7598		
	13.330	2.6275	22.616	386.404	21.8468	-0.4603		
	13.470	3.1275	22.616	0.6346	0.6346	-0.1207		

TABLE 27

Universal Velocity Distribution

Re	$\frac{u}{f_t}$ (sec)	$\frac{y}{V}$ (in.)	u^+	y^+	Equation (64)		Equation (70)	
					% Deviation	% Deviation	% Deviation	% Deviation
38,181	9.280	0.0775	13.533	25.147	-2.2247	-2.0440	-2.9332	0.3773
	10.020	0.1275	14.612	41.371	1.9332	0.3773	1.9332	0.3773
	11.630	0.3775	16.960	122.492	2.3818	0.4465	2.3818	0.4465
	12.520	0.6275	18.258	203.612	1.5984	0.1149	1.5984	0.1149
	13.710	1.1275	19.993	365.853	0.0339	-0.2380	0.0339	-0.2380
	14.620	1.6275	21.320	528.094	-0.7032	-0.0123	-0.7032	-0.0123
	15.240	2.1275	22.224	690.335	-0.4933	-0.0109	-0.4933	-0.0109
	15.610	2.6275	22.764	852.575	22.1263	0.1148	22.1263	0.1148
	15.700	3.1275	22.895	1014.816	1.0397		1.0397	
56,045	13.610	0.0775	14.258	35.184	14.2243	-2.9351	-2.4431	-2.4431
	14.680	0.1275	15.378	57.883	15.3399	-1.0605	-1.5497	-1.5497
	17.000	0.3775	17.809	171.380	17.7321	2.2871	0.2346	0.2346
	18.250	0.6275	19.118	284.877	18.9773	2.6293	0.2496	0.2496
	19.970	1.1275	20.920	511.870	20.5450	1.5340	-0.3695	-0.3695
	21.170	1.6275	22.177	738.864	21.4524	0.3540	-0.3657	-0.3657
	21.980	2.1275	23.026	965.857	22.0084	-0.1277	0.0978	0.0978
	22.510	2.6275	23.581	1192.851	22.5434	-0.0045	0.0302	0.0302
	22.710	3.1275	23.791	1419.844	23.0218	1.1391	-0.1781	-0.1781

7. Velocity Distribution Close to the Wall

Derivation of equation (65)

a) $u^+ = A \ln y^+ + B$, equation (64), valid at distance from the wall.

b) $u^+ = y^+ + Cy^+^4 + Dy^+^5$, equation (32), valid close to the wall

A smooth transition should occur at $y^+ = y_1^+$.

Equation a gives for the first and second derivatives:

$$c) \frac{du^+}{dy^+} = \frac{A}{y^+}$$

$$d) \frac{d^2u^+}{dy^+^2} = - \frac{A}{y^+^2}$$

Equation b gives for the first and second derivatives:

$$e) \frac{du^+}{dy^+} = 1 + 4C y^+^3 + 5D y^+^4$$

$$f) \frac{d^2u^+}{dy^+^2} = 12C y^+^2 + 20D y^+^3$$

Equate c and e and solve for C,

$$g) C = \frac{A}{4y_1^+^4} - \frac{5}{4} D y_1^+ - \frac{1}{4y_1^+^3}$$

Equate d and f and solve for C,

$$h) C = - \frac{A}{12y_1^+^4} - \frac{20}{12} D y_1^+$$

Equate g and h and solve for D,

$$i) D = \frac{3}{5} \frac{1}{y_1^+ 4} - \frac{4}{5} \frac{A}{y_1^+ 5}$$

Substituting expression for D back into equation h and obtain for C,

$$j) C = \frac{15}{12} A \frac{1}{y_1^+ 4} - \frac{1}{y_1^+ 3}$$

Finally, equating equation a and b and substituting for C and D from equations i and j, an equation with only y_1^+ as the unknown is obtained:

$$k) \ln y_1^+ - \frac{3}{5} \frac{1}{A} y_1^+ = - \frac{B}{A} + \frac{9}{20}$$

Based on the presently obtained constants A and B,

$$l) \ln y_1^+ - 0.217 y_1^+ = - 0.994$$

By trial-and-error solution,

$$y_1^+ \sim 18$$

the point at which a smooth transition should occur. The value of the constants are

$$C = - 1.403 (10^{-4})$$

$$D = 4.55 (10^{-6})$$

The correlation valid for $y^+ < 18$ is

$$u^+ = y^+ - 1.403 (10^{-4}) (y^+)^4 + 4.55 (10^{-6}) (y^+)^5$$

Calculated values are given in Table 28.

TABLE 28

Velocity Distribution Close to the Wall

y^+	Equation (31)	y^+	Equation (33)	Equation (35)
u^+	u^+	u^+	u^+	u^+
1.8607	1.835	1.0	1.000	1.000
2.8360	2.753	2.0	1.998	1.998
4.9897	4.588	4.0	3.976	3.969
9.1236	7.340	5.0	4.944	4.927
12.9388	9.175	7.0	6.801	6.740
18.1833	11.010	10.0	9.260	9.052
21.5816	11.930	15.0	12.036	11.352
25.6905	12.840	20.0	13.056	12.112
30.6900	13.760	25.0	13.965	14.629
33.5933	14.220			

8. Universal Velocity Distribution of Gill and Scher

The numerical integration of equation (39) was performed with a 4th order Legendre-Gauss quadrature formula, which is exact for a 7th degree polynomial. The computer program used to obtain the values given in Tables 29 to 32 is shown in the next two pages. Changing the limit of convergence from 1% to 0.1% barely changed the computed velocity profile. The time required in the latter case was 6 minutes and 12 seconds. A numerical integration using the trapezoidal rule was initially attempted but it required more than 50,000 increments and more than 1/2 hour of computing time to obtain the same convergence, hence it was discarded.


```

CC=(F*XK*(1.-EXP(-PF*XK/YM)))*2
D=1.-XK/YM
IF (D.GT.0.0) GO TO 131
X1=0.0
GO TO 132
131 X1=(-1.+SQRT(1.+4.*CC*D))/2./CC
132 XK=H/2.*(.1.+.8611363115)+A
CC=(F*XK*(1.-EXP(-PF*XK/YM)))*2
D=1.-XK/YM
IF (D.GT.0.0) GO TO 133
X2=0.0
GO TO 134
133 X2=(-1.+SQRT(1.+4.*CC*D))/2./CC
134 XK=H/2.*(.1.-.3399810435)+A
CC=(F*XK*(1.-EXP(-PF*XK/YM)))*2
D=1.-XK/YM
IF (D.GT.0.0) GO TO 135
X3=0.0
GO TO 136
135 X3=(-1.+SQRT(1.+4.*CC*D))/2./CC
136 XK=H/2.*(.1.+.3399810435)+A
CC=(F*XK*(1.-EXP(-PF*XK/YM)))*2
D=1.-XK/YM
IF (D.GT.0.0) GO TO 137
X4=0.0
GO TO 138
137 X4=(-1.+SQRT(1.+4.*CC*D))/2./CC
138 SUM=H/2.*(.3478548451*(X1+X2)+.6521451548*(X3+X4))
UC=UC+SUM
A=A+H
IF (K.LT.N) GO TO 130
DFL=ARS(UC-UPC(I,J))*100./UC
IF (DFL.LT..1) GO TO 103
UPC(I,J)=UC
N=N*2
FN=FN*2.
GO TO 101
103 UPC(I,J)=UC
E=UPC(I,J)-UP(I,J)
FP=100.*E/UP(I,J)
ERROR=ERROR+ARS(FP)
WRITE(6,7) J,N,H,YP(I,J),UP(I,J),UPC(I,J),E,FP,ERROR
IF (I.EQ.8) GO TO 109
IF (J.LT.9) GO TO 104
GO TO 105
109 IF (J.LT.8) GO TO 104
CALL EXIT
END

```


GILL AND SCHER - LEGENDRE GAUSS INTEGRATION

```

DIMENSION VI(9),P(9),UP(9,9),U(9,9),UPC(9,9),US(9),UA(9),Y(9,9),YP
1(9,9),RF(9),BF(9)
1 FORMAT (1X,9F7.4)
2 FORMAT (1X,8F7.1)
3 FORMAT (1X,8F6.3)
4 FORMAT (1X,8F6.1)
5 FORMAT (1H1HI,3X,5HRF(I),12X,2HYM,9X,1HJ,6X,1HN,7X,1HH,7X,7HYP(I,
1J),3X,7HUP(I,J),2X,8HUPC(I,J))
6 FORMAT (1H1X,I2,2X,F8.1,2X,F10.4)
7 FORMAT (1H 34X,I2,1X,I6,1X,F8.4,2X,F9.3,2X,F7.3,3X,F8.4,F9.5,F9.5,
1F10.5)
READ (5,1) ((U(I,J),J=1,9),I=1,8)
READ (5,1) ((Y(I,J),J=1,9),I=1,8)
READ (5,2) (RE(I),I=1,8)
READ (5,3) (UA(I),I=1,8)
RFAD (5,4) (P(I),I=1,8)
C=.316
F=.36
FF=23.
WRITE (6,5)
I=0
31 I=I+1
RF(I)=C/RF(I)**.25
US(I)=UA(I)*SQRT(RF(I)/8.)
VI(I)=.124933/P(I)
J=0
30 J=J+1
UP(I,J)=U(I,J)/US(I)
YP(I,J)=Y(I,J)*US(I)/VI(I)/12.
IF (I.EQ.8) GO TO 32
IF (J.LT.9) GO TO 30
GO TO 31
32 IF (J.LT.8) GO TO 30
140 I=0
105 I=I+1
YM=RF(I)/2.*SQRT(RF(I)/8.)
WRITE (6,6) I,RE(I),YM
J=0
FRROR=0.0
104 J=J+1
N=10
EN=10.
UPC(I,J)=0.0
101 H=YP(I,J)/EN
UC=0.0
PF=(YM-60.)/FF
SUM=0.0
A=0.0
K=0
130 K=K+1
XF=H/2.*(1.-.8611363115)+A

```


TABLE 29

Velocity Distribution of Gill and Scher

Equation (66)	Point No.	No. of Increments	Measured	Equation (39)	% Deviation
Re	y_m^+		y^+	u^+	
8,874	283.0564	1	11.539	10.662	-12.23233
		2	34.165	13.943	2.70229
		3	56.790	15.788	1.00822
		4	102.041	16.762	3.89458
		5	147.293	18.249	-0.38942
		6	192.544	18.966	-1.69165
		7	237.795	19.223	-1.53185
		8	283.046	19.581	-2.67838
		9	334.751	19.0569	
13,117	398.4499	1	9.874	8.395	0.04658
		2	16.244	11.108	-0.52255
		3	48.095	15.067	1.14850
		4	79.945	16.240	2.42738
		5	143.647	17.486	3.09298
		6	207.348	19.026	-1.26895
		7	271.050	20.126	-4.33717
		8	334.751	20.529	-4.83032
		9	398.4499	20.822	-5.55304

TABLE 30

Velocity Distribution of Gill and Scher

Re	y_m^+	Point No.	N	y^+	Measured		u^+	u^+	% Deviation
					No. of Increments	Equation (39)			
18,176	530.0655	1	320	13.135	10.498	9.9084	-5.61239	-5.61239	-2.04346
		2	320	21.610	12.492	12.2365	-4.15351	-4.15351	
		3	20	63.982	15.289	15.9243	2.76127	2.76127	
		4	20	106.355	16.785	17.2485	2.03922	2.03922	
		5	20	191.099	18.253	18.6252	-1.28823	-1.28823	
		6	40	275.844	19.638	19.3849	-2.61288	-2.61288	
		7	40	360.589	20.386	19.8531	-3.31347	-3.31347	
		8	80	445.334	20.829	20.1387	-4.46831	-4.46831	
		9	80	530.078	21.217	20.2686			
23,816	671.4733	1	1280	16.639	10.314	11.0242	6.88458	6.88458	
		2	320	27.374	12.882	13.0841	1.57081	1.57081	
		3	20	81.050	16.015	16.4934	2.98664	2.98664	
		4	20	134.725	17.386	17.7876	2.30993	2.30993	
		5	40	242.076	18.909	19.1639	1.34739	1.34739	
		6	40	349.427	20.062	19.9243	-0.68841	-0.68841	
		7	20	456.778	20.998	20.3591	-3.04293	-3.04293	
		8	80	564.128	21.629	20.6799	-4.38841	-4.38841	
		9	80	671.479	21.825	20.8097	-4.65195	-4.65195	

TABLE 31

Velocity Distribution of Gill and Scher

Equation (66)	Point No.	N	y^+	No. of Increments		Measured	Equation (39)	%
				Re	y^+ y_m			
28,987	797.4371	1	640	19.761	9.513	11.7574	23.58946	
		2	20	32.510	13.159	13.7320	4.35185	
		3	20	96.254	16.435	16.9089	2.88120	
		4	40	159.999	17.638	18.1980	3.17259	
		5	40	287.488	19.508	19.5735	0.33749	
		6	40	414.977	21.007	20.3344	-3.20103	
		7	80	542.466	21.895	20.8041	-4.98366	
		8	80	669.955	22.395	21.0898	-5.82783	
		9	80	797.444	22.617	21.2200	-6.17710	
32,711	886.3916	1	1280	21.965	11.048	12.1758	10.21267	
		2	2560	36.136	13.751	14.0037	1.83992	
		3	20	106.992	16.756	17.1672	2.45417	
		4	20	177.848	18.015	18.4528	2.42869	
		5	40	319.559	19.694	19.8308	0.69362	
		6	80	461.270	20.937	20.5925	-1.64353	
		7	80	602.981	21.860	21.0626	-3.64804	
		8	80	744.692	22.381	21.3481	-4.61299	
		9	40	886.404	22.616	21.4518	-5.14589	

TABLE 32

Velocity Distribution of Gill and Scher

Re	y^+_{m}	Point No.	N	y^+	Measured	Equation (39)		% Deviation
						No. of Increments	u^+	
38,181	1014.8105	1	640	25.147	13.533	12.6982	-6.16785	
		2	20	41.371	14.612	14.4602	-1.03876	
		3	20	122.492	16.960	17.5024	3.19906	
		4	20	203.612	18.258	18.7871	2.89954	
		5	40	365.853	19.993	20.1660	0.86484	
		6	80	528.094	21.320	20.9290	-1.83441	
		7	80	690.335	22.224	21.3983	-3.71659	
		8	80	852.575	22.764	21.6855	-4.73709	
		9	160	1014.816	22.895	21.8154	-4.71585	
56,045	1419.8364	1		35.184	14.258	13.8849	-2.61400	
		2	20	57.883	15.378	15.4271	0.31624	
		3	40	171.380	17.809	18.3542	3.06215	
		4	40	284.877	19.118	19.6401	2.72922	
		5	80	511.870	20.920	21.0219	0.48602	
		6	80	738.864	22.177	21.7839	-1.77368	
		7	160	965.857	23.026	22.2548	-3.34849	
		8	160	1192.851	23.581	22.5418	-4.40695	
		9	160	1419.844	23.791	22.6720	-4.70161	

9. Velocity Distribution of Pai

i) $\frac{u}{u_m} = 1 + a_1 \left(\frac{r}{R}\right)^2 + a_2 \left(\frac{r}{R}\right)^{2M}$ (42)

where

$$a_1 = \frac{S - M}{M - 1}$$

$$a_2 = \frac{1 - S}{M - 1}$$

$$S = 0.585 + 3.172 (10^{-3}) Re^{0.833}$$

$$M = -0.617 + 8.211 (10^{-3}) Re^{0.786}$$

Dimensionless velocity, u/u_m , was computed from equation (42) and compared with measured values in Tables 33 to 36.

ii)

$$\frac{u}{u_m} = 1 + \frac{2n^2}{(n+1)(2n+1)} \sqrt{\frac{f}{8}} \left[\ln \left(1 - \sqrt{1 - \frac{y}{R}} \right) + \sqrt{1 - \frac{y}{R}} \right] \quad (69)$$

where

$$n = \sqrt{\frac{1}{f}}$$

$$f = 0.316 Re^{-1/4}$$

and K was obtained by least squares for each run,

$$K = \frac{2n^2}{(n+1)(2n+1)} \sqrt{\frac{1}{f}} \frac{\sum_{1}^m \left(\frac{y}{R}\right)^2}{\sum_{1}^m \left(\frac{u}{u_m}\right) \left(\frac{y}{R}\right) - \sum_{1}^m \frac{y}{R}}$$

m = number of points measured in each run

Computed values are given in Tables 33 to 36.

TABLE 33

Velocity Distribution of Pai

Re	Point No.	Measured			Equation (42)			Equation (69)		
		$1 - \frac{y}{R}$	$\frac{u}{u_m}$	$\frac{u}{u_m}$	% Deviation	K	$\frac{u}{u_m}$	% Deviation	0	0
8,874	1	0	1.0000	1.0000	0	0.315	1.00000	1.00000	0	0.10813
	2	0.1599	0.9817	0.9912	0.9628		0.98276	0.98276	-0.4100	-1.06449
	3	0.3197	0.9686	0.9646	-0.4100		0.95829	0.95829	-1.2343	-0.82461
	4	0.4796	0.9319	0.9204	-1.2343		0.92422	0.92422	0.2766	0.87420
	5	0.6395	0.8560	0.8584	0.2766		0.87420	0.87420	-4.4137	0.78969
	6	0.7994	0.8063	0.7707	-4.4137		0.78969	0.78969	-4.5180	0.71385
	7	0.8793	0.7120	0.6798	-4.5180		0.71385	0.71385	27.9183	0.54819
	8	0.9592	0.5445	0.3925	27.9183		0.54819	0.54819	0.67833	0.67833
	9				0.283		1.00000	1.00000	0	0
13,117	1	0	1.0000	1.0000	0		0.98149	0.98149	-0.2573	-0.44713
	2	0.1599	0.9859	0.9910	0.5171		0.95522	0.95522	0.9190	-1.16741
	3	0.3197	0.9665	0.9640	-0.2573		0.91863	0.91863	0.8398	0.53991
	4	0.4796	0.9137	0.9190	0.5814		0.86493	0.86493	0.8560	2.99219
	5	0.6395	0.8398	0.8560	1.9294		0.77419	0.77419	0.7735	-0.73163
	6	0.7994	0.7799	0.7735	-0.8220		0.69278	0.69278	0.7236	-4.25972
	7	0.8793	0.5335	0.7079	-2.1721		0.51491	0.51491	0.5335	-3.48389
	8	0.9592	0.4032	0.4664	12.5835		0.43238	0.43238	16.4305	0.43238
	9	0.9752		0.3370	0.4032		7.23820	7.23820		

TABLE 34

Velocity Distribution of Pai

Re	Point No.	Measured			Equation (42)			Equation (69)		
		$1 - \frac{Y}{R}$	$\frac{u}{u_m}$							
18,176	1	0	1.0000	1.0000	1.0000	1.0000	1.0000	1.0000	1.0000	1.0000
	2	0.1599	0.9817	0.9910	0.9448	0.98362	0.98362	0.98346	0.98346	0.98346
	3	0.3197	0.9608	0.9639	0.3252	0.96036	0.96036	0.95999	0.95999	0.95999
	4	0.4796	0.9256	0.9188	-0.7332	0.92798	0.92798	0.92730	0.92730	0.92730
	5	0.6395	0.8603	0.8557	-0.5401	0.88044	0.88044	0.88089	0.88089	0.88089
	6	0.7994	0.7911	0.7742	-2.1351	0.80012	0.80012	0.80041	0.80041	0.80041
	7	0.8793	0.7206	0.7203	-0.0481	0.72805	0.72805	0.73427	0.73427	0.73427
	8	0.9592	0.5888	0.5269	10.5109	0.57061	0.57061	-3.08890	-3.08890	-3.08890
	9	0.9752	0.4948	0.3981	19.5486	0.49756	0.49756	0.55776	0.55776	0.55776
					0.299					
23,816	1	0	1.0000	1.0000	1.0000	1.0000	1.0000	1.0000	1.0000	1.0000
	2	0.1599	0.9910	0.9910	0.0009	0.98346	0.98346	-0.76059	-0.76059	-0.76059
	3	0.3197	0.9621	0.9641	0.2037	0.95999	0.95999	-0.21979	-0.21979	-0.21979
	4	0.4796	0.9192	0.9191	-0.0089	0.92730	0.92730	0.88089	0.88089	0.88089
	5	0.6395	0.8664	0.8562	-1.1779	0.87931	0.87931	1.49017	1.49017	1.49017
	6	0.7994	0.7966	0.7753	-2.6794	0.79824	0.79824	0.20561	0.20561	0.20561
	7	0.8793	0.7338	0.7259	-1.0804	0.72549	0.72549	-1.13249	-1.13249	-1.13249
	8	0.9592	0.5902	0.5728	-2.9411	0.56657	0.56657	-4.00450	-4.00450	-4.00450
	9	0.9752	0.4726	0.4509	-4.5842	0.49282	0.49282	4.27933	4.27933	4.27933

TABLE 35

Velocity Distribution of Pai

Re	Point No.	Measured			Equation (42)			Equation (69)		
		$1 - \frac{y}{R}$	$\frac{u}{u_m}$							
28,987	1	0	1.0000	1.0000	0	0	0	1.00000	1.00000	0
	2	0.1599	0.9902	0.9911	0.0865	0.0865	0.0865	0.98247	0.98247	-0.78035
	3	0.3197	0.9681	0.9643	-0.3977	-0.3977	-0.3977	0.95759	0.95759	-1.08552
	4	0.4796	0.9288	0.9195	-0.9963	-0.9963	-0.9963	0.92295	0.92295	-0.63020
	5	0.6395	0.8625	0.8570	-0.6427	-0.6427	-0.6427	0.87209	0.87209	1.11178
	6	0.7994	0.7799	0.7765	-0.4392	-0.4392	-0.4392	0.78616	0.78616	0.80329
	7	0.8793	0.7267	0.7287	0.2768	0.2768	0.2768	0.70906	0.70906	-2.42690
	8	0.9592	0.5818	0.6023	3.5281	3.5281	3.5281	0.54063	0.54063	-7.07636
	9	0.9752	0.4206	0.4893	16.3346	16.3346	16.3346	0.46248	0.46248	9.95624
					0.299	0.299	0.299	1.00000	1.00000	0
32,711	1	0	1.0000	1.0000	0	0	0	0.98400	0.98400	-0.56602
	2	0.1599	0.9896	0.9911	0.1510	0.1510	0.1510	0.96128	0.96128	-0.55011
	3	0.3197	0.9666	0.9644	-0.2276	-0.2276	-0.2276	0.92965	0.92965	0.41629
	4	0.4796	0.9258	0.9199	-0.6391	-0.6391	-0.6391	0.88322	0.88322	1.42666
	5	0.6395	0.8708	0.8576	-1.5210	-1.5210	-1.5210	0.80478	0.80478	1.02669
	6	0.7994	0.7966	0.7774	-2.4084	-2.4084	-2.4084	0.73439	0.73439	-0.87881
	7	0.8793	0.7409	0.7303	-1.4357	-1.4357	-1.4357	0.58062	0.58062	-4.50384
	8	0.9592	0.6080	0.6185	1.7221	1.7221	1.7221	0.50927	0.50927	4.25095
	9	0.9752	0.4885	0.5124	4.8902	4.8902	4.8902			

TABLE 36

Velocity Distribution of Pai

Re	Point No.	Measured			Equation (42)			Equation (69)		
		$1 - \frac{Y}{R}$	$\frac{u}{u_m}$	% Deviation	$1 - \frac{Y}{R}$	$\frac{u}{u_m}$	% Deviation	$1 - \frac{Y}{R}$	$\frac{u}{u_m}$	% Deviation
38,181	1	0	1.0000	0	0	1.0000	0	1.00000	0	0
	2	0.1599	0.9943	-0.3168	0.9912	0.98588	-0.84713	0.98588	-0.84713	-0.84713
	3	0.3197	0.9707	-0.6260	0.9646	0.96583	-0.50196	0.96583	-0.50196	-0.50196
	4	0.4796	0.9312	-1.1614	0.9204	0.93791	0.72075	0.93791	0.72075	0.72075
	5	0.6395	0.8732	-1.6894	0.8584	0.89693	2.71774	0.89693	2.71774	2.71774
	6	0.7994	0.7975	-2.3435	0.7788	0.82769	3.78619	0.82769	3.78619	3.78619
	7	0.8793	0.7408	-1.1583	0.7322	0.76557	3.34340	0.76557	3.34340	3.34340
	8	0.9592	0.6382	-0.2315	0.6367	0.62985	-1.30894	0.62985	-1.30894	-1.30894
	9	0.9752	0.5911	-8.4944	0.5409	0.56687	-4.09894	0.56687	-4.09894	-4.09894
	56,045	1	0	1.0000	1.0000	1.00000	0	1.00000	0	0
	2	0.1599	0.9912	0.0122	0.9913	0.98621	-0.50345	0.98621	-0.50345	-0.50345
	3	0.3197	0.9679	-0.2679	0.9653	0.96663	-0.13092	0.96663	-0.13092	-0.13092
	4	0.4796	0.9322	-1.1024	0.9219	0.93937	0.76966	0.93937	0.76966	0.76966
	5	0.6395	0.8793	-2.0604	0.8612	0.89936	2.28138	0.89936	2.28138	2.28138
	6	0.7994	0.8036	-2.5528	0.7831	0.83176	3.50365	0.83176	3.50365	3.50365
	7	0.8793	0.7486	-1.4763	0.7375	0.77109	3.00460	0.77109	3.00460	3.00460
	8	0.9592	0.6464	0.6704	0.6704	0.63857	-1.21144	0.63857	-1.21144	-1.21144
	9	0.9752	0.5993	0.6037	0.5993	0.57708	-3.70797	0.57708	-3.70797	-3.70797

TABLE 37
Entrance Velocity Profiles

Re	u (ft/sec)	y (in.)	u^+	y^+	% Deviation
8,790	2.820	0.3775	14.524	33.906	8.074
	3.420	1.1275	17.614	101.269	-0.438
	3.780	2.1275	19.468	191.087	-4.434
	3.780	3.1275	19.468	280.905	-1.106
13,000	4.370	0.3775	16.146	47.576	0.743
	4.860	1.1275	17.956	142.099	0.835
	5.140	2.1275	18.991	268.129	0.965
	5.290	3.1275	19.545	394.160	1.418
	6.120	0.3775	16.715	63.948	0.293
18,000	6.740	1.1275	18.408	190.996	1.064
	7.090	2.1275	19.364	360.394	1.590
	7.290	3.1275	19.910	529.792	2.058
	7.670	0.3775	17.078	78.528	0.180
23,000	8.490	1.1275	18.904	234.544	0.240
	9.010	2.1275	20.062	442.565	-0.222
	9.250	3.1275	20.596	650.585	0.335
	9.500	0.3775	17.721	93.979	-1.749
28,200	10.330	1.1275	19.269	280.691	-0.093
	10.860	2.1275	20.258	529.641	0.303
	11.050	3.1275	20.612	778.591	1.722
	11.260	0.3775	18.121	109.199	-2.523
33,500	12.240	1.1275	19.698	326.150	-0.985
	12.890	2.1275	20.744	615.418	-0.829
	13.090	3.1275	21.066	904.686	0.732
	12.960	0.3775	18.311	124.718	-2.315
39,000	14.080	1.1275	19.893	372.502	-0.834
	14.790	2.1275	20.896	702.881	-0.484
	14.990	3.1275	21.179	1033.260	1.248
	17.960	0.3775	19.013	168.953	-3.235
55,000	19.430	1.1275	20.569	504.622	-1.608
	20.210	2.1275	21.394	952.180	-0.414
	20.520	3.1275	21.723	1399.738	1.064

TABLE 38
Center-Line Velocity

Baro. press.	688.0 mm Hg
Flowing temp.	531.6°R
Orifice press.	694.1 mm Hg
Orifice press. diff.	2.28 mm Hg
Press. at probe loc.	688.0 mm Hg
Average velocity	3.052 ft/sec
Reynolds number	8,760
Flow rate	35.12 SCFM

Pt. of Measurement (in.)	Δh (in. alc.)	u (ft/sec)	$\frac{u}{u_{FD}}$
310	0.0041	4.05	1.000
220	0.0040	4.00	0.988
130	0.0039	3.95	0.975
26	0.0036	3.79	0.936
0	0.0057	4.77	1.178

Baro. press	691.5 mm Hg
Flowing temp.	531.6°R
Orifice press.	706.4 mm Hg
Orifice press. diff.	4.93 mm Hg
Press. at probe loc.	692.2 mm Hg
Average velocity	4.49 ft/sec
Reynolds number	13,000
Flow rate	52.00 SCFM

Pt. of Measurement (in.)	Δh (in. alc.)	u (ft/sec)	$\frac{u}{u_{FD}}$
310	0.0092	6.05	1.000
265	0.0091	6.01	0.993
220	0.0091	6.01	0.993
130	0.0086	5.85	0.967
46	0.0074	5.42	0.896
26	0.0077	5.53	0.914
16	0.0083	5.74	0.949
0	0.0122	6.96	1.150

TABLE 39

Center-Line Velocity

Baro. press	694.0 mm Hg
Flowing temp.	531.6°R
Orifice press.	723.0 mm Hg
Orifice press. diff.	9.63 mm Hg
Press. at probe loc.	695.0 mm Hg
Average velocity	6.31 ft/sec
Reynolds number	18,300
Flow rate	73.34 SCFM

Pt. of Measurement (in.)	Δh (in. alc.)	u (ft/sec)	\bar{u} \bar{u}_{FD}
310	0.0181	8.46	1.000
265	0.0180	8.44	0.998
220	0.0179	8.41	0.994
130	0.0166	8.10	0.957
46	0.0150	7.70	0.910
26	0.0151	7.73	0.914
16	0.0159	7.93	0.937
0	0.0200	8.90	1.052

Baro. press	696.6 mm Hg
Flowing temp.	531.6°R
Orifice press.	742.0 mm Hg
Orifice press. diff.	14.96 mm Hg
Press at probe loc.	698.8 mm Hg
Average velocity	7.91 ft/sec
Reynolds number	23,000
Flow rate	92.4 SCFM

Pt. of Measurement (in.)	Δh (in. alc.)	u (ft/sec)	\bar{u} \bar{u}_{FD}
310	0.0280	10.50	1.000
265	0.0280	10.50	1.000
220	0.0277	10.44	0.994
130	0.0255	10.02	0.954
46	0.0228	9.47	0.902
26	0.0235	9.62	0.916
16	0.0253	9.98	0.950
0	0.0369	12.06	1.149

TABLE 40

Center-Line Velocity

Baro. press	696.5 mm Hg
Flowing temp.	531.6°R
Orifice press.	764.0 mm Hg
Orifice press. diff.	22.06 mm Hg
Press. at probe loc.	700.0 mm Hg
Average velocity	9.70 ft/sec
Reynolds number	28,300
Flow rate	113.5 SCFM

Pt. of Measurement (in.)	Δh (in. alc.)	u (ft/sec)	$\frac{u}{u_{FD}}$
310	0.0422	12.88	1.000
265	0.0423	12.89	1.000
265	0.0421	12.86	0.998
220	0.0418	12.80	0.994
130	0.0374	12.12	0.941
60	0.0338	11.52	0.894
26	0.0346	11.66	0.905
16	0.0374	12.12	0.941
0	0.0539	14.55	1.130

Baro. press	695.7 mm Hg
Flowing temp.	531.6°R
Orifice press.	791.5 mm Hg
Orifice press diff.	29.85 mm Hg
Press. at probe loc.	700.7 mm Hg
Average velocity	11.43 ft/sec
Reynolds number	33,400
Flow rate	134.0 SCFM

Pt. of Measurement (in.)	Δh (in. alc.)	u (ft/sec)	$\frac{u}{u_{FD}}$
310	0.0578	15.06	1.000
265	0.0577	15.05	0.999
220	0.0567	14.92	0.991
130	0.0517	14.25	0.946
36	0.0460	13.44	0.892
26	0.0476	13.64	0.906
16	0.0517	14.25	0.946
0	0.0747	17.12	1.137

TABLE 41

Center-Line Velocity

Baro. press	689.0 mm Hg
Flowing temp.	531.6°R
Orifice press.	825.0 mm Hg
Orifice press. diff.	39.50 mm Hg
Press. at probe loc.	695.8 mm Hg
Average velocity	13.47 ft/sec
Reynolds number	39,000
Flow rate	156.8 SCFM

Pt. of Measurement (in.)	Δh (in. alc.)	u (ft/sec)	$\frac{u}{u_{FD}}$
--------------------------------	--------------------------	---------------	--------------------

307	0.0791	17.68	1.000
261	0.0786	17.63	0.997
216	0.0767	17.41	0.985
126	0.0690	16.51	0.934
46	0.0624	15.70	0.888
26	0.0643	15.94	0.902
16	0.0701	16.64	0.941
7	0.0815	17.95	1.015
0	0.1016	20.04	1.133

Baro. press	696.1 mm Hg
Flowing temp.	531.6°R
Orifice press.	1026.0 mm Hg
Orifice press. diff.	63.0 mm Hg
Press at probe loc.	709.6 mm Hg
Average velocity	18.54 ft/sec
Reynolds number	55,000
Flow rate	220.0 SCFM

Pt. of Measurement (in.)	Δh (in. alc.)	u (ft/sec)	$\frac{u}{u_{FD}}$
--------------------------------	--------------------------	---------------	--------------------

310	0.1511	24.20	1.000
265	0.1502	24.13	0.997
220	0.1476	23.92	0.988
130	0.1343	22.81	0.943
46	0.1193	21.50	0.888
26	0.1231	21.84	0.902
16	0.1340	22.79	0.942
0	0.2015	27.94	1.155

TABLE 42

Center-Line Velocity Using Wall Taps

Baro. press	701.8 mm Hg
Flowing temp.	531.6°R
Orifice press.	747.0 mm Hg
Orifice press. diff.	14.89 mm Hg
Press. at probe loc.	704.0 mm Hg
Average velocity	7.86 ft/sec
Reynolds number	23,000
Flow rate	92.50

Pt. of Measurement (in.)	Δh (in. alc.)	u (ft/sec)
280	0.0264	10.16
220	0.0257	10.02
114	0.0211	9.08
26	0.0195	8.73

Baro. press	698.1 mm Hg
Flowing temp.	531.6°R
Orifice press.	766.0 mm Hg
Orifice press. diff.	21.80 mm Hg
Press. at probe loc.	701.6 mm Hg
Average velocity	9.63 ft/sec
Reynolds number	28,200
Flow rate	112.99 SCFM

Pt. of Measurement (in.)	Δh (in. alc.)	u (ft/sec)
280	0.0396	12.46
220	0.0385	12.30
114	0.0332	11.41
26	0.0311	11.04

TABLE 43

Center-Line Velocity Using Wall Taps

Baro press.	704.3 mm Hg
Flowing temp.	531.6°R
Orifice press.	837.4 mm Hg
Orifice press. diff.	38.68 mm Hg
Press. at probe loc.	711.3 mm Hg
Average velocity	13.15 ft/sec
Reynolds number	39,000
Flow rate	156.47 SCFM

Pt. of Measurement (in.)	Δh (in. alc.)	u (ft/sec)
280	0.0752	17.05
220	0.0732	16.82
114	0.0628	15.58
26	0.0595	15.17

Baro press.	706.0 mm Hg
Flowing temp.	531.6°R
Orifice press.	1030.0 mm Hg
Orifice press. diff.	63.6 mm Hg
Press. at probe loc.	718.3 mm Hg
Average velocity	18.43 ft/sec
Reynolds number	55,200
Flow rate	221.37 SCFM

Pt. of Measurement (in.)	Δh (in. alc.)	u (ft/sec)
280	0.1450	23.56
220	0.1419	23.31
114	0.1219	21.60
26	0.1163	21.10

A P P E N D I X B

AN ERROR ANALYSIS

An error analysis was undertaken to test the fit of the experimental data to the universal velocity distribution correlation. The aim of this analysis was to see to what extent the correlation is sensitive to errors which arise in the measurement of the velocity and the distance from the wall.

1. Error in Measured Velocity

$$u = \sqrt{\frac{2g_c \Delta P}{\rho_{air}}}$$

or

$$u = \text{constant} \sqrt{\frac{\rho_{alc} T \Delta h}{P}} \quad (1)$$

The error variance is

$$E_u = \left(\frac{\partial u}{\partial \rho_{alc}} \right)^2 E_{\rho_{alc}} + \left(\frac{\partial u}{\partial T} \right)^2 E_T + \left(\frac{\partial u}{\partial (\Delta h)} \right)^2 E_{\Delta h} + \left(\frac{\partial u}{\partial P} \right)^2 E_P \quad (2)$$

Estimates of experimental errors:

$E_{\rho_{alc}}$	= 0.0155	$\pm 5^\circ F$
E_T	= 1.0	$\pm 1.0^\circ C$
$E_{\Delta h}$	= $2.5 (10^{-8})$	$\pm 0.0005 \text{ in. alc. for } u = 18.8 \text{ ft/sec}$
	= $4.0 (10^{-8})$	$\pm 0.0002 \text{ in. alc. for } u = 3.06 \text{ ft/sec}$
E_P	= 9.0	$\pm 3 \text{ mm Hg}$

The first derivatives of equation (1) with respect to each of ρ_{alc} , T, Δh and P were obtained and substituted into equation (2). With the estimated variances, the following limiting conditions were obtained:

Standard deviation = 0.40% , for $u = 18.8 \text{ ft/sec}$

Standard deviation = 5.10% , for $u = 3.06 \text{ ft/sec}$

2. Error in Measured Flow Rate

$$Q = CFY \sqrt{\frac{2g_C \Delta P}{\rho_{\text{air}}}}$$

or

$$Q = \text{constant} \quad CY \sqrt{\frac{\Delta PT}{P}} \quad (3)$$

The error variance is

$$\begin{aligned} E_Q &= \left(\frac{\partial Q}{\partial C} \right)^2 E_C + \left(\frac{\partial Q}{\partial Y} \right)^2 E_Y + \left(\frac{\partial Q}{\partial (\Delta P)} \right)^2 E_{\Delta P} \\ &+ \left(\frac{\partial Q}{\partial T} \right)^2 E_T + \left(\frac{\partial Q}{\partial P} \right)^2 E_P \end{aligned} \quad (4)$$

Estimates of experimental errors:

$$E_C = 0.0004 \quad \pm 0.02$$

$$E_Y = 0.000025 \quad \pm 0.005$$

$$E_{\Delta P} = 0.25 \quad \pm 0.5 \text{ mm Hg} \quad \text{for } Re = 56,000$$

$$= 0.0013 \quad \pm 0.036 \text{ mm Hg} \quad \text{for } Re = 8870$$

$$E_T = 3.24 \quad \pm 1.8^\circ\text{F}$$

$$E_P = 64.0 \quad \pm 8.0 \text{ mm Hg} \quad \text{for } Re = 56,000$$

$$= 16.0 \quad \pm 4.0 \text{ mm Hg} \quad Re = 8,870$$

The first derivatives of equation (3) with respect to each of C , Y , ΔP , T and P were obtained and substituted into equation (4). With the estimated variances, a nearly constant standard deviation was obtained for all flow rates.

Standard deviation = 1.15%

3. Universal Velocity Distribution

$$u^+ = A \ln y^+ + B \quad (5)$$

For simplicity:

$$u = u^+$$

$$y = y^+$$

and

$$u = A \ln y + B \quad (5a)$$

From least squares the following expression for A was obtained:

$$A = \frac{\sum_{i=1}^n u_i \ln y_i - \frac{1}{n} \sum_{i=1}^n u_i \sum_{i=1}^n \ln y_i}{\sum_{i=1}^n (\ln y_i)^2 - \frac{1}{n} (\sum_{i=1}^n \ln y_i)^2} \quad (6)$$

n = number of points

The error variance is

$$E_A = \sum_{i=1}^n \left(\frac{\partial A}{\partial u_i} \right)^2 E_{u_i^+} + \sum_{i=1}^n \left(\frac{\partial A}{\partial y_i} \right)^2 E_{y_i^+} \quad (7)$$

values of $E_{u_i^+}$, based upon the sum of the errors in the flow rate and the point velocity ranged from

0.06 for $Re = 56,000$ and $u_i = 13.65$

to 1.30 $Re = 8,870$ and $u_i = 14.0$

The variance $E_{y_i^+}$ was a function of flow rate only. Based upon an uncertainty of ± 0.03 inches in measured y_i ,

$E_{y_i^+} = 7.33$ for $Re = 8,870$

$= 185.0$ for $Re = 56,000$

Differentiating equation (6) with respect to all u_i 's and y_i 's, and substituting into equation (7) gives

$$E_A = \frac{1}{D^2} \sum_1^n E_{u_i} + (\ln y_i - \frac{1}{n} \sum_1^n \ln y_i)^2$$

$$+ \frac{1}{D^4} \sum_1^n E_{y_i} \left(\frac{D}{y_i} (u_i - \frac{1}{n} \sum_1^n u_i) \right)$$

$$- \frac{2C}{y_i} (\ln y_i - \frac{1}{n} \sum_1^n \ln y_i)^2$$

where

$$C = \sum_1^n u_i \ln y_i - \frac{1}{n} \sum_1^n u_i \sum_1^n \ln y_i$$

$$D = \sum_{i=1}^n (\ln y_i)^2 - \frac{1}{n} \left(\sum_{i=1}^n \ln y_i \right)^2$$

With the estimated variances the following standard deviation of A was obtained:

$$\pm 0.078$$

$$\text{or, } \pm 2.8\% \quad \text{for } A = 2.77$$

From least squares (equation 5a) the following expression for B was obtained:

$$B = \frac{1}{n} \sum_{i=1}^n u_i - \frac{A}{n} \sum_{i=1}^n \ln y_i \quad (8)$$

n = number of points.

A from equation (6)

The error variance is

$$E_B = \sum_{i=1}^n \left(\frac{\partial B}{\partial u_i} \right)^2 E_{u_i^+} + \sum_{i=1}^n \left(\frac{\partial B}{\partial y_i} \right)^2 E_{y_i^+} \quad (9)$$

The values of $E_{u_i^+}$ and $E_{y_i^+}$ are as previously. Differentiating equation (8) with respect to all u_i 's and y_i 's, and substituting into equation (9) gives

$$\begin{aligned}
 E_B &= \sum_{i=1}^n E_{u_i^+} \left((1 - \sum_{i=1}^n \ln y_i) (\ln y_i - \frac{1}{n} \sum_{i=1}^n \ln y_i) \frac{1}{D} \frac{1}{n} \right)^2 \\
 &+ \sum_{i=1}^n E_{Y_i^+} \left((\frac{c}{y_i} + \sum_{i=1}^n \ln y_i \frac{u_i}{y_i} - \frac{\sum_{i=1}^n u_i}{n}) \right. \\
 &\quad \left. - \frac{c}{D} \sum_{i=1}^n \ln y_i \left(\frac{2 \ln y_i}{y_i} - \frac{1}{n y_i} \right) \right) \frac{1}{n D}^2
 \end{aligned}$$

where C and D are defined as previously. The obtained standard deviation of B is

$$\pm 0.45$$

$$\text{or, } \pm 11.5\% \quad \text{for } B = 4.0$$

A P P E N D I X C

OPERATION AND MAINTENANCE OF AIR SUPPLY UNIT

Preliminary to startup of the new blower or its modifications, certain recommended checks were carried out. (listed on page 11 in "Instruction and Service Manual", CY-3, October 1963, Gardner-Denver Company, Quincy, Illinois)

From experience obtained with the present blower unit, a few additional checks are recommended at more frequent intervals:

i) The alignment of the motor and blower direct coupling is not perfect and should be tested periodically. An incorrect alignment was assumed to be the cause of failure of one blower-bearing shortly after the initial startup.

ii) The blower air discharge temperature varies with operating conditions. It should in no case exceed 350°F. A temperature shut-down switch was installed for this purpose. However, the setting of the switch changed with time, hence periodic checks with a standard thermometer are recommended. The last temperature settings were:

cut in at 245°F

cut out at 300°F

iii) Oil should be changed at least every 1000 hours of operation. Since the last oil-change, January 1965, there have been approximately 100 hours of blower operation. (May 1965) The type of oil presently being used is Teresso 65 - viscosity 555 at 100°F - Imperial Oil. (for further details see Instruction and Service Manual)

Performance of the Blower

The blower was tested for maximum performance shortly after installation, August 21, 1964, and a flow rate of 234 SCFM was obtained. Comparable flow rates have been obtained during the test period, and it may be concluded that the maximum performance has not changed.

The blower speed was measured with a tactometer and recorded. It was found that the speed was practically constant with time and with change in back pressure. Values recorded on August 20th, 1964 were:

Back-Pressure (psig)	rpm
2.0	3620
2.0	3618
3.3	3615
7.0	3595
10.0	3580
3.3	3618
2.0	3635
2.0	3630 (after 1 hour)

B29834